ANALYSIS OF HYBRID DIVERSITY RECEIVERS IN RAYLEIGH FADING CHANNELS

by

Paraskevas Polydorou

M.A.Sc., Simon Fraser University, 1997

B.A.Sc., Simon Fraser University, 1993

A THESIS SUBMITTED IN PARTIAL FULFILLMENT
OF THE REQUIREMENTS FOR THE DEGREE OF
DOCTOR OF PHILOSOPHY
in the School
of
Engineering Science

SIMON FRASER UNIVERSITY

April 2004

Approval

Name:	Paraskevas Polydorou
Degree:	Doctor of Philosophy
Title of Thesis:	Analysis of Hybrid Diversity Receivers in Rayleigh Fading Channels
Examining Committee:	
Chair:	Dr. Steve Hardy

Dr. Paul Ho
Senior Supervisor

Dr. Shawn Stapleton
Supervisor

Dr. James K. Cavers
Supervisor

Dr. Dong In Kim
Internal Examiner

Dr. Witold A. Krzymien
External Examiner
University of Alberta

Date Approved: April 8, 2004

SIMON FRASER UNIVERSITY

Partial Copyright Licence

Abstract

This thesis analyses the performance of hybrid diversity receivers which are essentially a hybrid of the three classical receivers: Selection Combining (SC), Equal Gain Combining (EGC) and Maximal Ratio Combining (MRC).

The hybrid selection/maximal ratio combining (H-S/MRC) receiver uses channel statistical information (CSI) to select and combine only the strongest of the available diversity branches. The average output SNR of this receiver and the SEP are derived. Lower computational complexity expressions are derived to compensate for an $N!$-fold increase in complexity (N is the number of diversity branches) in receivers with unequal branch statistics. Furthermore, an asymptotical SEP expression valid at high SNR is derived which provides further insight into the factors affecting the asymptotic SEP of the H-S/MRC receiver.

The selection combining (SC) and the double selection/equal gain combining (2S/EGC) receivers which do not use CSI are analysed and exact expressions for their SEP are derived. Furthermore, asymptotic SEP expressions are derived which are enlightening about the factors affecting their SEP at high SNR. It is found that while uneven distribution of the branch signal powers affects the error floor of the receivers, uneven distribution of the branch noise powers affects the asymptotic area above the error floor. The hybrid selection/equal gain combining (H-S/EGC) receiver which allows combining of an arbitrary number of selected branches is a generalization of the SC and 2S/EGC receivers. The asymptotic analysis of this receiver provides a closed form expression for the SEP and indicates that in some environments the asymptotic SEP may actually deteriorate with an increase in the number of combined branches. The asymptotic SEP of the H-S/MRC receiver, on the other hand, is proven to always improve by the combining of additional diversity branches.

A reduced complexity hybrid diversity receiver (RHDR) which tackles the problem of maintaining differential phase reference in selective diversity receivers at switch time is described and simulated. The RHDR uses two branches and achieves a SEP which is upper bounded by the SC receiver and lower bounded by the 2S/EGC receiver.

Acknowledgments

I acknowledge the help and support of my supervisor, Paul Ho, throughout my studies and express my gratitude for his help in the completion of my degree.

I also express special thanks to my wife, Janis, for her patience and support throughout the many years of my studies. I am especially grateful for the long days she spent raising our two children, Andreas and Catherine, in the last two years.

Playing intramural soccer has been a very enjoyable activity over the years. I am grateful to all the team mates and friends I have met over the years, and especially my team mates from "High Geer".

Dedication

To my parents.

Table of Contents

List of Tables

List of Figures

List of Abbreviations

2EGC	Equal gain combining receiver with two diversity branches
2S/EGC	Double selection/equal gain combining
2S/MRC	Double selection/maximal ratio combining
BPSK	Binary phase shift keying
CSI	Channel statistical information
DPSK	Differential phase shift keying
EGC	Equal gain combining
H-S/EGC	Hybrid selection/equal gain combining
H-S/MRC	Hybrid selection/maximal ratio combining
IF	Intermediate frequency
MMSE	Minimum mean squared error
MPSK	Multiple phase shift keying
MRC	Maximal ratio combining
PDF	Probability density function
PSGC	Previous symbol gain combining
PSK	Phase shift keying
RF	Radio frequency
SC	Selection combining
SDR	Software defined radio
SNR	Signal to noise ratio
SPN	Signal plus noise

Chapter 1

Introduction

In the ever expanding world of wireless communications the engineer faces a myriad problems ranging from limited bandwidth to radio channel variations causing unreliable communications. In our research, we investigated proposed remedies to the unpredictability (or randomness) of the radio channel. Specifically, we analysed the performance of a range of hybrid diversity receivers (HDR) and in particular, receivers operating in radio channels with unknown statistical parameters having diversity branches with non-identical statistics.

1.1 The Radio Channel

The wireless communication medium is continuously varying, thus, making reliable communications difficult. Many factors cause the variations. To name a few: Moving receiver and/or transmitter, moving objects in the environment, large obstacles in the line of sight, reflections of the signal at large objects, random arrival delay of the reflected signals, etc [1]-[2]. A simple urban environment with a mobile receiver surrounded by high buildings and other objects is shown in Figure 1.1. As can be seen in this picture, versions of the transmitted signal are reflected by objects in the environment of the mobile receiver and arrive at the receiver at slightly different times and with different phase. The direct path, shown as a solid line in Figure 1.1, is generally not available in urban areas because of the multitude of tall buildings and other obstacles in the line of sight. The result is a rapidly fluctuating signal, which is the superposition of the reflected replicas of the transmitted signal. The amplitude and phase variation is called fading and an example of a signal undergoing such fading is shown in Figure 1.2. In the interval shown in Figure 1.2 it is observed that the instantaneous power of the received signal varies from about 4 times above average down to 0.003 times below average or a dynamic range of approximately 30dB. This is not an unusual occurrence in wireless communications where the receiver designer must accommodate large dynamic gains at the receiver.

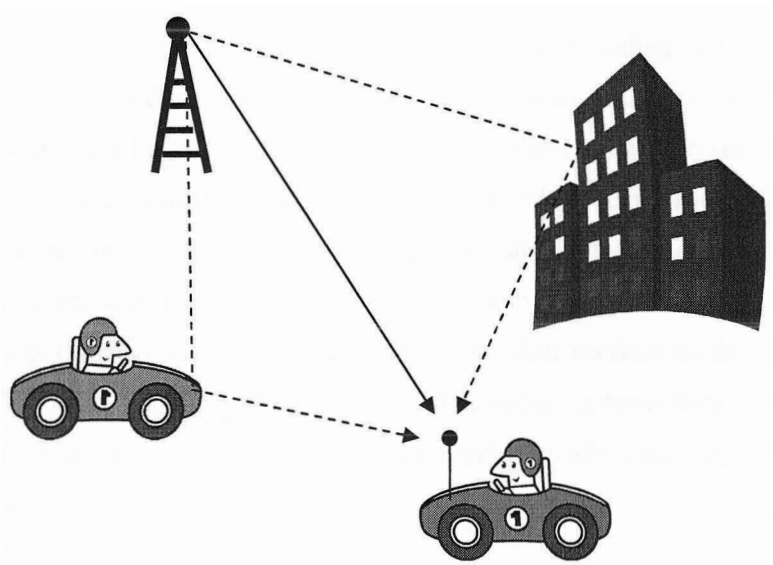

Figure 1.1: An urban fading environment.

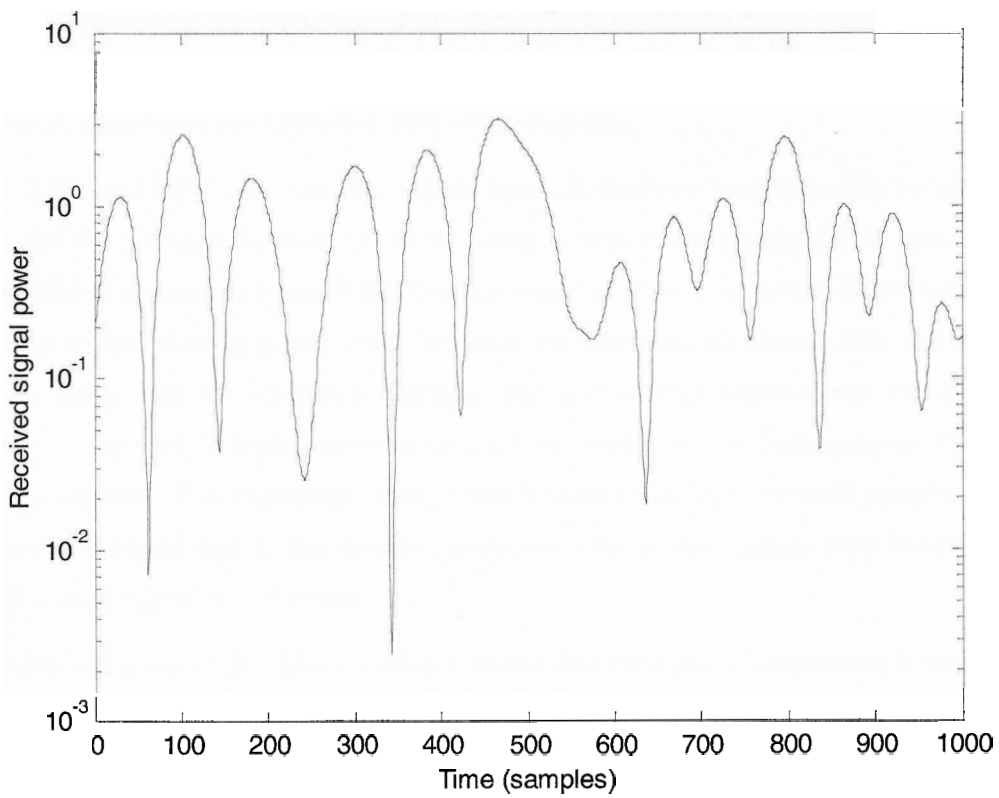

Figure 1.2: A signal from a Rayleigh fading channel with normalized average power equal to 1 and normalized fade rate $f_D = 0.01$.

1.2 The Benefits of Diversity at the Receiver

As already mentioned, the radio channel can be unreliable due to fading and, as a result, a lot of effort and energy has been expended over the years on ways to overcome the limitations of the medium. Many proposals have appeared which in some way remedy the situation such as, for example, the three classic methods of receiver diversity, which have been studied and been in use for decades. These are in order of increasing complexity and performance: Selection combining (SC), equal gain combining (EGC) and maximal ratio combining (MRC). The basic idea behind receiver diversity is that by capturing a number of *independent* versions of the transmitted signal the probability that at any one time all versions would be suffering from deep fading is very small and, thus, the signal-to-noise ratio at the receiver would be adequate for detection with low probability of error.

In a SC receiver there is, actually, no combining involved. The receiver simply compares the instantaneous signal-to-noise ratio (SNR) of all the branches and selects the branch with the largest value for detection. A demonstration of the operation of such a receiver is shown in Figure 1.3, where a receiver with two diversity branches, each with average power normalized to 1, continuously monitors the magnitude of the signals from each branch and selects the branch with the largest instantaneous magnitude and, hence, power. In the example of Figure 1.3, the power of the selected signal does not fall below 60% of the average.

In EGC and MRC receivers the signals from all diversity branches must be cophased, to ensure that the phase contamination due to fading is removed, and weighted to provide a linear combination of the signals from all the diversity branches. This ensures that all received branches contribute to the resulting signal. MRC provides the maximum combined SNR and on average performs better than the other two methods. The performance improvement of MRC comes, however, at the cost of higher complexity since knowledge of the instantaneous SNR at each branch is required. This knowledge ensures that branches with stronger SNR contribute more to the combined signal sent to the detector. Branches with weaker signals have lower SNR and, therefore, are assigned lower weight.

When using one of the three diversity methods described above an increase in the number of diversity branches normally improves the error performance of the diversity receiver. The improvement, however, comes at the cost of increased power consumption and more expensive implementation while at the same time the benefit from each additional branch diminishes [3]. To

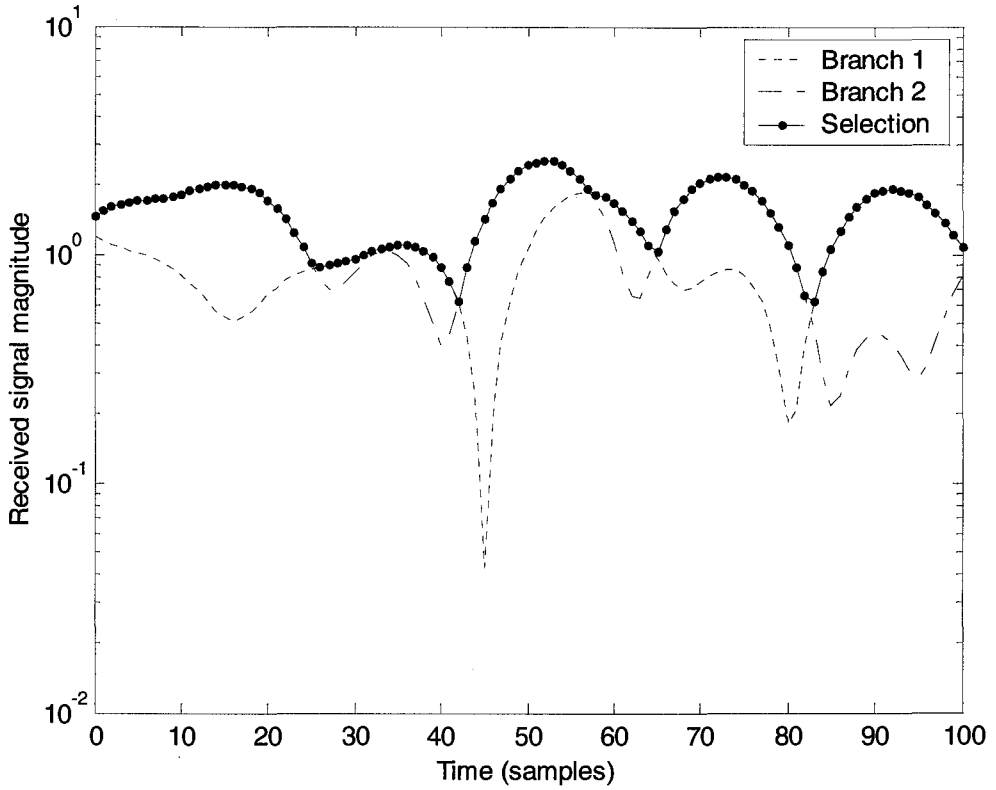

Figure 1.3: Demonstration of 2-branch selection diversity reception in a fast Rayleigh fading channel with normalized fade rate $f_D = 0.03$.

address this issue, a new, hybrid method has recently been proposed to limit the diversity branches used for detection to those branches that produce the maximum benefit, for example, the branches with the maximum SNR or signal plus noise (SPN) power. This method ensures that the branches with the strongest SNR, SPN, or any other criterion, are used in the combining process whereas the weaker branches are ignored.

The effect of the omission of the weaker signals should be obvious. In the case of MRC receivers, these signals would have very low weights so their effect in the combined signal would be very small, almost negligible. In the case of EGC receivers, where no weighting is performed, the inclusion of the weaker branches may even be detrimental to the performance of the receiver. As we see in Chapter 5, diversity receivers with no channel statistical information (noCSI) operating in hybrid mode and employing EGC with fewer than the maximum number of branches could result in better average error rates than classical EGC (Also see [4]).

1.3 Classical and Hybrid Diversity Receivers – A Historical Overview

1.3.1 Classical Diversity Receivers

The classical diversity receivers employing SC, EGC and MRC have been studied extensively over the years even though in many particular cases there are still no closed-form expressions for their average SEP. As Schwartz in [1] describes: "it was first discovered that the fading fluctuations of the signal received on two antennas placed sufficiently far apart were independent... It was then suggested that a switch to the strongest antenna signal at each instant would greatly reduce the fading depth... EGC and MRC can also be used as linear combinations of all available signals and other methods of obtaining diversity such as frequency, angle, polarization, time and multipath can be used..." An overview of the early work in diversity is provided in the paper by Eng et al [4] where they refer to early papers by Van Wambeck and Ross [5], Kahn [6] and others. The paper by Brennan [7] is also a classic reference for introduction to classical diversity techniques.

The performance of coherent versions of many diversity receivers is easier to calculate and it is documented by many researchers. The unrealistic coherent receivers have knowledge of the exact fading gain at each instant and use this value to cophase and optimally combine the diversity signals. It was found that MRC provides the best performance of the three techniques followed by EGC and SC in descending order of performance [1]. However, MRC is limited to channels with good estimates of both the phase and the magnitude of the fading since co-phasing and optimum weighting of each diversity signal is very important. EGC on the other hand only requires estimation of the phase and SC, in fact, does not perform combining but still requires estimation of the fading phase when angle modulations are used.

The analysis of the classical SC, EGC and MRC diversity receivers is abundant and we do not attempt to enumerate here the accomplishments of all the researchers. In fact much of the analysis appears in textbooks such as [1], [2] and [8]. In general, however, the performance of non-coherent versions of these receivers has not been as thorough and some systems do not have easy to understand solutions. Neasmith and Beaulieu in [9] provided an analysis of a SC system using signal-plus-noise, as opposed to signal-to-noise ratio, as the selection criterion for coherent, differentially coherent and non-coherent diversity receivers in a uniform signal profile. Zhang has studied the MRC and non-coherent EGC receiver operating in Rayleigh and Rice channels with correlated branches in various papers. (e.g. [10]-[11]) In general, Zhang uses hypergeometric functions for EGC, or gives efficient ways to calculate integral expressions. Lombardo also

investigated in [12] the bit error rate MRC using differential phase shift keying (DPSK) and correlated diversity branches.

1.3.2 Hybrid Diversity Receivers

The, so called, hybrid diversity schemes which select the L strongest branches out of N available and then combine them using either MRC (H-S/MRC) or EGC (H-S/EGC), can be thought of as generalized diversity combining schemes with SC, MRC and EGC being special cases. Hybrid diversity receivers (HDR), as we refer to them in this thesis, began appearing in the literature in the mid 1990s with an early paper appearing in 1994 by Erben et al [13]. This new hybrid technique was named "hybrid selection combining/maximal-ratio combining" by Erben and was analysed in the case of a RAKE receiver which uses a subset of the strongest signal paths out of all possible RAKE "arms" (fingers) in the combining. As was discussed in this paper, the "classical RAKE receiver consisting of fixed branch delay time differences" is not optimal since, in order to keep the RAKE receiver practical, the number of fingers is limited to some number N, with the possibility of omitting branches arriving with delays outside of that range. In [13] the hybrid SC/MRC 2DPSK RAKE receiver in a spread spectrum system, which monitors and selects the N *strongest* signal paths was analysed and an expression for the mean bit error rate (BER) was derived. The branches were assumed to have equal average SNR and the authors used a probability density function (pdf) for the combined SNR to arrive at rather long expressions for the average BER. Furthermore, the effect of the observation time in estimating the multipath intensity profile was investigated. It was argued that longer observation times produce better estimates due to the effect of the noise and the synchronization times.

Kong, Milstein et al, initially used the name "selection combining scheme" as it applied to the RAKE receiver. In [14] they derived expressions for the BER of this scheme for selection of a subset of the available branches in a uniform and exponential multipath intensity profile (MIP) and compared its performance to the SC receiver. In [4] they investigated receivers selecting 2 (SC2) or 3 (SC3) branches and then combining the signals using MRC in coherent communications or EGC in noncoherent communications. Their results were compared with SC, MRC and EGC receivers operating in similar environments. One interesting conclusion from their results was that the SC2 and SC3 receivers operating non-coherently performed in some cases better than the EGC receiver did. In later papers, Kong et al renamed this type of receiver "generalized selective combining" (GSC) scheme and concentrated their efforts in obtaining expressions for the average output SNR of the GSC. The rationale was that the average SNR is directly linked to the error performance of the receivers. For example, in [15] they derived a

generalized expression for the average SNR of a coherent GSC system consisting of branches with unequal average branch SNR. In the latest paper, [16], Kong derives an expression for the average Signal-to-Interference-plus-Noise Ratio under similar conditions. The expressions arrived at by Kong, Milstein et al were, in general, very long except for the special case of uniform SNR profile.

Alouini et al, in addition to their work in the classical diversity receivers (e.g. [17]-[18]), made significant contributions in the HDR area. They referred to the HDR as the "hybrid selective combining/maximal-ratio combining" (hybrid SC/MRC). As an example of Alouini and Simon's contribution to the analysis of HDR's, the performance of 2 specific coherent receivers in Nakagami fading channels employing hybrid SC/MRC was compared with that of SC and MRC in [19]. In general, Alouini et al investigated coherent receivers operating in channels with general power profiles and performing SC/MRC. Their results are usually in the form of a confluent hypergeometric functions which, although compact, are not very enlightening [19].

Annamalai et al produced many papers mainly for the classical diversity receivers but they also have a contribution in the HDR area. Their efforts were concentrated in deriving frameworks for obtaining expressions for many different diversity receivers. Like the other researchers, their expressions involved hypergeometric functions or were too complex for any useful conclusions. In [20], for example, they considered coherent, differentially coherent and noncoherent EGC systems over various fading channels including Rayleigh and Nakagami fading channels and provided closed-form expressions using the Appell hypergeometric function. Another area relevant to this thesis in which Annamalai et al contributed is analysis of diversity receivers with Gaussian channel estimation errors. In [21] and [22] they analysed receivers with Gaussian errors in their channel estimates. Their expressions, although useful to produce plots, do not help in gaining understanding of the factors influencing the receivers' behaviour.

For the research described so far, the effort was concentrated on deriving a probability density function for the combined SNR and then proceeding to derive an expression for the average SEP of the receiver. While this is a good technique it did not help to produce simple, concise expressions for the SEP, and in many cases resulted in expressions, which were just as cryptic as the problem itself. Instead, Win and Winters avoided deriving the pdf of the sum by expressing the output SNR as the sum of the individual branch SNR's. The problem of the ordered variables, which arises from the need to sort the branches according to their instantaneous signal magnitude or power, was tackled by a simple linear transformation resulting in a set of independent variables. Consequently, the integration with variable limits was transformed into

integration with the constant limits $[0,\infty)$. Their results were more presentable and could be used to extract meaningful information, such as what is the effect of unequal mean signal and/or noise powers in the diversity branches.

Papers by Win and Winters began appearing in 1999 (e.g. [23]-[24]) in which the authors were using the "virtual branch technique" to analyse coherent hybrid diversity systems in which the exact fading gain was available at the receiver. The diversity receivers were employed in channels with both uniform and non-uniform average SNR profiles. The SNR profile was in effect decided by the arriving average signal powers because the noise power in each branch was considered to be uniform in all cases. They also tackled the problem of correlated branches for the HDR in Nakagami fading in [25].

Polydorou and Ho initially investigated in [26] the hybrid selection maximal ratio combining (H-S/MRC) receiver operating in a Rayleigh fading environment. The H-S/MRC uses minimum mean squared error (MMSE) channel estimation. Annamalai et al later investigated a similar receiver in [21] and [22]. Polydorou and Ho provided closed form expressions for the SEP as well as lower complexity bounds and an asymptotic expression for high SNR. Polydorou and Ho later investigated in [27] the SC receiver operating in a Rayleigh fading channel without CSI and using DPSK. The SC receiver was operating in an environment with general signal and noise power profiles, an environment not considered previously for the SC receiver. The effect of the signal and noise profiles was evaluated by comparing the performance of this receiver and its coherent equivalent. Later, in [28], Polydorou and Ho, also analysed the double selection equal gain combining (2S/EGC) receiver operating in a similar environment as the SC from [27]. An exact expression for the SEP was derived and asymptotic analysis was performed to extract meaningful information on the factors affecting its performance.

From this discussion it should be apparent that a common application for the hybrid receiver is a CDMA receiver with a RAKE demodulator. The RAKE demodulator is used in a frequency selective channel to take advantage of the time dispersive nature of this channel by combining the time delayed despread replicas of the transmitted signal. While such a receiver may have a large number of possible replicas at its disposal, practical considerations limit the number that it can combine. Such a RAKE demodulator is modelled as a hybrid diversity receiver which is able to select a subset of the available replicas and combine them using appropriate weights.

1.4 Goals and Contributions of this Thesis

The goal of this thesis is to evaluate the performance of diversity receivers which are as general as possible and are operating in an environment which is as realistic as possible. A unique feature of our work is the analysis of the receiver performance with respect to different power and/or noise power profiles. Furthermore, we aim to derive expressions, which help us understand the factors affecting the performance of these receivers and not to merely replace integration with equally cryptic infinite hypergeometric series. In cases where an exact descriptive expression was not possible, we derived approximate, asymptotic expressions. The asymptotic expressions have the additional advantage of more clearly identifying the factors affecting the receiver performance due to their simplicity. Apart from the theoretical analysis of the hybrid diversity receivers we developed a reduced complexity hybrid diversity receiver (RHDR) which only requires the signals from two of the branches to be demodulated.

In Chapter 3 we investigate the effect of using linear MMSE channel estimation in hybrid selection maximal ratio combining (H-S/MRC) receivers as opposed to the perfectly coherent receivers studied, for example, by Win and Winters in [23]-[25]. We analyse the hybrid diversity receiver using linear MMSE channel estimation aided by PSAM or DPSK and obtain compact closed form expressions for the average symbol error probability (SEP) and the average output signal to noise ratio (SNR).

In Chapter 4 we investigate receivers operating in radio channels with unknown channel statistical information (CSI) and obtain symbol error probability (SEP) expressions for two special cases of HDR's analysed in part in [27]-[28]. We identify these receivers as *noCSI* to indicate the fact that they do not have access to the channel statistical information (CSI). Furthermore, we contrast the performance of these receivers to that of the H-S/MRC receivers analysed in Chapter 3 and observe the effect of the branch power profiles on their SEP.

To gain insight into the effect of the signal power profile and the noise power profile on the performance of HDR's operating in channels with known and unknown CSI we derive, in Chapter 5, compact and descriptive asymptotic approximations to the SEP of H-S/MRC and H-S/EGC receivers. These expressions indicate that absence of CSI has an effect on the error performance, which is related to the general arithmetic mean and the general geometric mean of the signal and/or noise power profiles. We find that the effect of the power profiles varies depending on the SNR region of interest. From the derived asymptotic expressions, we also observe that in general at high SNR a H-S/EGC receiver monitoring N and combining L branches

would perform better than an EGC receiver combining L branches with a more pronounced advantage in uniform power profiles.

Finally, in Chapter 6, we derive a reduced complexity hybrid diversity receiver, which can operate in channels with unknown CSI using DPSK. The RHDR selects 2 diversity branches out of all available while maintaining differential phase continuity between symbols. The common problem with DPSK in any selective diversity receiver is that it requires the previous symbol in every branch as a differential phase reference. This problem has been addressed by a more intelligent selection algorithm, which ensures that at least one of the two strongest branches can be correctly used for differential detection at any one time. It is shown by simulation that the SEP of this receiver is bound by the SEP of the SC and 2S/EGC receivers analysed in Chapter 4.

Chapter 2

Background

In this chapter, we provide background material, which is used in the main body of the thesis. The topics described in this chapter are: complex random variables, linear MMSE estimation, baseband system model, fading, channel estimation with or without channel statistical information (CSI) and ordered variables. CSI, in this thesis, refers to information about the channel statistics such as the maximum Doppler spread, the autocorrelation function of the fading process, the average power of the signal and the noise in each branch, etc.

2.1 Complex Random Variables

Since most of the analysis in this thesis involves statistical averaging of complex random variables (rv), we begin by explaining the notation used for our analysis. Let z be a complex rv defined in terms of the independent and identically distributed (iid) real variables x and y as follows

$$z = x + jy. \tag{2.1}$$

The rv's x and y have zero mean and, hence, z also has zero mean, that is

$$E[x] = E[y] = E[z] = 0, \tag{2.2}$$

where $E[\bullet]$ denotes expectation (statistical average). [1] Using (2.2) and considering the fact that x and y are iid, the variance of x and y is defined as

$$\sigma_x^2 = \sigma_y^2 = E[x^2] = E[y^2] = \sigma^2 \tag{2.3}$$

and the variance of z is defined as

$$\sigma_z^2 = \frac{1}{2}E[|z|^2] = \sigma^2. \tag{2.4}$$

---

[1] In this thesis we do not distinguish between the random variable and actual values taken by the random variable, usually denoted by capital and lower case letters respectively. For example, the rv could be denoted by X and its expectation in (2.2) could be written as $E[X]$.

The ½ factor introduced in (2.4) is used merely for convenience as this equates the variance of the complex rv z to the variance of the real rv's x and y.

Now let z_1 and z_2 be two complex, zero-mean rv's with variances σ_1^2 and σ_2^2 respectively. The covariance of z_1 and z_2, which in this case is equal to their correlation, is defined as

$$\sigma_{z_1 z_2} = \frac{1}{2} E[z_1 z_2^*]. \tag{2.5}$$

Note the absence of the square in the covariance symbol as opposed to the square in the variance symbol.

2.2 Linear MMSE Estimation

For the analysis of the average symbol error probability (SEP) of the various diversity receivers we make extensive use of linear minimum mean-squared error (MMSE) estimation theory. In the case of the Gaussian random variables that we are investigating, linear MMSE estimation is also the optimum MMSE estimation method [29].[2]

According to basic estimation theory, the MMSE estimate $\hat{g}$ of a random variable g can be calculated from a set of N observations. Let the $N \times 1$ column vector $\mathbf{h}$ consisting of the N observations be denoted by

$$\mathbf{h} = [h_1, h_2, \ldots, h_N]^T, \tag{2.6}$$

where ^{T} denotes transpose. The estimate $\hat{g}$ is, then,

$$\hat{g} = \mathbf{w}^\dagger \mathbf{h} + \mu, \tag{2.7}$$

where † denotes conjugate transpose,

$$\mu = E[g] - \mathbf{w}^\dagger E[\mathbf{h}] \tag{2.8}$$

and the vector $\mathbf{w}$ is calculated from the Wiener-Hopf equation. In this thesis the variable g is used to represent the fading gain of the channel and, therefore, based on our assumption of using the Rayleigh fading model, it is a zero-mean Gaussian variable. In light of this information, $\mu = 0$ and (2.7) becomes

$$\hat{g} = \mathbf{w}^\dagger \mathbf{h}. \tag{2.9}$$

Let $\mathbf{R}$ be the $N \times N$ correlation matrix of the observations defined as

---

[2] The material in this section is based on [29].

$$\mathbf{R} = \frac{1}{2} E[\mathbf{h}\mathbf{h}^{\dagger}], \tag{2.10}$$

and let $\mathbf{p}$ be the cross-correlation vector between the variable g and the observations vector $\mathbf{h}$, defined as

$$\mathbf{p} = \frac{1}{2} E[\mathbf{h}g^{*}], \tag{2.11}$$

where * denotes complex conjugation. Since the correlation matrix $\mathbf{R}$ is for our purposes positive definite and, hence, non-singular, the vector $\mathbf{w}$ is calculated by solving the Wiener-Hopf equation

$$\mathbf{R}\mathbf{w} = \mathbf{p}. \tag{2.12}$$

To measure the quality of the estimation, we define the estimation error as

$$e = g - \hat{g}, \tag{2.13}$$

and its variance, in this case the minimum mean squared error variance, is obtained from the expression

$$\sigma_e^2 = \frac{1}{2} E[|e|^2] = \sigma_g^2 - \sigma_{\hat{g}}^2, \tag{2.14}$$

where

$$\sigma_{\hat{g}}^2 = \mathbf{p}^{\dagger}\mathbf{R}^{-1}\mathbf{p}. \tag{2.15}$$

The error variable, e, has the property that it is zero-mean, Gaussian and statistically independent of the estimate $\hat{g}$. As we will see in the following chapters, this property of the estimation error greatly assists in the derivation of the SEP expressions.

When the MMSE estimation is based on a single observation h, the expression shown in (2.9) takes the scalar form

$$\hat{g} = w^{*}h, \tag{2.16}$$

and

$$w = \frac{\sigma_{gh}}{\sigma_h^2}. \tag{2.17}$$

σ_{gh} is the covariance of the random variable g and the observation h, defined as

$$\sigma_{gh} = \frac{1}{2} E[gh^{*}], \tag{2.18}$$

and σ_h^2 is the variance of the observation, defined as

$$\sigma_h^2 = \frac{1}{2} E\left[|h|^2\right]. \tag{2.19}$$

The MMSE error variance is given by (2.14), where the variance of the estimate, $\hat{g}$, a special case of (2.15) and is shown below:

$$\sigma_{\hat{g}}^2 = \frac{\sigma_{gh}^2}{\sigma_h^2}. \tag{2.20}$$

2.3 Baseband System Model

For our analysis of communication systems, we use the discrete-time, complex baseband model shown in Figure 2.1. This baseband equivalent model removes unnecessary bandpass details without affecting the analysis [2]. The source in Figure 2.1 generates a random sequence of symbols, which are sent to the channel encoder for appropriate formatting before being transmitted through the channel. The channel encoder, for example, could introduce pilot symbols in the data stream or perform differential encoding in order to assist in the channel estimation at the receiver. The modulation we consider is phase shift keying (PSK) in which all transmitted symbols, $s[k]$, have equal energy and for the purposes of this analysis, the energy is set to 1. In effect, the symbol energy is incorporated into the channel gain. The channel we consider is the Rayleigh fading channel with Doppler spread and normalized fade rate f_D. This channel introduces both multiplicative Rayleigh fading gain, $g[k]$, as well as additive white Gaussian noise (AWGN), $n[k]$ [2]. At the receiver, the channel decoder attempts to remove as much of the channel uncertainty as possible, aided by the channel pilot symbols or the differential encoding introduced in the transmitter by the channel encoder. The result is then passed to the detector which makes a symbol-by-symbol decision on the transmitted data.

Based on the variables shown in Figure 2.1 we may express the signal arriving at the receiver at time k as

$$r[k] = g[k]s[k] + n[k]. \tag{2.21}$$

For convenience, we omit from now on the time index k, except when absolutely necessary, and the expression shown in (2.21) becomes

$$r = g \cdot s + n. \tag{2.22}$$

The complex gain g is a zero-mean, complex Gaussian rv and it may be represented in polar form as

$$g = |g| e^{j\theta}, \tag{2.23}$$

and the transmitted symbol s may be written as

$$s = e^{j\varphi}, \tag{2.24}$$

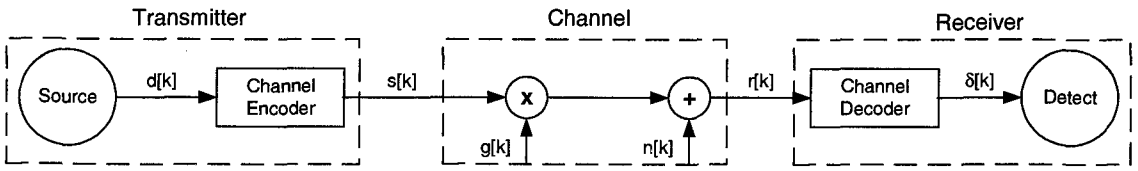

Figure 2.1: Baseband equivalent system model for the fading channel.

where

$$\varphi = \frac{2\pi k}{M},\ k \in \{0,1,\ldots,M-1\} \tag{2.25}$$

and M is the constellation size of PSK.

Since in PSK the information is conveyed through the angle φ, the random rotation θ introduced by fading on the received signal must be removed as it directly affects the detection of the received symbol. To better illustrate the effect of fading in PSK communications we present two diagrams in Figure 2.2 corresponding to a binary PSK (BPSK) transmitted symbol s=1. The symbol received from an AWGN channel is shown on the left and the symbol received from a fading channel is shown on the right. The transmitted signal is the small light coloured circle and the received symbol without the effect of AWGN is the dark circle of equal size. Note that when the channel is only affected by AWGN and assuming phase lock has already been achieved, the received symbol is attenuated by a constant real valued factor and is affected only by AWGN. The larger fuzzy disc represents the uncertainty arising from the AWGN and the resultant received symbol is likely to be within the circle. By testing whether the received symbol is in the right or left hand plane the detector can reproduce the transmitted symbol with a certain probability of error. When the channel is also affected by fading in addition to the AWGN, the received symbol suffers a random phase rotation in addition to a real valued attenuation. The phase rotation could randomly move the received symbol into the wrong plane and make phase lock difficult. As shown in the example in Figure 2.2, the rotation would result in erroneous detection. Therefore, for PSK modulation, estimation of the phase rotation is necessary. Pilot symbol assisted modulation (PSAM) or differential PSK (DPSK) may be used to assist in the estimation of the random rotation θ. The estimate $\hat{\theta}$ can be used to rotate the symbol back to approximately its original position. Based on the diagram in Figure 2.2, at the receiver we perform the following operation

$$\delta = r \cdot e^{-j\hat{\theta}}. \tag{2.26}$$

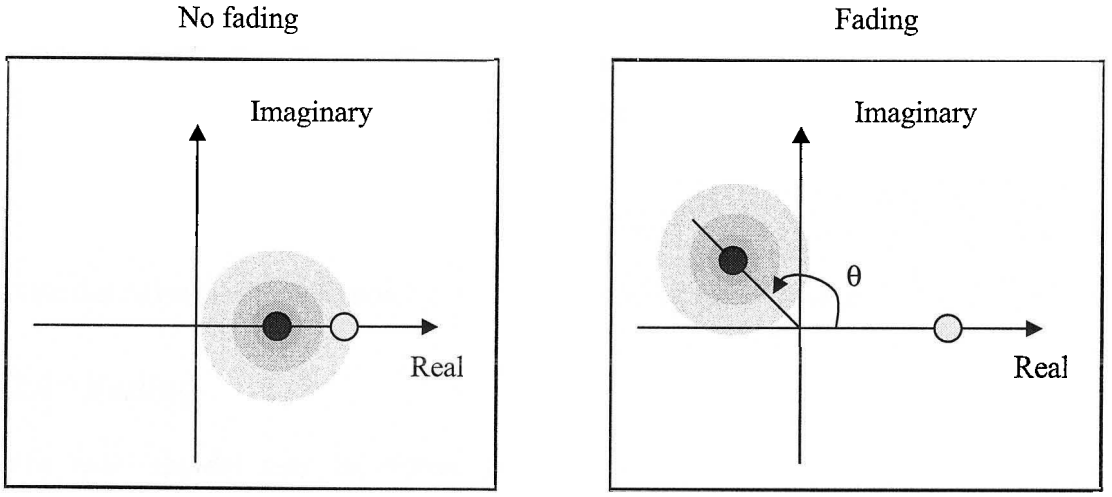

Figure 2.2: Comparison of Fading and AWGN channels

A useful measure of the signal quality, which is used for the symbol error probability (SEP) calculation, is the instantaneous SNR. In the case of the ideal coherent PSK receiver, that is the receiver which has complete and perfect knowledge about the channel state, we may deduce from equation (2.22) that the 1st term on the right hand side (rhs) is the useful part of the signal and the 2nd term is the noise. Therefore, the instantaneous SNR is defined as

$$\gamma = \frac{\frac{1}{2}|gs|^2}{\frac{1}{2}E[|n|^2]} \tag{2.27}$$

To simplify the readability of the expressions and without loss of generality we may assume that the transmitted symbol is 1. The expression shown in (2.27) is not affected by this simplification because any other transmitted symbol, based on the representation of (2.24), is merely a rotation and does not affect the magnitude of the numerator. In this case, (2.27) becomes

$$\gamma = \frac{\frac{1}{2}|g|^2}{\sigma_n^2}. \tag{2.28}$$

If MMSE estimation is employed, we can use (2.13) to express the fading gain in terms of the channel estimate $\hat{g}$ and the estimation error e as

$$g = \hat{g} + e. \tag{2.29}$$

Consequently, the received symbol shown in (2.22) can be expressed as

$$r = (\hat{g} + e) + n = \hat{g} + v, \tag{2.30}$$

where

$$v = e + n \tag{2.31}$$

and it may be thought of as the *effective* noise in the received symbol as it merges the AWGN and the estimation error into a new, zero-mean, Gaussian, random variable. The variance of v is denoted by

$$\mathcal{N} \equiv \sigma_v^2 = \sigma_e^2 + \sigma_n^2 . \tag{2.32}$$

Note that as explained in Section 2.2, v is statistically independent of $\hat{g}$.

2.4 Fading

The radio channel may be represented by different models depending on the operating environment. The most popular model used for urban communications is the Rayleigh fading model but Nakagami and Rician models are also common [2]. In fact, the Rayleigh model is a special case of the Nakagami model. For our research we used the Rayleigh model but the results can also be extended to the Nakagami model.

2.4.1 Rayleigh Fading

The fading gain in a Rayleigh fading environment is modelled as a complex Gaussian random variable with its real and imaginary parts being iid, zero-mean Gaussian variables like the variables used in (2.1). The magnitude of the fading gain at the receiver, is defined as

$$|g| = \sqrt{x^2 + y^2} . \tag{2.33}$$

The magnitude of the fading gain can be shown to be a Rayleigh distributed random variable characterized by the following pdf:

$$f_{|g|}(x) = \frac{x}{\sigma_g^2} \exp\left(-\frac{x^2}{2\sigma_g^2} \right), \; |g| > 0 \tag{2.34}$$

where σ_g^2 is the variance of the fading gain g and is defined below:

$$\sigma_g^2 = \frac{1}{2} E[|g|^2] . \tag{2.35}$$

Furthermore, the phase of the fading gain, defined as

$$\theta = \arctan\left(\frac{y}{x} \right), \tag{2.36}$$

can be shown to be a uniform random variable characterized by the following pdf:

$$f_\theta(\theta)=\begin{cases}\dfrac{1}{2\pi} & -\pi<\theta\le\pi \\ 0 & otherwise\end{cases}. \tag{2.37}$$

With the magnitude of the fading gain $|g|$ being Rayleigh distributed the pdf of the instantaneous SNR, γ, defined in (2.28), can be shown to be exponentially distributed as shown below:

$$f_\gamma(\gamma)=\frac{1}{\Gamma}\exp\left(-\frac{\gamma}{\Gamma}\right), \tag{2.38}$$

where

$$\Gamma=E[\gamma]=\frac{\sigma_g^2}{\sigma_n^2} \tag{2.39}$$

is the average signal to noise ratio.

2.4.2 Nakagami Fading

The Nakagami distribution used for the fading signal envelope is a more general pdf than the Rayleigh distribution. By choosing an appropriate value for the parameter m the distribution of the variable can vary from the one-sided Gaussian ($m=\frac{1}{2}$) to the Rayleigh ($m=1$) and to distributions with tails which decay faster than the Rayleigh distribution [2]. The Nakagami pdf is shown below:

$$f_{|g|}(x)=\frac{2}{\Gamma(m)}\left(\frac{m}{2\sigma_g^2}\right)^m x^{2m-1}\exp\left(-\frac{mx^2}{2\sigma_g^2}\right), \tag{2.40}$$

where $\Gamma(\bullet)$ is the gamma function defined by

$$\begin{aligned}&\Gamma(m)=\int_0^\infty t^{m-1}e^{-t}dt, \quad m>0\\ &\Gamma(m)=(m-1)!, \quad m\text{ integer and } m>0.\\ &\Gamma\left(\tfrac{1}{2}\right)=\sqrt{\pi}, \quad \Gamma\left(\tfrac{3}{2}\right)=\tfrac{1}{2}\sqrt{\pi}\end{aligned} \tag{2.41}$$

In (2.41), m is the Nakagami fading parameter and σ_g^2 is the variance of the fading gain or, alternatively, the average power. From the expression shown in (2.40) we observe that the Nakagami pdf is similar to the Rayleigh pdf and, in fact, it reduces to a Rayleigh pdf when m=1.

2.4.3 The Doppler Effect

In cases where at least one of the communication nodes or the surrounding objects are moving, the signal spectrum will be spread because of the Doppler effect. The Doppler effect, or Doppler spread, is also commonly observed in the case of sound with the well-known example of the train horn changing its pitch as the train passes by an observer. As the train approaches the observer, the pitch of the horn seems higher whereas as the train moves away the pitch seems lower. Similarly, in the case of radio communications, depending on the direction of motion, the Doppler effect distorts the frequencies of the various arriving paths and produces an effect at the receiver, which is equivalent to a U-shaped spectrum [8]. The Doppler spread reduces the temporal correlation of the channel gain between consecutive received symbols with detrimental effects on the error rate at the receiver. This Doppler spread has the effect of reducing the receiver's ability to predict the current channel state based on previous observations.

2.5 Channel Estimation using CSI

From this point forward and without loss of generality, we set the transmitted symbols $s[k]$ (for all k) in (2.21) to unity. This means that for any time index k, $r[k]$ can be written as $r[k]=g[k]+n[k]$. It should also be noted that we assume that the Rayleigh fading channel suffers Doppler spread with maximum normalized Doppler frequency f_D. The autocorrelation function of $g[k]$ based on the average received power, σ_g^2, and the normalized fade rate, f_D, is shown in [8] to be

$$R_{gg}[\tau]=\frac{1}{2}E[g[k]g[k+\tau]^*]=\sigma_g^2 J_0(2\pi f_D\tau), \tag{2.42}$$

where $J_0(\bullet)$ is the zero order Bessel function of the first kind, f_D is the normalized fade rate and τ is the temporal separation in number of samples.

With CSI available at the receiver an estimator can use observations to calculate an optimum MMSE estimate of the fading gain as discussed in Section 2.2. The observations may be obtained in several ways and in this thesis we focus on using differential encoding or pilot symbols, which are introduced by the transmitter into the data stream.

Unfortunately, in many situations, the receiver has no knowledge about the statistics of the channel it is operating in. The signal and noise powers as well as the correlation between the fading gain and the observations are not available or they are continuously changing making their

estimation difficult. To overcome this difficulty we may use a modulation, which works with or without optimum channel estimation such as DPSK.

2.5.1 Pilot Symbol Assisted Modulation

With PSAM the transmitter periodically inserts known pilot symbols in the data stream, which may be used at the receiver to calculate the optimum MMSE estimate of the fading gain of every received symbol. The estimator may use any number of pilot symbols for the calculation of the fade estimates and according to [30] 11 pilot symbols provide a good compromise between performance and delay or energy waste.[3] Following the analysis in [30] we define a frame of length M which consists of $M-1$ data symbols and 1 pilot symbol. The pilot symbol is assumed to be the 1st symbol in the frame. In general the receiver uses K pilot symbols to calculate the optimum channel estimates.

Let the received pilot symbols be placed in the following column vector

$$\mathbf{h}=\left[r\left[\left(\lfloor -K/2\rfloor+1\right)M\right],r\left[\left(\lfloor -K/2\rfloor+2\right)M\right],\cdots,r\left[\left(\lfloor -K/2\rfloor+K\right)M\right]\right]^T, \tag{2.43}$$

where $r[kM]$ is a pilot symbol and the $\lfloor\bullet\rfloor$ notation indicates the largest integer which is less than or equal to the number inside the brackets. The goal is to calculate the fading estimates $\hat{g}[1],\hat{g}[2],\ldots,\hat{g}[M-1]$ in the current frame. The autocorrelation matrix $\mathbf{R}$ was defined in (2.10) and the cross-correlation vector was defined in (2.11). The element in row i ($i=1,2,\ldots,K$) and column j ($j=1,2,\ldots,K$) of the autocorrelation matrix is given by

$$R_{ij}=\sigma_g^2 J_0\left(2\pi f_D M\left|i-j\right|\right)+\sigma_n^2\delta_{ij}, \tag{2.44}$$

where δ_{ij} is the Kronecker delta function. The cross-correlation vector is different for each estimate and is a function of the symbol's position in the frame. For the m-th symbol in the frame, the i-th element of the cross-correlation vector is given by

$$p_i[m]=\sigma_g^2 J_0\left(2\pi f_D\left|\left(\lfloor -K/2\rfloor+i\right)M-m\right|\right) \tag{2.45}$$

Based on the analysis in [30] and in Section 2.2 in this chapter we derive the optimum estimation coefficients and ultimately the variance of the estimation error and the average power of the estimates. The estimate of $g[k]$ is given by

---

[3] Note that the PSAM transmitter introduces a higher number of non-data symbols than DPSK and, thus, provides a lower energy per bit.

$$\hat{g}[k] = \mathbf{w}[k]^{\dagger}\mathbf{h}, \tag{2.46}$$

where $\mathbf{w}[k]$ is calculated using (2.12) as

$$\mathbf{w}[k] = \mathbf{R}^{-1}\mathbf{p}[k]. \tag{2.47}$$

The variance of the error and of the estimates can be calculated using (2.14) and (2.15) respectively.

2.5.2 Differential Phase Shift Keying

With DPSK the transmitter conveys information as the angular difference from the previous transmitted symbol and it is, therefore, a simpler system to implement and to analyse since the observation is a single scalar value. The symbol received in the previous instant is used as the observation and the optimum estimate of the fading gain can be calculated following the analysis in Section 2.5.1.

Let the observation be defined as

$$h = r[k-1]. \tag{2.48}$$

The optimum MMSE estimate is, then, given by

$$\hat{g} = w^{*}h, \tag{2.49}$$

where w was defined in (2.17) and the values of the required statistics are

$$\sigma_{gh} = \sigma_g^2 J_0(2\pi f_D), \tag{2.50}$$

$$\sigma_h^2 = \sigma_g^2 + \sigma_n^2, \tag{2.51}$$

The variance of the error and of the estimates can be calculated using (2.14) and (2.15) respectively.

The optimum channel estimate derived in (2.49) uses CSI which may not be available in certain situations. When CSI is not available at the receiver, DPSK may be used with the unmodified previous received symbol providing an estimate of the channel. In effect, the signal plus noise of the previous symbol becomes the *raw* channel estimate for the current symbol. Therefore, when CSI is not available the observation h shown in (2.48) is used as the estimate.

When the receiver does not employ diversity, that is it uses a single receive branch, the two fading gain estimates shown in (2.49) and in (2.48) perform identically. In a multiple branch diversity receiver, however, where the signals from multiple branches must be combined to produce the decision variable, the use of the raw channel estimate shown in (2.48) has detrimental effects on the symbol error rate. The difference in performance is caused by the weighting factor

w^* which places more weight on signals with higher SNR and helps produce a combined output signal which is closer to the optimum MRC signal. This issue will become clear when we consider the receivers with no CSI in chapters 4 and 5.

2.6 Ordered Random Variables

The SEP analysis of the hybrid diversity receivers (HDR) inevitably leads to the study of ordered variables. The HDR's we analyse in the following chapters select a number of the strongest branches for diversity combining and, thus, ordering has to be done to assist in the selection. Unfortunately, the ordered variables representing the received signal in the diversity branches are not independent, making averaging calculations more complicated than for their independent unordered counterparts used in MRC and EGC. In this section, we briefly review some of the concepts related to the order statistics of independent, exponentially distributed variables. These variables represent the instantaneous SNR in the diversity branches and are used for the evaluation of the SEP of the H-S/MRC receiver in Chapter 3.

Let $\{x_1, x_2, \ldots, x_N\}$ be a set of N independent, exponentially distributed variables with not necessarily equal parameters. We denote the exponential pdf of the individual variables as

$$f_{x_i}(x) = \frac{1}{X_i} \exp\left(-\frac{x}{X_i}\right), \tag{2.52}$$

where

$$X_i = E[x_i]. \tag{2.53}$$

The joint pdf of the variables $\{x_1, x_2, \ldots, x_N\}$ is given by

$$f_{x_1, x_2, \ldots, x_N}(x_1, x_2, \ldots, x_N) = \prod_{i=1}^{N} \left(\frac{1}{X_i} \exp\left(-\frac{x_i}{X_i}\right) \right) \tag{2.54}$$

Now let us define the following transformation:

$$\begin{aligned} x_{(1)} &= \text{largest of } \{x_1, x_2, \ldots, x_N\} \\ x_{(2)} &= 2^{\text{nd}} \text{ largest of } \{x_1, x_2, \ldots, x_N\} \\ &\vdots \\ x_{(N)} &= \text{smallest of } \{x_1, x_2, \ldots, x_N\}. \end{aligned} \tag{2.55}$$

This transformation creates the set of variables $\{x_{(1)}, x_{(2)}, \ldots, x_{(N)}\}$, where $x_{(1)} > x_{(2)} > \cdots > x_{(N)}$, to represent the original set $\{x_1, x_2, \ldots, x_N\}$ when arranged in descending order of magnitude. The joint pdf of the ordered variables is given by

$$f_{x_{(1)},x_{(2)},\ldots,x_{(N)}}(x_{(1)}, x_{(2)}, \ldots, x_{(N)}) = \sum_{\mathbf{P}_k} \prod_{i=1}^{N} \left(\frac{1}{X_{k_i}} \exp\left(-\frac{x_{(i)}}{X_{k_i}} \right) \right), \tag{2.56}$$

where $\mathbf{P}$ denotes the set of the $N!$ permutations of the integers $1, 2, \cdots, N$ and the subscript k denotes the k-th permutation in that set. As already stated, the variables $\{x_{(1)}, x_{(2)}, \ldots, x_{(N)}\}$ are no longer independent, thus, any averaging performed on the ordered set of variables is non-trivial. Fortunately, for the case of exponentially distributed rv's a simple linear transformation was introduced to the field of HDR's by Win and Winters in [23] to express the dependent variables in terms of a set of N independent variables $\{u_1, u_2, \ldots, u_N\}$. A modified version of that transformation applied to variables having the pdf shown in (2.56) is shown below:

$$x_{(i)} = \sum_{n=i}^{N} u_n \,. \tag{2.57}$$

This transformation can also be expressed in a more concise form using matrix notation. Let the column vector $\mathbf{x}$ consist of the variables $\{x_{(1)}, x_{(2)}, \ldots, x_{(N)}\}$ as follows:

$$\mathbf{x} = [x_{(1)}, x_{(2)}, \ldots, x_{(N)}]^T \,, \tag{2.58}$$

and the vector $\mathbf{u}$ consist of the variables $\{u_1, u_2, \ldots, u_N\}$ as follows:

$$\mathbf{u} = [u_1, u_2, \ldots, u_N]^T \,. \tag{2.59}$$

The linear transformation shown in (2.57) can be written in vector notation as

$$\mathbf{x} = \mathbf{T}\mathbf{u} \,, \tag{2.60}$$

where $\mathbf{T}$ is the upper triangular matrix shown below:

$$\mathbf{T} = \begin{bmatrix} 1 & 1 & \cdots & 1 \\ 0 & 1 & \cdots & 1 \\ \vdots & \vdots & \ddots & \vdots \\ 0 & 0 & \cdots & 1 \end{bmatrix}. \tag{2.61}$$

What this transformation does, is ensure that the new variables $\{u_1, u_2, \ldots, u_N\}$ can vary independently while the ordering of the variables $\{x_{(1)}, x_{(2)}, \ldots, x_{(N)}\}$ still holds. The joint pdf of the resulting variables $\{u_1, u_2, \ldots, u_N\}$ is given by

$$f_{u_1,u_2,\ldots,u_N}(u_1,u_2,\ldots,u_N)=\sum_{\mathbf{P}_k}\left(\prod_{i=1}^{N}\left(\frac{1}{X_{k_i}}\exp\left(-b_{k_i}u_i\right)\right)\right), \tag{2.62}$$

where

$$b_{k_i}=\sum_{n=1}^{i}\frac{1}{X_{k_n}}, \tag{2.63}$$

This transformation restores the independence of the variables and in some cases, as we will see in Chapter 3, considerably simplifies the average SEP and SNR derivations as well as produces results which are concise and easily interpreted.

Chapter 3

Hybrid Diversity Receivers Using Optimum MMSE Channel Estimation

The hybrid diversity receivers (HDR's) are a hybrid of two of the classical diversity methods. One example is the hybrid of selection combining (SC) and maximal ratio combining (MRC). Another example, more common in receivers without channel statistical information (CSI), is the hybrid of SC and equal gain combining (EGC). The HDR's provide performance, which is bounded by the performance of the classical SC receiver and the performance of MRC or EGC receivers. Since only a subset of the monitored diversity branches are combined, the HDR's have reduced complexity over the MRC and EGC receivers [31]. In this chapter we analyse the performance of a class of HDR's which use optimum MMSE channel estimation to aid in selection and combining, called the hybrid selection/maximal ratio combining (H-S/MRC) receivers. As shown in Chapter 2, CSI is necessary for optimum MMSE estimation of the channel gain since statistical parameters of the channel are needed to calculate the optimum estimator coefficients. For example, in (2.16) and (2.17) the channel estimate for a receiver using DPSK is shown to be a function of the joint statistics of the fading gain and the observation variable. The transmitter communicating with such a receiver also participates in the channel estimation process by either periodically introducing pilot symbols in the data stream or by differentially encoding the transmitted symbols.

The analysis in this chapter was inspired by the work of Win and Winters who in numerous papers (for example [24], [32]) analysed the operation of coherent diversity receivers using the "virtual branch technique" we described in Section 2.6. The two researchers and their associates investigated coherent receivers operating in Rayleigh and Nakagami fading channels with both independent and correlated diversity branches. They considered channels with branches having both equal and unequal (also called uneven, unbalanced or non-uniform) average SNR's and derived expressions for the average combined SNR and for the average SEP of the H-S/MRC receiver. We extend the analysis performed previously to investigate the H-S/MRC receiver operating in a Rayleigh fading environment with Doppler spread and unequal branch SNR's. Our

H-S/MRC receiver does not have perfect knowledge of the channel state but uses its knowledge of the CSI to employ MMSE channel estimation and to perform optimum hybrid diversity combining. Since the MMSE estimation, in our analysis, does not predict the channel state perfectly, the maximum *estimated* SNR is used as the branch selection criterion. Furthermore, the estimated fading gain is used to calculate the optimum weights for the combined branches. The uncertainty in the fading gain estimates is modelled as a Gaussian error and has the effect of reducing the combined output SNR relative to the SNR of HDR's with perfect channel state information. Some of the analysis in this chapter appeared in [26] which incidentally was the first paper to appear investigating imperfect channel estimation in HDR's. Other papers analysing classical diversity with errors include [33]-[36]. Annamalai and Tellambura also analysed HDR's with Gaussian errors in the channel estimates, in [21] and more recently in [22]. They analysed channels with iid diversity branches and assumed constant correlation between the estimate and the actual fading gain for all SNR's. As we see in Section 3.4 this is not true in the case of MMSE estimation since the correlation increases at high SNR due to the reduction of the influence of the AWGN on the uncertainty of the channel.

Specifically, in this chapter we investigate the effect of the Gaussian error, introduced by the MMSE channel estimation, and of the non-uniform average SNR profile on the SEP of the H-S/MRC receiver. To the best of our knowledge no other analysis of hybrid diversity receivers has appeared in the literature which properly models the MMSE (PSAM or DPSK) estimation error in relation to the fade rate and the channel statistics. The ideal coherent receiver is a special case of the H-S/MRC receiver analysed in this chapter and is used as a reference in evaluating the effects of the estimation error. The main contributions of this chapter are: a) Derivation of the average SEP and average combined SNR for the H-S/MRC receiver using MMSE channel estimation, b) analysis of the effect of uneven average branch SNR's on the SEP, c) derivation of lower computational complexity bounds for the SEP and d) asymptotic analysis of the SEP at high SNR.

3.1 System Model

The model we use for the H-S/MRC receiver is directly derived from the system model shown in Figure 2.1. The transmitter is identical to that of Figure 2.1 and the channel affects the signal with Rayleigh fading with Doppler spread and with AWGN. The receiver, shown in Figure 3.1, consists of N diversity branches, which are independently affected by fading and AWGN,

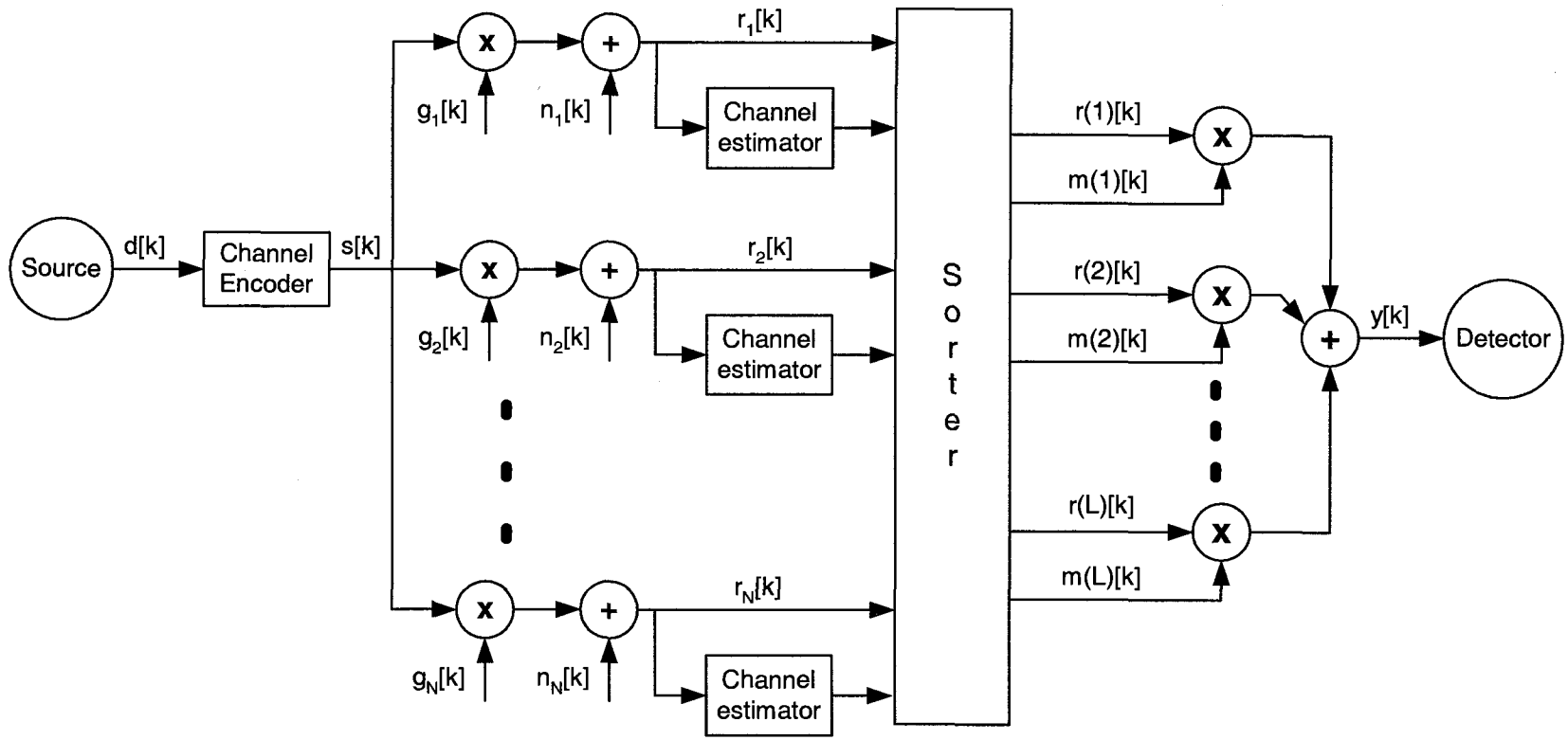

Figure 3.1: H-S/MRC receiver system model.

indicated by the variables $g_i[k]$ and $n_i[k]$ respectively. The N branches represent the independent versions of the received signal that are acquired, for example, by multiple antennas or by a RAKE receiver. The symbols received from the N branches, $r_1[k], r_2[k], \ldots, r_N[k]$, are sorted according to their estimated SNR, which is calculated by the MMSE estimators. Using the notation introduced in Section 2.6, the symbols from the L strongest branches can be written as $r_{(1)}[k], r_{(2)}[k], \ldots, r_{(L)}[k]$, $(1 \le L \le N)$. These L symbols are combined using MRC to produce the decision variable, y, which is used for a symbol-by-symbol decision by the detector. The detector computes the decoding metrics $C_n = \mathrm{Re}\left(y e^{-j2\pi n/M}\right)$, $n = 0,1,\ldots,M-1$, and decides that $\hat{s} = e^{j2\pi k/M}$ is the transmitted symbol if C_k is the largest amongst the C_n's.

As in equation (2.22), in any symbol interval the signal from the i-th branch at the receiver can be written as

$$r_i = g_i + n_i \tag{3.1}$$

where g_i is the fading gain affecting the i-th branch and n_i is the corresponding AWGN term. Note that as discussed in Chapter 2, we have set, without loss of generality, the transmitted data symbols to 1. The g_i's are complex Gaussian random variables with zero mean and variance $\sigma_{g_i}^2$. The set $\left\{\sigma_{g_1}^2, \sigma_{g_2}^2, \ldots, \sigma_{g_N}^2\right\}$ defines the signal power profile (SPP) of the channel. The SPP is called uniform if all the $\sigma_{g_i}^2$'s are equal. In this thesis, the analysis is general in the sense that it is not limited to any particular profile. The n_i's are also complex Gaussian random variables with zero mean and variance $\sigma_{n_i}^2$. The set $\left\{\sigma_{n_1}^2, \sigma_{n_2}^2, \ldots, \sigma_{n_N}^2\right\}$ defines the noise power profile (NPP) of the channel which as for the SPP is not limited to any particular profile. In this chapter we will also use the average SNR profile to refer to the set $\left\{\sigma_{g_1}^2/\sigma_{n_1}^2, \sigma_{g_2}^2/\sigma_{n_2}^2, \ldots, \sigma_{g_N}^2/\sigma_{n_N}^2\right\}$ of actual average SNR's in each branch.

At each symbol interval the bank of N channel estimators produces the estimates $\hat{g}_i$ of the complex multiplicative fading gains g_i. The optimum MMSE channel estimate in each branch is calculated by the expression

$$\hat{g}_i = \mathbf{w}_i^{\dagger}\mathbf{h}_i, \tag{3.2}$$

where $\mathbf{h}_i$ is the observations vector and $\mathbf{w}_i$ is the MMSE estimator coefficients vector. Just as in equation (2.29), in each branch we can express the channel fading in terms of the estimate and the MMSE estimation error as

$$g_i = \hat{g}_i + e_i . \tag{3.3}$$

Equation (3.3) allows the expression of the received symbol in branch i as a function of the channel estimate $\hat{g}_i$, the estimation error e_i and the AWGN n_i as

$$r_i = (\hat{g}_i + e_i) + n_i = \hat{g}_i + v_i , \tag{3.4}$$

where $v_i = e_i + n_i$, defined in (2.31), is the *effective* noise in each branch with variance defined in (2.32) as $\mathcal{N}_i \equiv \sigma_{v_i}^2 = \sigma_{e_i}^2 + \sigma_{n_i}^2$.

Using (2.9), (2.14) and (2.15) the approximate instantaneous SNR in r_i based on the estimate $\hat{g}_i$, can be expressed as

$$\gamma_i = \frac{\frac{1}{2}|\hat{g}_i|^2}{\mathcal{N}_i} = \frac{\frac{1}{2}\mathbf{w}_i^{\dagger}\mathbf{h}_i\mathbf{h}_i^{\dagger}\mathbf{w}_i}{\sigma_{g_i}^2 - \mathbf{p}_i^{\dagger}\mathbf{R}_i^{-1}\mathbf{p}_i + \sigma_{n_i}^2} \tag{3.5}$$

and its probability density function (pdf) is exponential and is defined as

$$f_{\gamma_i}(\gamma_i) = \frac{1}{\Gamma_i} e^{-\frac{\gamma_i}{\Gamma_i}}, \tag{3.6}$$

where

$$\Gamma_i = E[\gamma_i] = \frac{\frac{1}{2}\mathbf{w}_i^{\dagger}\mathbf{R}_i\mathbf{w}_i}{\sigma_{g_i}^2 - \mathbf{p}_i^{\dagger}\mathbf{R}_i^{-1}\mathbf{p}_i + \sigma_{n_i}^2} \tag{3.7}$$

is the average estimated SNR of branch i. For the special case of channel estimation using a single observation value, as for example in DPSK, the vector expressions shown in (3.2), (3.5) and (3.7) are reduced to the scalar expressions, respectively,

$$\hat{g}_i = \frac{\sigma_{g_i h_i}^*}{\sigma_{h_i}^2} h_i , \tag{3.8}$$

$$\gamma_i = \frac{\frac{1}{2}|h_i|^2 \left|\sigma_{g_i h_i}\right|^2}{\sigma_{h_i}^4 \sigma_{g_i}^2 - \sigma_{h_i}^2 \left|\sigma_{g_i h_i}\right|^2 + \sigma_{h_i}^4 \sigma_{n_i}^2}, \tag{3.9}$$

$$\Gamma_i = \frac{\left|\sigma_{g_i h_i}\right|^2}{\sigma_{g_i}^2 \sigma_{h_i}^2 - \left|\sigma_{g_i h_i}\right|^2 + \sigma_{n_i}^2 \sigma_{h_i}^2} . \tag{3.10}$$

Before deriving the optimal H-S/MRC strategy in the presence of imperfect channel estimation, it is instructive to derive the optimal classical MRC strategy. For MRC, the combined signal, i.e. the decision variable for the demodulator, is the sum

$$y = \sum_{i=1}^{N} m_i r_i, \tag{3.11}$$

where m_i is the weighting coefficient for the i-th branch and is a function of $\hat{g}_i$. Given the channel estimates $\hat{g}_i$ from (3.2) or (3.8), the combined signal can be written as

$$r = \sum_{i=1}^{N} m_i \hat{g}_i + \sum_{i=1}^{N} m_i v_i, \tag{3.12}$$

where the first term is the signal component and the second is the effective noise component. The corresponding instantaneous estimated SNR at the detector is, thus,

$$\gamma_{mrc} = \frac{\frac{1}{2}\left|\sum_{i=1}^{N} m_i \hat{g}_i\right|^2}{\frac{1}{2}E\left[\left|\sum_{i=1}^{N} m_i v_i\right|^2\right]}. \tag{3.13}$$

Based on the independence of the v_i with the $\hat{g}_i$ and hence with the m_i, we may simplify the denominator of (3.13) and rewrite the instantaneous estimated SNR as

$$\gamma_{mrc} = \frac{\left|\sum_{i=1}^{N} m_i \hat{g}_i\right|^2}{2\sum_{i=1}^{N} |m_i|^2 \mathcal{N}_i}. \tag{3.14}$$

The optimum values for the m_i that maximize the overall SNR can be obtained by applying the Schwarz's inequality on (3.14) based on the assumption that the signals in all branches are independent. By rewriting (3.14) as

$$\gamma_{mrc} = \frac{\left|\sum_{i=1}^{N}\left(m_i\sqrt{\mathcal{N}_i}\right)\left(\frac{\hat{g}_i}{\sqrt{\mathcal{N}_i}}\right)\right|^2}{2\sum_{i=1}^{N} |m_i|^2 \mathcal{N}_i}, \tag{3.15}$$

we may use Schwarz's inequality to separate the two terms in the numerator as follows:

$$\frac{\left|\sum_{i=1}^{N}\left(m_i\sqrt{\mathcal{N}_i}\right)\left(\frac{\hat{g}_i}{\sqrt{\mathcal{N}_i}}\right)\right|^2}{2\sum_{i=1}^{N} |m_i|^2 \mathcal{N}_i} \le \frac{\sum_{i=1}^{N}\left|m_i\sqrt{\mathcal{N}_i}\right|^2 \sum_{i=1}^{N}\left|\frac{\hat{g}_i}{\sqrt{\mathcal{N}_i}}\right|^2}{2\sum_{i=1}^{N} |m_i|^2 \mathcal{N}_i}. \tag{3.16}$$

After cancellations the inequality is simplified to

$$\frac{\left|\sum_{i=1}^{N} m_i \hat{g}_i\right|^2}{2\sum_{i=1}^{N} |m_i|^2 \mathcal{N}_i} \leq \frac{1}{2}\sum_{i=1}^{N}\left|\frac{\hat{g}_i}{\sqrt{\mathcal{N}_i}}\right|^2 . \tag{3.17}$$

The conclusion should now be obvious, as our goal is to maximize the left hand side. The maximum value is achieved at equality which implies that the two numerator terms shown in (3.16) must be equal as shown below:

$$m_i\sqrt{\mathcal{N}_i} = \left(\frac{\hat{g}_i}{\sqrt{\mathcal{N}_i}}\right)^* . \tag{3.18}$$

The value of m_i is

$$m_i = \frac{\hat{g}_i^*}{\mathcal{N}_i} = \frac{\mathbf{h}_i^\dagger \mathbf{w}_i}{\sigma_{g_i}^2 - \frac{1}{2}\mathbf{p}_i^\dagger \mathbf{R}_i^{-1}\mathbf{p}_i + \sigma_{n_i}^2} \tag{3.19}$$

and using this value for m_i the corresponding maximum SNR in (3.14) is simplified to

$$\gamma_{mrc} = \sum_{i=1}^{N} \frac{\frac{1}{2}|\hat{g}_i|^2}{\mathcal{N}_i} = \sum_{i=1}^{N} \gamma_i . \tag{3.20}$$

The expression in (3.20) indicates that the total SNR at the output of the MRC receiver is the sum of the individual SNR's from the independent branches. Therefore, branches with larger instantaneous SNR contribute more to the total combined SNR than branches with lower instantaneous SNR. At this point it should be noted that the *optimum* diversity combining strategy described above requires that the receiver has knowledge of the statistics of each branch which are used to calculate the m_i in (3.19). Furthermore, in spite of the assumption of mutual independence of the branches it was recently shown in [37] that these weights are still optimal even with correlated branches.

Based on the analysis for MRC and the fact that the instantaneous SNR, γ_i, is a positive quantity, it can be deduced that the *optimum* H-S/MRC receiver should combine, at each symbol interval, the L branches, $1 \leq L \leq N$, with the largest instantaneous SNR. The weighting coefficients were derived in (3.19). The instantaneous SNR at the output of the H-S/MRC receiver can, thus, be written as

$$\gamma_h = \sum_{i=1}^{N} a_i \gamma_{(i)} \tag{3.21}$$

where

$$a_i = \begin{cases} 1 & i = 1,2,\cdots,L \\ 0 & \text{otherwise} \end{cases} \tag{3.22}$$

and $\gamma_{(1)} > \gamma_{(2)} > \cdots > \gamma_{(N)}$, are the instantaneous branch SNR's arranged in descending order. As shown in (2.56) the joint pdf of the sorted variables is

$$f(\gamma_{(1)}, \gamma_{(2)}, \cdots, \gamma_{(N)}) = \sum_{\mathbf{P}_k} \left(\prod_{i=1}^{N} \left(f_{\gamma_{k_i}}(\gamma_{(i)}) \right) \right), \tag{3.23}$$

where $\mathbf{P}$ denotes the set of the $N!$ permutations of the integers $1,2,\cdots,N$ and the subscript k denotes the k-th permutation in that set.

3.2 Symbol Error Probability Analysis

The necessary background is now established to allow us to derive the SEP of the H-S/MRC receiver with independent Rayleigh faded branches. For this derivation we use an alternative expression for the conditional SEP of PSK receivers derived by Pawula et al in [38] and used widely in the literature. This technique can also be used to calculate the SEP of M-AM and square M-QAM modulations [44]. The expression defines the SEP conditioned on the combined SNR as

$$P_{e|\gamma_h} = \frac{1}{\pi} \int_0^{\Phi} \exp(-K(\varphi)\gamma_h) d\varphi \tag{3.24}$$

where $K(\varphi) = \sin^2(\pi/M)/\sin^2(\varphi)$, $\Phi = \pi(M-1)/M$, and M is the constellation size in PSK. The *unconditional* average SEP for the fading channel is obtained by the expression

$$P_e = \frac{1}{\pi} \sum_{\mathbf{P}_k} \int_0^{\Phi} \int_0^{\infty} \int_0^{\gamma_{(1)}} \cdots \int_0^{\gamma_{(N-1)}} \exp\left(-K(\varphi) \sum_{i=1}^{N} a_i \gamma_{(i)} \right) \left(\prod_{i=1}^{N} f_{\gamma_{k_i}}(\gamma_{(i)}) \right) d\gamma_{(N)} \cdots d\gamma_{(2)} d\gamma_{(1)} d\varphi. \tag{3.25}$$

One possible approach to obtaining a solution would be to directly evaluate the nested integral with the variable upper limits, a very tedious procedure. An alternative approach is to use the "virtual branch technique" which was described in Section 2.6. With the simple linear transformation $\gamma_{(i)} = \sum_{n=i}^{N} u_n$, defined in (2.57), the sorted variables can be converted into the new set of independent, exponentially distributed, random variables $\{u_1, u_2, \ldots, u_N\}$. The joint pdf of the new, independent variables is

$$f_{u_1,u_2,\ldots,u_N}(u_1,u_2,\ldots,u_N) = \frac{1}{(\Gamma_0)^N} \sum_{\mathbf{P}_k} \left(\prod_{i=1}^{N} \exp(-b_{k_i} u_i) \right), \tag{3.26}$$

where

$$b_{k_i} = \sum_{n=1}^{i} \frac{1}{\Gamma_{k_n}} \tag{3.27}$$

and Γ_0 is the geometric mean of the average branch SNR's defined as

$$\Gamma_0 = \left(\prod_{i=1}^{N} \Gamma_i \right)^{1/N}. \tag{3.28}$$

Using the independent variables u_i the expression in (3.25) becomes

$$P_e = \frac{1}{\pi(\Gamma_0)^N} \sum_{\mathbf{P}_k} \int_0^{\Phi} \int_0^{\infty} \int_0^{\infty} \cdots \int_0^{\infty} \exp\left(-K(\varphi) \sum_{i=1}^{N} c_i u_i \right) \left(\prod_{i=1}^{N} \exp\left(-b_{k_i} u_i\right) \right) du_N \cdots du_2 du_1 d\varphi \tag{3.29}$$

where

$$c_i = \sum_{n=1}^{i} a_n \tag{3.30}$$

or in other words

$$c_i = \begin{cases} i & i \le L \\ L & L < i \le N \end{cases}. \tag{3.31}$$

After simplification, the integrand in (3.29) becomes a product of exponentials and (3.29) can be written more conveniently as

$$P_e = \frac{1}{\pi(\Gamma_0)^N} \sum_{\mathbf{P}_k} \int_0^{\Phi} \int_0^{\infty} \int_0^{\infty} \cdots \int_0^{\infty} \exp\left(-\sum_{i=1}^{N} \left(K(\varphi) c_i + b_{k_i} \right) u_i \right) du_N \cdots du_2 du_1 d\varphi . \tag{3.32}$$

The N inner integrals, each of which can be evaluated separately due to the independence of the variables, produce the closed-form expression for the SEP

$$P_e = \frac{1}{\pi(\Gamma_0)^N} \sum_{\mathbf{P}_k} \left(\int_0^{\Phi} \left(\prod_{i=1}^{N} \frac{1}{K(\varphi) c_i + \sum_{n=1}^{i} \left(1/\Gamma_{k_n}\right)} \right) d\varphi \right), \tag{3.33}$$

where b_{k_i} was replaced with the sum defined in (3.27). It is interesting to note that the SPP and NPP do not independently influence the SEP of the H-S/MRC receiver but instead the profile of the average branch SNR's is the influencing factor.

A special case of interest because of its simpler form, as well as its potential for comparison with the literature, is the case of the uniform SNR profile, i.e. where all the branches have equal average SNR. In this special case, the SEP is simplified to

$$P_e = \frac{1}{\pi} \int_0^{\Phi} \prod_{i=1}^{N} \left(\frac{1}{\Gamma K(\varphi) c_i / i + 1} \right) d\varphi . \tag{3.34}$$

While (3.34) appears to be of the same form as the result in [24], it should be noted that the variable Γ in (3.34) is the average *estimated* SNR and not the actual SNR in the branches as was the assumption in [24].

In comparing (3.33) with (3.34), we observe that unequal SNR in the different branches leads to $N!$-fold increase in computational complexity. While for many diversity receivers of practical interest N is a small integer and this $N!$-fold increase in computational complexity is manageable there are cases such as dense multipath channels where the number of branches could be high. We therefore derive, in Section 3.2.1, bounds with adjustable complexity and accuracy.

3.2.1 Upper and Lower Bounds on the SEP

To reduce the complexity in the evaluation of (3.33) we derive lower computational complexity expressions which provide upper and lower bounds. Let

$$\boldsymbol{\Gamma} = \left[\Gamma_{(1)}, \Gamma_{(2)}, \cdots, \Gamma_{(N)}\right], \qquad \Gamma_{(1)} > \Gamma_{(2)} > \cdots \Gamma_{(N)} \tag{3.35}$$

be the average branch SNR's arranged in descending order, derived from the set of unsorted SNR's $\{\Gamma_1, \Gamma_2, \cdots, \Gamma_N\}$. Then it can be easily shown that for any permutation $\mathbf{P}_k$, the term $\sum_{n=1}^{i}\left(1/\Gamma_{k_n}\right)$ in (3.33) satisfies

$$A_i \le \sum_{n=1}^{i} \frac{1}{\Gamma_{k_i}} \le B_i, \tag{3.36}$$

where

$$A_i = \sum_{n=1}^{i} \frac{1}{\Gamma_{(n)}} \tag{3.37}$$

and

$$B_i = \sum_{n=1}^{i} \frac{1}{\Gamma_{(N-n+1)}}. \tag{3.38}$$

Consequently, we can obtain a lower bound and an upper bound on the SEP by using (3.36) to bound every product term in (3.33). The upper and lower bounds obtained this way will be independent of the permutation $\mathbf{P}_k$. As such, their computation complexity will be identical to that of the exact SEP of a uniform power profile (3.34). However, depending on how substantial is the variation in the SNR profile, these bounds may not be tight. By making a sacrifice in computational complexity, we can obtain tighter bounds by applying (3.36) only to the last *N-t* terms in the integrand of (3.33) while allowing the first t terms to be averaged over all possible permutations $\mathbf{P}_k$. These more general upper and lower bounds can be written as

$$P_e \le \frac{(N-t)!}{\pi(\Gamma_0)^N}\sum_{\mathbf{P}_k^t}\left(\int_0^{\Phi}\left(\prod_{i=1}^{t}\frac{1}{K(\varphi)c_i+b_{k_i}}\right)\left(\prod_{i=t+1}^{N}\frac{1}{K(\varphi)c_i+A_i}\right)d\varphi\right) \tag{3.39}$$

and

$$P_e \ge \frac{(N-t)!}{\pi(\Gamma_0)^N}\sum_{\mathbf{P}_k^t}\left(\int_0^{\Phi}\left(\prod_{i=1}^{t}\frac{1}{K(\varphi)c_i+b_{k_i}}\right)\left(\prod_{i=t+1}^{N}\frac{1}{K(\varphi)c_i+B_i}\right)d\varphi\right) \tag{3.40}$$

where $\mathbf{P}^t$ denotes the set of the $N!/(N-t)!$ permutations of the t integers taken from the set $\{1,2,\cdots,N\}$ and the subscript k denotes the k -th permutation from that set.

$$\mathbf{P}_k^t = (k_1,k_2,\cdots,k_t), \qquad k=1,2,\cdots,N!/(N-t)! \tag{3.41}$$

is the k-th possible t-tuple that can be constructed from the set $\{1,2,\cdots,N\}$ without repetition.

3.2.2 Asymptotic Analysis

To reach meaningful conclusions from the expression in (3.33) we assume that the channel fading is slow enough that there is no irreducible error floor in the region of interest. This means that at large channel SNR, the term $\sum_{n=1}^{i}\left(1/\Gamma_{k_n}\right)$ in (3.33) will be insignificant compared to the term $K(\varphi)c_i$ [26][40][41]. Consequently, the SEP may be approximated by

$$P_e \approx \frac{N!}{\pi(\Gamma_0)^N}\int_0^{\Phi}\left(\prod_{i=1}^{N}\frac{1}{K(\varphi)c_i}\right)d\varphi = \left(\frac{N!}{L!L^{N-L}}\right)\frac{K_\varphi}{\pi(\Gamma_0)^N}, \tag{3.42}$$

where, for convenience of notation, we used the following substitution:

$$K_\varphi = \int_0^{\Phi}\frac{d\varphi}{K(\varphi)^N}. \tag{3.43}$$

In [40] the term $\left(N!/\left(L!L^{N-L}\right)\right)^{1/N}$ is called the upper bound for the SNR penalty and indicates the additional SNR required by the H-S/MRC receiver to achieve the same SEP as the classical MRC receiver with N branches. The integral in (3.43) has a known evaluation according to the integral tables in [42]. For the general case of PSK with $M \ge 2$, the integral is given by [39 eq.2.513 1]

$$K_\varphi = \frac{1}{2^{2N}}\binom{2N}{N}\frac{\pi(M-1)}{M} + \frac{(-1)^N}{2^{2N-1}}\sum_{k=0}^{N-1}(-1)^k\binom{2N}{k}\frac{\sin\left(\pi(2N-2k)(M-1)/M\right)}{2N-2k} \tag{3.44}$$

and for the special case of BPSK ($M=2$) the integral is simplified to [39 eq.3.621 3]

$$K_\varphi = \frac{(2N-1)!!}{(2N)!!}\frac{\pi}{2}, \tag{3.45}$$

where the notation $2k!!$ denotes the product $2\cdot 4\cdot 6\cdots 2k$ and the notation ($2k$-1)!! denotes the product $1\cdot 3\cdot 5\cdots(2k-1)$ where k is any integer. In spite of the existence of the exact solution to the integral, in most expressions we retain the integral form since it is more compact than the right hand side of (3.44).

The approximation in (3.42) leads to a very simple expression for the degradation in profile efficiency caused by having a non-uniform SNR profile compared to having a uniform SNR profile. Recall that Γ_0 represents the geometric mean of the branch SNR's. Since the geometric mean is less than or equal to the arithmetic mean, let us consider two H-S/MRC systems having the same number of branches and equal total average SNR but with different SNR profiles amongst their respective branches. For the uniform power profile, Γ_0 is also equal to the average SNR of all the branches defined by

$$\Gamma_{avg} = \frac{1}{N}\sum_{i=1}^{N}\Gamma_i \,. \tag{3.46}$$

We can, therefore, express the asymptotic SEP of the H-S/MRC receiver operating in a uniform SNR profile in terms of Γ_{avg} as

$$P_e^u \approx \left(\frac{N!}{L!L^{N-L}}\right)\frac{K_\varphi}{\pi\left(\Gamma_{avg}\right)^N}. \tag{3.47}$$

From (3.42) and (3.47) it is clear that the receiver operating in the uniform SNR profile will perform better than the receiver operating in a non-uniform SNR profile by a factor $\left(\Gamma_{avg}/\Gamma_0\right)^N$. We, therefore, define the *profile efficiency ratio* as shown below:

$$\delta_p = \left(\frac{\Gamma_0}{\Gamma_{avg}}\right)^N. \tag{3.48}$$

δ_p is the ratio of the SEP of the H-S/MRC receiver in the uniform SNR profile over the SEP of the receiver in a non-uniform SNR profile shown in (3.42) and (3.47) respectively. Alternatively, the profile efficiency can be expressed in logarithmic terms as

$$\delta_{\text{pdB}} = 10N\bullet\log\left(\frac{\Gamma_0}{\Gamma_{avg}}\right)\text{dB}. \tag{3.49}$$

In (3.48) we observe that the degradation in energy efficiency caused by a non-uniform profile is only dependent upon the total number of branches N and not on the number of selected branches L. In Section 3.4 we use (3.48) to explain the behaviour of various receivers operating in the asymptotic region.

3.3 Output SNR Analysis

SNR analysis for the ideal coherent H-S/MRC receiver has been done by Kong and Milstein in [43] and [15] and by Win et al in [32] and [31]. We extend the analysis to the H-S/MRC receiver which uses MMSE channel estimation. In this section we derive a closed-form expression for the average SNR of the H-S/MRC system whose SEP was analysed in Section 3.2. With most of the framework established in Sections 3.1 and 3.2, here we briefly derive the final expression.

The average SNR is calculated as the expectation of the instantaneous SNR γ_h, defined in (3.21), as follows:

$$\Gamma_h = E[\gamma_h] = \int_0^\infty \gamma_h f_{\gamma_h}(\gamma_h) d\gamma_h , \tag{3.50}$$

where $f_{\gamma_h}(\gamma_h)$ is the pdf of γ_h defined in (3.6). The expression in (3.50) can be modified by replacing γ_h with the sum of the sorted random variables shown in (3.21) to obtain the alternative expression

$$\Gamma_h = \sum_{\mathbf{P}_k} \int_0^\infty \int_0^{\gamma_{(1)}} \cdots \int_0^{\gamma_{(N-1)}} \left(\sum_{i=1}^{N} (a_i \gamma_{(i)}) \right) \left(\prod_{i=1}^{N} \left(f_{\gamma_{k_i}}(\gamma_{(i)}) \right) \right) d\gamma_{(N)} \cdots d\gamma_{(2)} d\gamma_{(1)} . \tag{3.51}$$

As in Section 3.2, we use the "virtual branch technique" from Section 2.6 to convert the dependent variables into a set of independent variables u_i with exponential pdf. The average SNR in (3.51) can now be written as

$$\Gamma_h = \frac{1}{(\Gamma_0)^N} \sum_{\mathbf{P}_k} \int_0^\infty \int_0^\infty \cdots \int_0^\infty \left(\sum_{i=1}^{N} (c_i u_i) \right) \left(\prod_{i=1}^{N} \left(\exp\left(-b_{k_i} u_i\right) \right) \right) du_N \cdots du_2 du_1 , \tag{3.52}$$

where c_i and b_{k_i} were defined in (3.30) and (3.27) respectively. We can easily solve (3.52) by reversing the summation and integration order as follows

$$\Gamma_h = \frac{1}{(\Gamma_0)^N} \sum_{\mathbf{P}_k} \sum_{i=1}^{N} c_i \int_0^\infty \int_0^\infty \cdots \int_0^\infty u_i \left(\prod_{n=1}^{N} \left(\exp\left(-b_{k_n} u_n\right) \right) \right) du_N \cdots du_2 du_1 . \tag{3.53}$$

The inner multiple integrals are evaluated independently as

$$\int_0^\infty \int_0^\infty \cdots \int_0^\infty u_i \left(\prod_{n=1}^{N} \left(\exp\left(-b_{k_n} u_n\right) \right) \right) du_N \cdots du_2 du_1 = \frac{1}{b_{k_i}} \prod_{n=1}^{N} \left(\frac{1}{b_{k_n}} \right) \tag{3.54}$$

and the expression in (3.53) is simplified to

$$\Gamma_h = \frac{1}{(\Gamma_0)^N} \sum_{\mathbf{P}_k} \left(\left(\prod_{n=1}^{N} \frac{1}{b_{k_n}} \right) \left(\sum_{i=1}^{N} \frac{c_i}{b_{k_i}} \right) \right) . \tag{3.55}$$

Let us now consider two special cases for the SNR of the H-S/MRC receiver: The SNR of the H-S/MRC receiver operating in a uniform profile and the SNR of the classical MRC receiver. For a uniform SNR profile (3.55) can be simplified even further as shown below:

$$\Gamma_h = \Gamma \sum_{i=1}^{N} \frac{c_i}{i}. \tag{3.56}$$

For ideal coherent detection, the SNR Γ in (3.56) becomes equal to the SNR used in [32], [43] and [15]. In other words, for the special case $\hat{g}_i = g_i$ the expression in (3.56) is identical to those in [32], [43] and [15].

For the classical MRC receiver we note that there is no selection involved and, hence, no need for ordered branches. The average SNR of the MRC receiver can, thus, be written as

$$\Gamma_{mrc} = \int_0^\infty \int_0^\infty \cdots \int_0^\infty \left(\sum_{i=1}^{N} \gamma_i \right) \left(\prod_{i=1}^{N} f_{\gamma_i}(\gamma_i) \right) d\gamma_N \cdots d\gamma_2 d\gamma_1 . \tag{3.57}$$

The final expression is easily obtained by direct calculation of the multiple integrals and is shown below:

$$\Gamma_{mrc} = \sum_{i=1}^{N} \Gamma_i . \tag{3.58}$$

We observe in (3.58) that the average SNR of the MRC receiver is simply the sum of the average SNR's of the individual branches.

3.4 Results

In this section we use the expressions derived in Sections 3.2 and 3.3 to examine the behaviour of the H-S/MRC receiver operating under various scenarios and demonstrate the tightness of the low-complexity SEP bounds for various parameters t. Furthermore, in this section we demonstrate the significance of the asymptotic SEP expression and the profile efficiency ratio in explaining the difference in the performance of the H-S/MRC receiver operating in various SNR profiles. All systems evaluated in this section operate in a Rayleigh fading environment with Doppler spread and employ 8-PSK (M=8) modulation. For the two types of channel estimators considered in this study, namely the DPSK and the PSAM we use the MMSE estimator parameters $\mathbf{w}_i$ derived in Section 2.5. In this section we provide results for these two estimation methods as well as for the ideal coherent receiver (CPSK) for comparison. It is worthwhile to note that the ideal coherent receiver is a special case of our receiver when $\hat{g}_i = g_i$.

We begin by explaining the convention we follow for defining the SNR profiles. The general form of the SNR profile is exponential, meaning that the actual input SNR's at the various branches are distributed according to

$$\tilde{\Gamma}_i = Ge^{-a(i-1)}, \tag{3.59}$$

where i is the branch index with values $i=1,2,\ldots,N$, a is the profile decay factor, and G is some constant. The tilde (~) over Γ_i indicates that the $\tilde{\Gamma}_i$ shown in (3.59) is the actual input SNR from branch i and not the SNR estimated by the channel estimator. The input SNR is defined as

$$\tilde{\Gamma}_i = \frac{\sigma_{g_i}^2}{\sigma_{n_i}^2}. \tag{3.60}$$

When $a=0$, the SNR profile is uniform and all branches have identical average branch SNR's, i.e. $\tilde{\Gamma}_i = \tilde{\Gamma}$ for all i. When $a>0$, the average SNR in each branch decreases exponentially with increasing branch index i. For the plots in this section the abscissa represents the mean value of the SNR's from all branches as shown below[1]:

$$\tilde{\Gamma} = \frac{1}{N}\sum_{i=1}^{N}\tilde{\Gamma}_i. \tag{3.61}$$

For the general exponential profiles the value of G can be calculated using (3.59) and (3.61) as

$$G = \frac{N\tilde{\Gamma}(1-e^{-a})}{(1-e^{-aN})}, \tag{3.62}$$

For the uniform profile $\tilde{\Gamma}=G$. With this convention for the SNR, we ensure that the total received SNR, irrespective of the profile, is identical for all receivers. The values of a and the corresponding profile efficiency ratio, defined in (3.48), for a receiver using N=4 branches are shown in Table 3.1.

We first compare the performance of the DPSK, PSAM and coherent PSK (CPSK) receivers. The SEP of the CPSK receiver is used as a lower bound on the average SEP that can be achieved by the two types of MMSE receivers analysed in this chapter. In Figures 3.2-3.5 we compare the DPSK, PSAM and CPSK receivers which operate in a fast fading channel with fade rate $f_D = 0.01$ and combine 1, 2, 3 and 4 branches respectively from a total of N=4 diversity branches. The PSAM receiver uses 11 pilot symbols for channel estimation and a frame of 15

[1] Note that some authors use the total received SNR on the abscissa, i.e. $N\tilde{\Gamma}$.

Table 3.1. Profile efficiency values for the four SNR profiles used in Section 3.4.

Profile name	a	δ_p	δ_{pdB} (dB)
uniform	0	1	0
exp1	0.5	0.547	-2.62
exp2	1	0.109	-9.63
exp3	2	$8.8\text{x}10^{-4}$	-30.55

symbols. The PSAM receiver illustrates the utility of more elaborate estimators in which a sacrifice in energy efficiency and complexity improves the SEP over that of the simpler DPSK receiver. In Figures 3.2-3.5 we observe that as the number of combined branches increases, the error floor of the DPSK receiver is reduced. The maximum incremental improvement occurs when the number of combined branches is increased from 1 to 2 while the benefit of increasing the number of combined branches to 3 and 4 is gradually diminished. We also observe that, apart from the change in the error floor of the DPSK receiver, the *relative* performance of the 3 receivers remains approximately constant as we increase the number of combined branches. In Figure 3.6 we compare the same three receivers as in Figures 3.2-3.5 but in a slower fading environment with $f_D = 0.002$. We observe that the error floor of the DPSK receiver is now shifted to a much lower level due to the higher temporal correlation of the channel. Another consequence of the increased temporal correlation is the reduction in the estimation error, which can be observed in Figure 3.6 where the performance the DPSK and PSAM receivers is closer to the performance of the CPSK than in Figures 3.2-3.5.

We, now, demonstrate the utility of the profile efficiency ratio, defined in (3.48), in predicting the degradation in the SEP of the H-S/MRC receiver as the SNR profile becomes more non-uniform, i.e. as the decaying factor a becomes larger. In Figure 3.7 we use the exact SEP expression shown in (3.33) and the asymptotic SEP expression shown in (3.48) to plot the exact and asymptotic SEP respectively of a DPSK receiver employing 2/4[2] H-S/MRC. We generate

[2] In this thesis we use the notation L/N to specify the number of selected branches, L, and the total number of available branches, N, of HDR's.

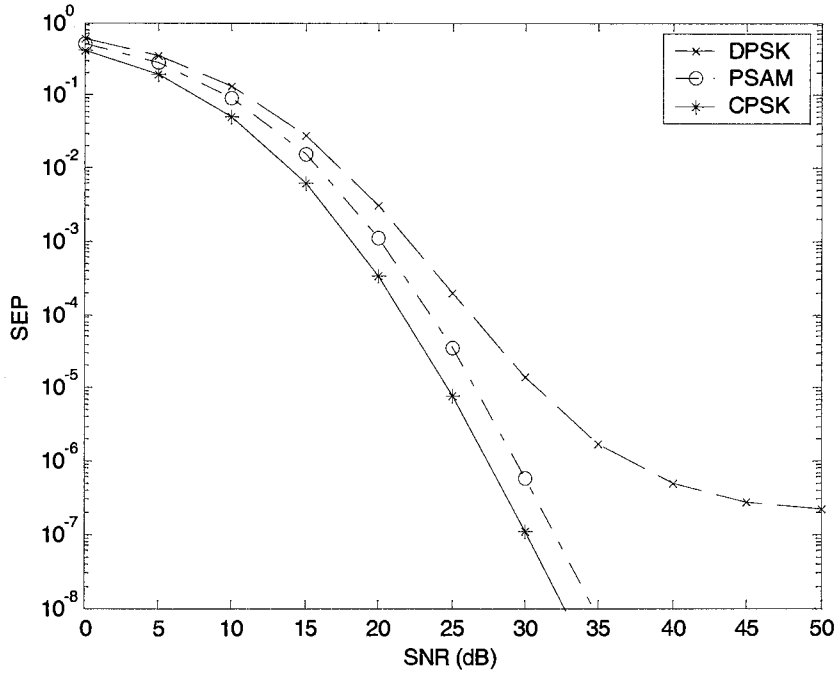

Figure 3.2: SEP of the DPSK, PSAM and CPSK receivers in a Rayleigh fading channel with normalized fade rate $f_D = 0.01$ and SNR profile exp2. The receivers combine 1 out of 4 available branches.

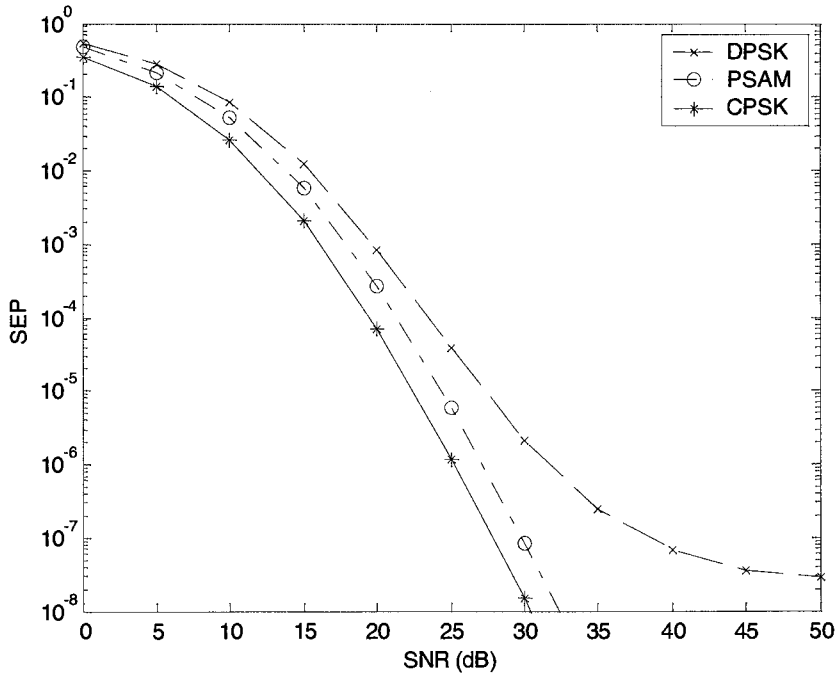

Figure 3.3: SEP of the DPSK, PSAM and CPSK receivers in a Rayleigh fading channel with normalized fade rate $f_D = 0.01$ and SNR profile exp2. The receivers combine 2 out of 4 available branches.

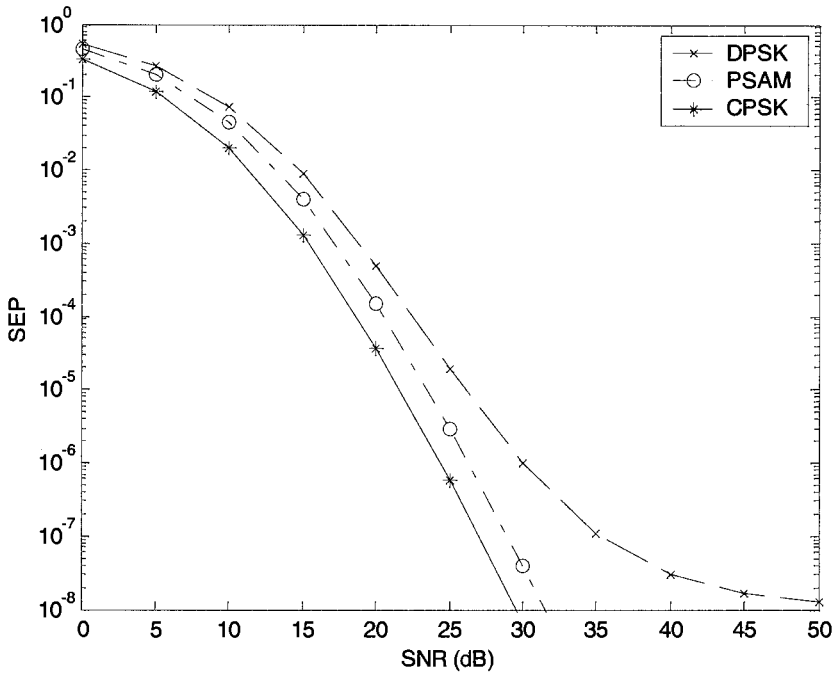

Figure 3.4: SEP of the DPSK, PSAM and CPSK receivers in a Rayleigh fading channel with normalized fade rate $f_D = 0.01$ and SNR profile exp2. The receivers combine 3 out of 4 available branches.

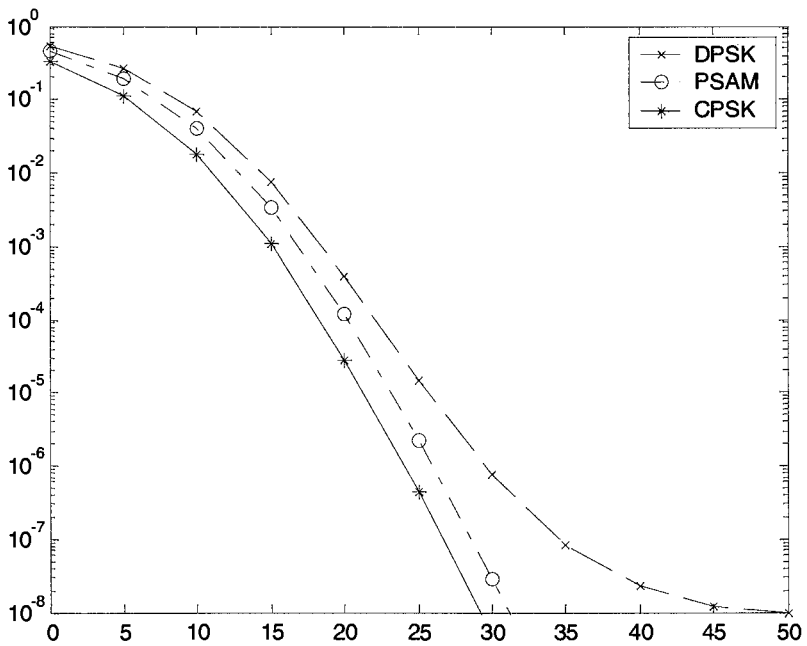

Figure 3.5: SEP of the DPSK, PSAM and CPSK receivers in a Rayleigh fading channel with normalized fade rate $f_D = 0.01$ and SNR profile exp2. The receivers combine all 4 available branches.

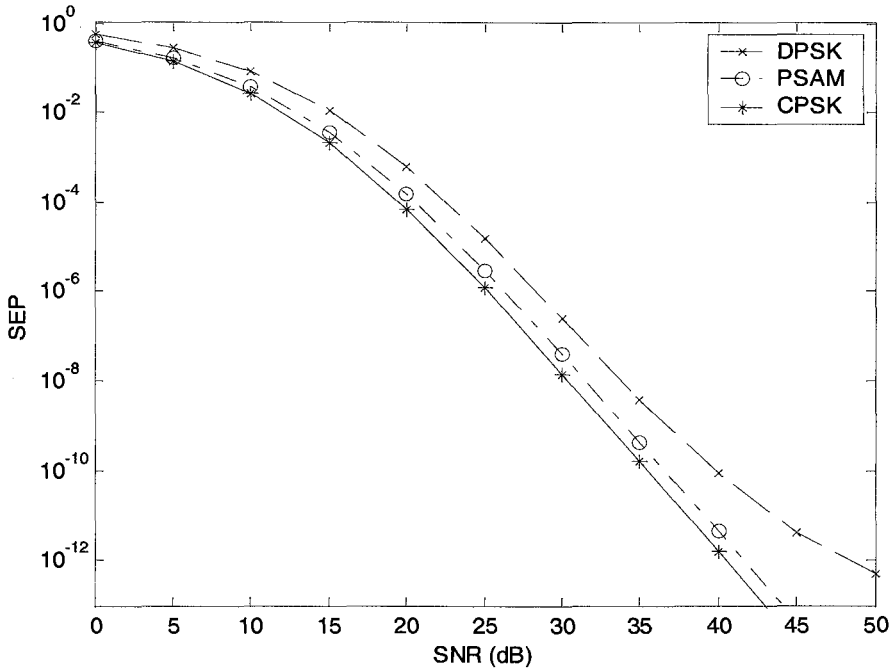

Figure 3.6: SEP of the DPSK, PSAM and CPSK receivers in a Rayleigh fading channel with normalized fade rate $f_D = 0.002$ and SNR profile exp2. The receivers combine 2 out of 4 available branches.

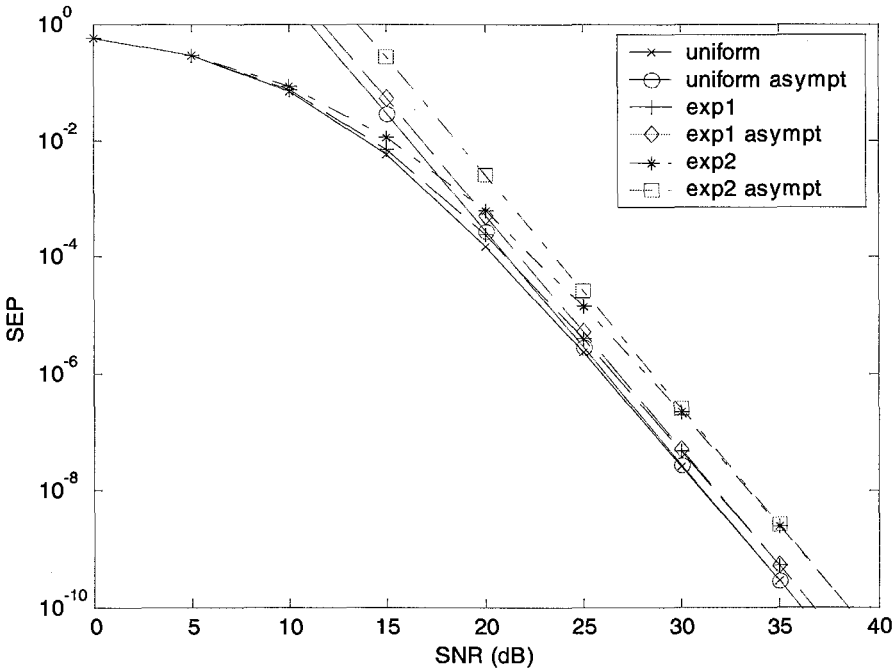

Figure 3.7: The exact and the asymptotic SEP of the DPSK H-S/MRC receiver in a static Rayleigh fading environment for three SNR profiles: uniform, exp1 and exp2. The receiver combines 2 out of 4 branches.

three such pairs of curves using the first three SNR profiles in Table 3.1 (a=0, 0.5, 1). We observe that at high SNR the SEP in the uniform profile is about 0.5 and 0.1 times smaller than in the exponential profiles exp1 and exp2 respectively as predicted by Table 3.1. The exact values calculated directly from the expression in (3.33) are: 0.55 and 0.11.

We, next, investigate two scenarios where N diversity branches could be exploited but due to practical limitations, the receivers can only combine L branches. Similar scenarios were investigated by Win and Kostic in [31] for the case of dense multipath channels. Let receiver A be the ideal H-S/MRC receiver, which is able to monitor N branches and at every symbol interval combine the L strongest branches using the optimum weights derived in (3.19). We identify receiver A as L/N H-S/MRC. Let receiver B have more limited resources so that it cannot monitor more than L branches, i.e. it combines the *same* L branches at all times. Receiver B is the classical MRC receiver with L diversity branches and we identify it as LMRC where L indicates the total number of diversity branches it uses. In Figure 3.8 we compare the performance of the two receivers operating in static Rayleigh fading channel and a uniform SNR profile with L=2 and N=4. We observe that in this profile the 2/4 H-S/MRC receiver outperforms the 2MRC receiver with a large margin even at very low SNR's. In Figures 3.9-3.10 we compare the two receivers operating in the exponential SNR profiles exp2 and exp3 with profile decay parameters a=1 and a=2 respectively. The 2MRC receiver in these two figures always combines the two branches with the largest *average* SNR's, i.e. the branches with indices i=1,2 in (3.59). In contrast, the 2/4 H-S/MRC receiver monitors all four branches and at each symbol interval selects the two branches with the largest *instantaneous* SNR in that interval. In Figure 3.10 we observe that the disparity in the performance of the two receivers is lower than in Figure 3.9 and even lower than in Figure 3.8. In fact, we observe that the two receivers in Figure 3.10 perform very similarly at low SNR's up to 15dB. To understand the difference in comparative performance of the two receivers in different SNR profiles we need to consider the selection process. The 2MRC receiver completely ignores two of the four available branches at all times whereas the 2/4 H-S/MRC receiver monitors all four of them and selects the strongest two at each symbol interval. In the exponential SNR profiles, the 2MRC receiver ignores the two branches with the lowest average SNR. Since the probability that any of these two branches has instantaneous SNR in the top two is very low, especially for large a's, ignoring them does not penalize considerably the 2MRC receiver. On the other hand, in the uniform SNR profile the 2MRC receiver ignores two branches, which have average SNR which are identical to the SNR of the two branches it combines. In this case the probability that any of the two ignored branches have instantaneous SNR in the top two

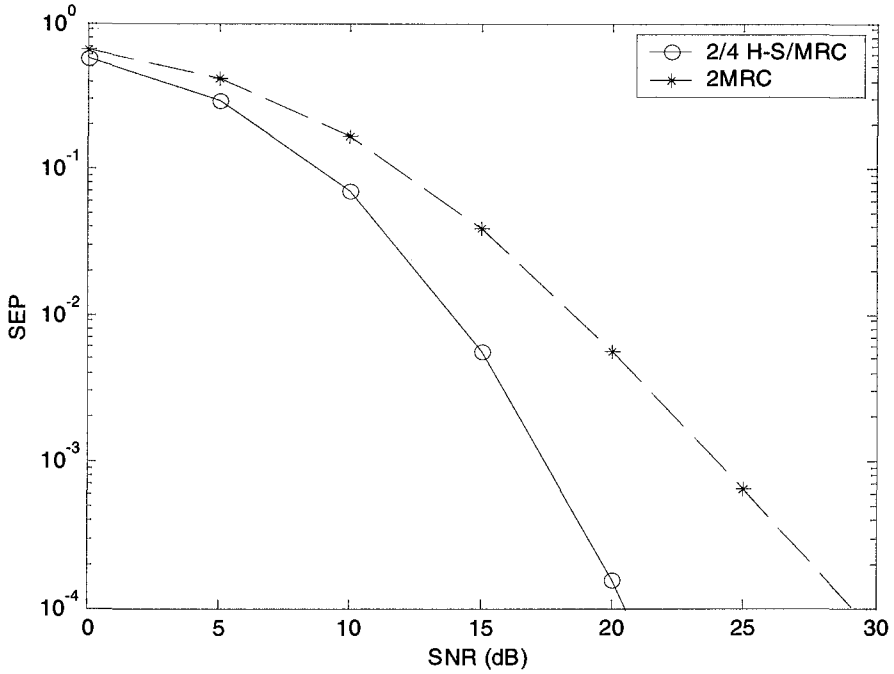

Figure 3.8: SEP of the 2/4 H-S/MRC and 2MRC receivers using DPSK in a static Rayleigh fading channel with uniform SNR profile.

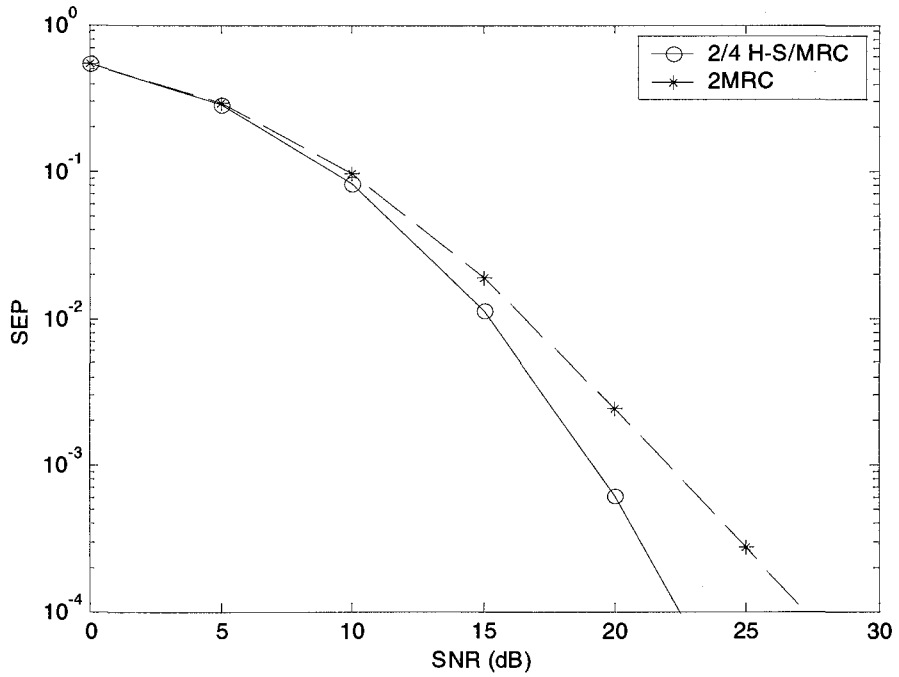

Figure 3.9: SEP of the 2/4 H-S/MRC and 2MRC receivers using DPSK in a static Rayleigh fading channel with exp2 SNR profile.

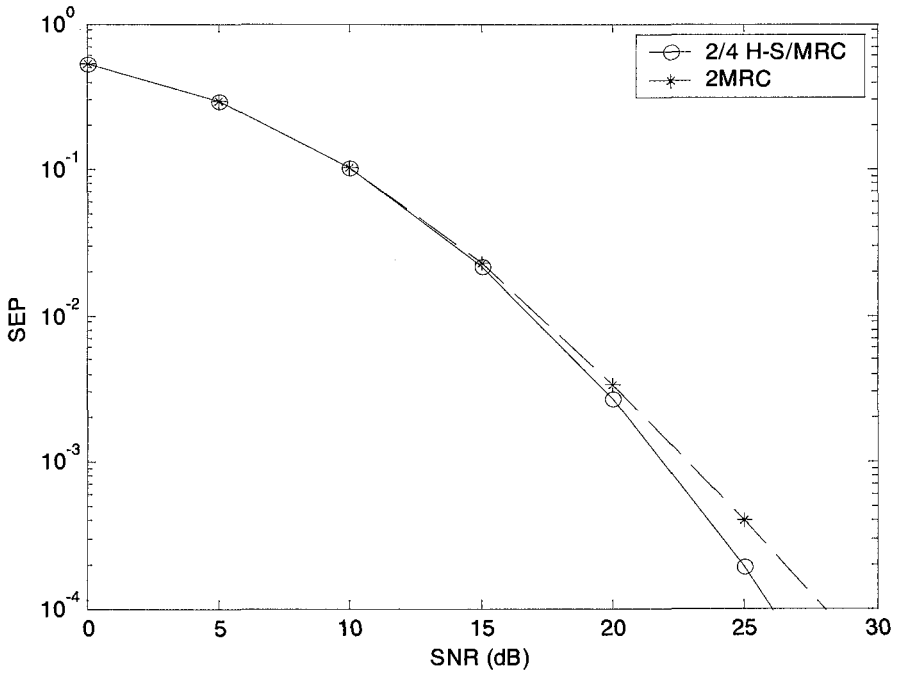

Figure 3.10: SEP of the 2/4 H-S/MRC and 2MRC receivers using DPSK in a static Rayleigh fading channel with exp3 SNR profile.

is much higher and the 2MRC is penalized by a more dramatic drop in performance compared to the 2/4 H-S/MRC receiver. We can, therefore, conclude that use of a H-S/MRC receiver over the classical MRC receiver described in this paragraph would make more sense in channels with uniform SNR profile or low profile decays. In highly unbalanced SNR profiles the simpler 2MRC receiver would provide a better performance-complexity balance.

In Figure 3.11 we demonstrate the effect of different normalized fade rates on the SEP of a 1/4 H-S/MRC (SC) receiver using DPSK and operating in a uniform SNR profile. We observe that as the fade rate increases, the SEP deteriorates and the unavoidable error floor for DPSK moves to a higher SEP and occurs at lower SNR's. To explain this phenomenon we need to examine the effect of the fade rate on the variance of the estimation error and on the correlation between the fading gain and the observation. We may obtain a more convenient visual correspondence of the SEP with the normalized correlation w_i using the following transformation:

$$\bar{\rho}_{g_i h_i} = 1 - \frac{\sigma_{g_i h_i}}{\sigma_{h_i}^2} = 1 - w_i . \tag{3.63}$$

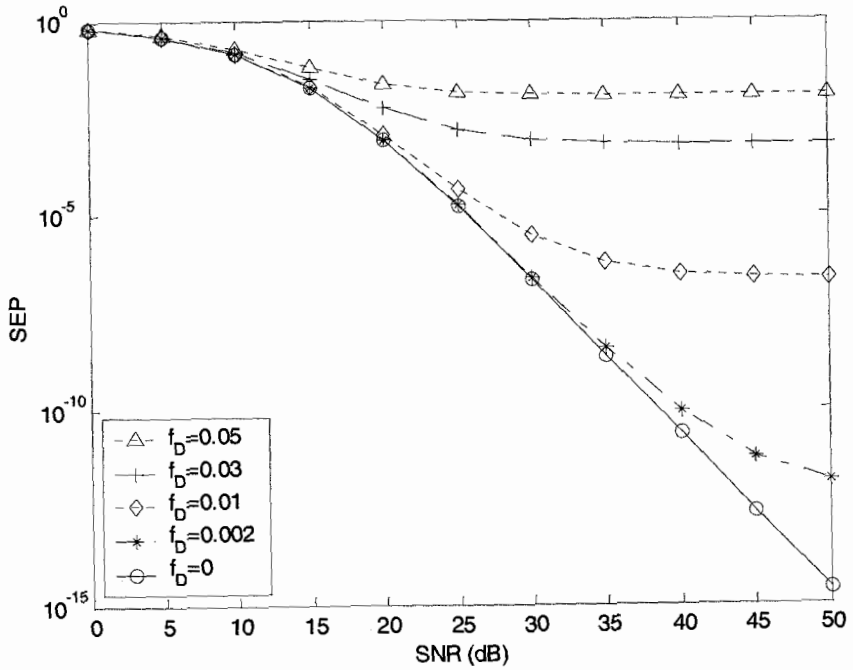

Figure 3.11: SEP of the 1/4 H-S/MRC receiver using DPSK in a Rayleigh fading environment for various fade rates. The receiver operates in uniform profile.

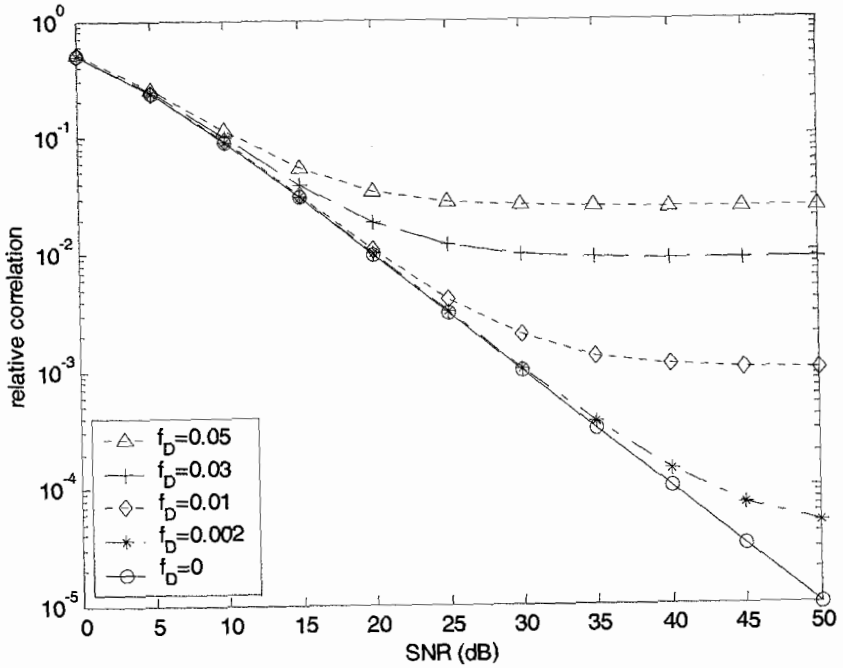

Figure 3.12: The variable $\overline{\rho}_{g_i h_i}$ as a function of SNR for the 1/4 H-S/MRC receiver in Figure 3.11.

In (3.63) we normalize and transform the correlation function $\sigma_{g_i h_i}$ to better illustrate the effect of higher received SNR on the correlation. The variable $\bar{\rho}_{g_i h_i}$ would approach zero at high SNR if the two variables were completely correlated. In Figure 3.12 we plot $\bar{\rho}_{g_i h_i}$ versus the SNR for the fade rates used in Figure 3.11. We observe in Figure 3.12 that $\bar{\rho}_{g_i h_i}$ reaches a floor, which depends on the fade rate. This floor has a relation to the SEP error floor we observed in Figure 3.11. To complete the observations, we plot in Figure 3.13 the normalized variance of the MMSE estimation error in the DPSK receiver, defined as

$$\frac{\sigma_e^2}{\sigma_g^2} = 1 - \frac{\sigma_{\hat{g}}^2}{\sigma_g^2}. \tag{3.64}$$

In (3.64) the error variance is normalized with the power of the signal power $\sigma_{g_i}^2$ for clearer comparison. We observe that the estimation error follows the same pattern as the SEP of the receiver, which demonstrates that the estimation cannot be improved indefinitely for non-zero fade rates.

In Figure 3.14 we plot the SEP of a 2/4 DPSK H-S/MRC receiver. We observe that there is some improvement over the SEP in Figure 3.11 but the additional branch does not improve the SEP dramatically. We also plot in Figure 3.15 the SEP of the 2/4 H-S/MRC receiver operating in the exponential SNR profile exp2 with a=1. It appears that while the performance of the receiver in the uniform profile is slightly better in the region above the error floor, the two profiles produce identical error floors. Finally, in Figure 3.16 we plot the SEP of the 2/4 H-S/MRC receiver using PSAM. In this figure we observe that at high fade rates the error floor is higher than for the equivalent DPSK receiver whereas at low fade rates the error floor is not present in the SNR region 0-50dB. This can be explained by considering the spacing of the pilot symbols with respect to the symbol of interest. Some of the pilot symbols are separated from the estimated symbols by long time intervals indicating that it is possible that a larger number of pilot symbols can be detrimental to the fading gain estimation. As we have seen in Figures 3.2-3.6, PSAM has the potential to provide better error performance than DPSK but in Figure 3.14 and Figure 3.16 we observe that in cases of fast fading the opposite may occur.

We next demonstrate the effect of the number of selected branches, L, on the combined output SNR and the SEP of a H-S/MRC receiver with a fixed total number of branches N=4. The plots of the *normalized* combined SNR of a DPSK H-S/MRC receiver operating in the uniform and the exponential profiles with a=0.5, a=1 and a=2 from Table 3.1 are shown in Figure 3.17.

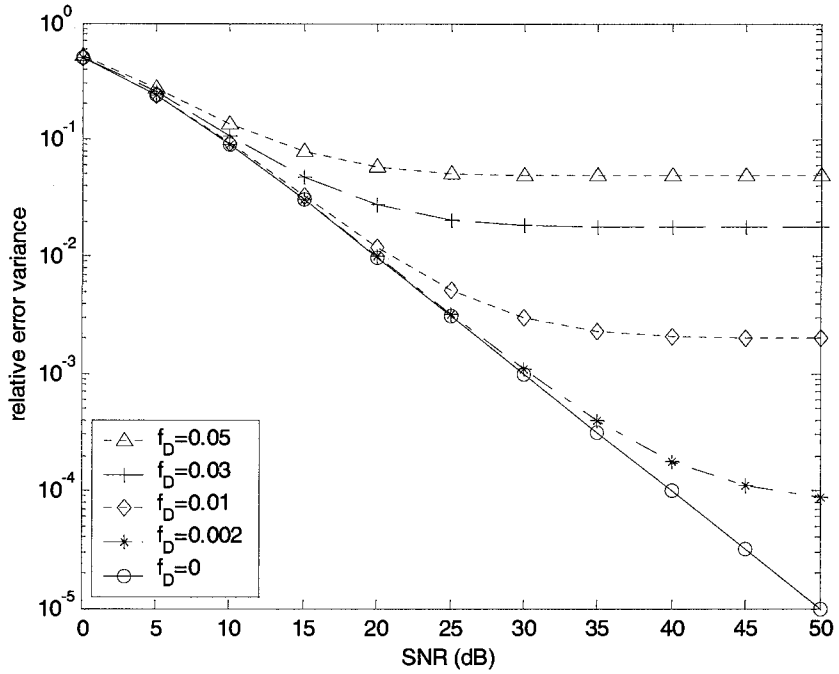

Figure 3.13: Normalized estimation error as a function of SNR for the 1/4 H-S/MRC receiver in Figure 3.11.

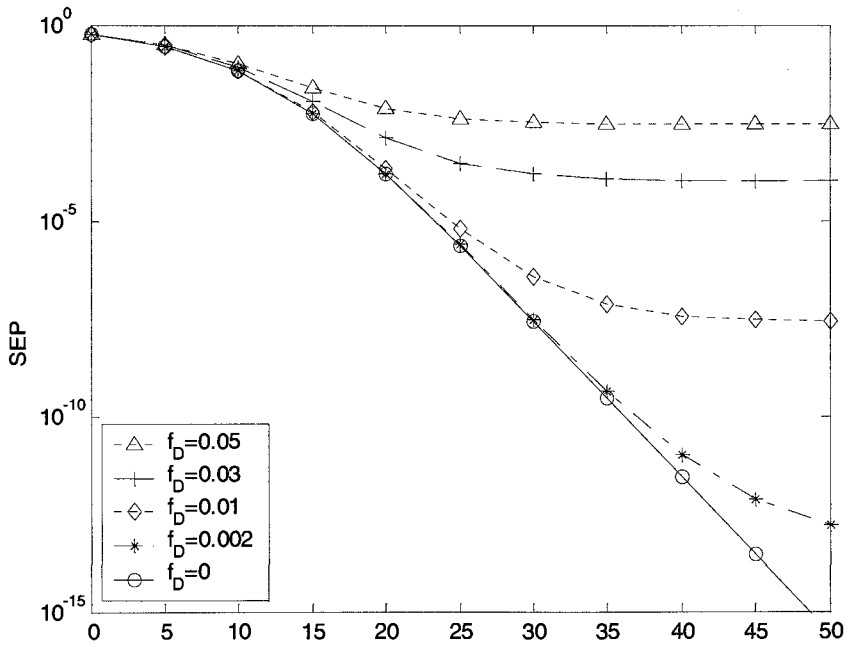

Figure 3.14: SEP of the 2/4 H-S/MRC receiver using DPSK in a Rayleigh fading environment for various fade rates. The receiver operates in uniform profile.

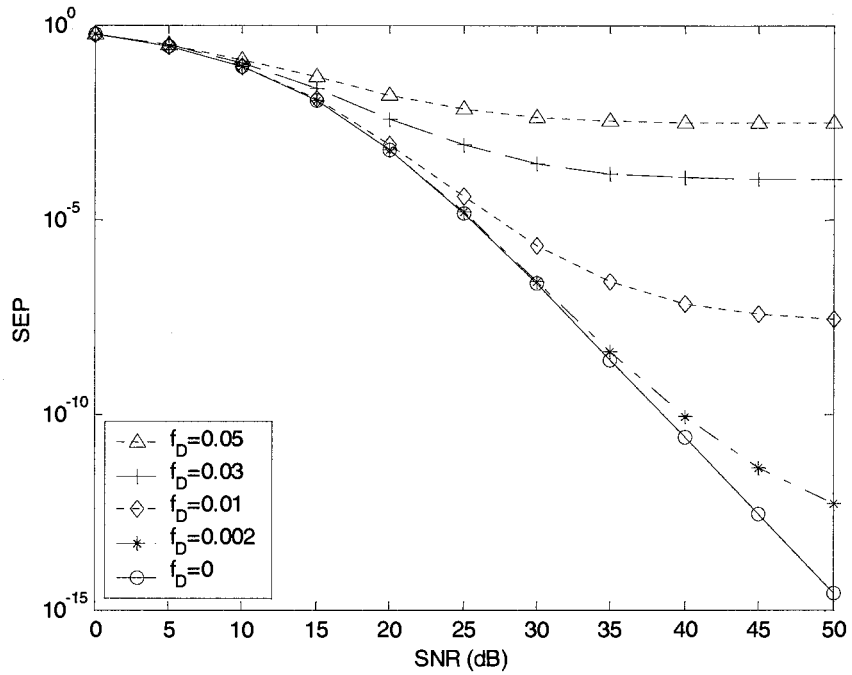

Figure 3.15: SEP of the 1/4 H-S/MRC receiver using DPSK in a Rayleigh fading environment for various fade rates. The receiver operates in the exp2 SNR profile.

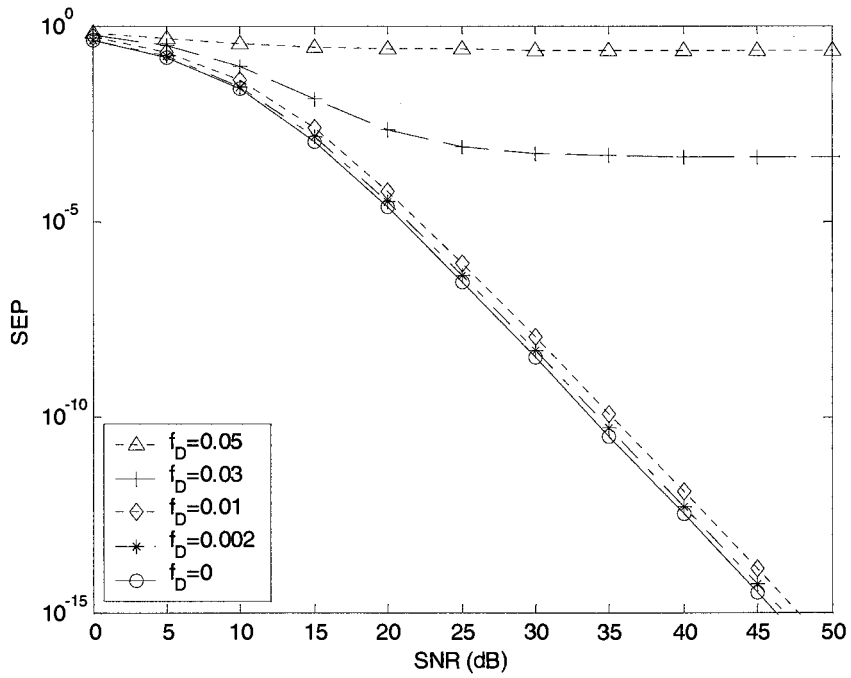

Figure 3.16: SEP of the 2/4 H-S/MRC receiver using PSAM in a Rayleigh fading

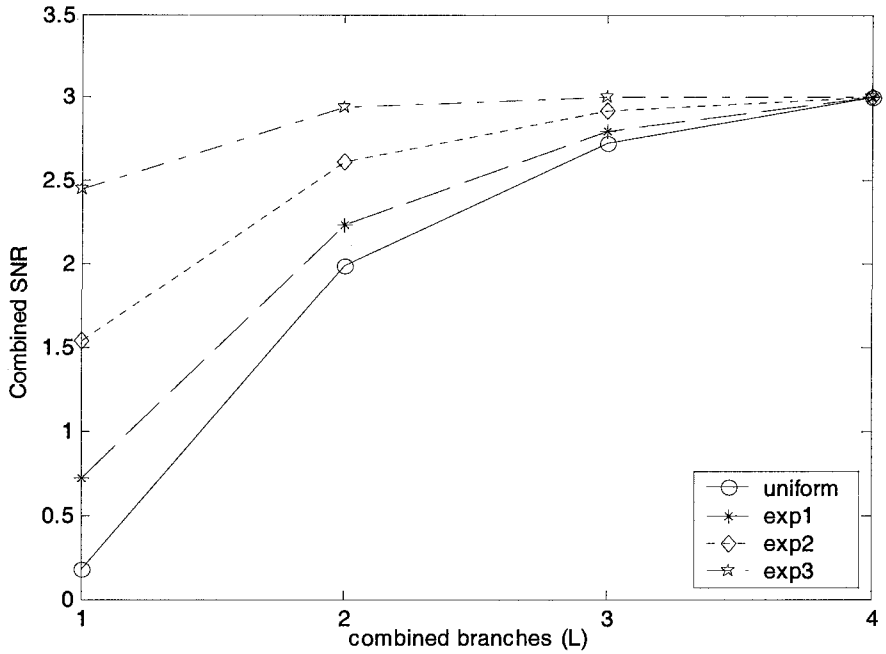

Figure 3.17: Normalized combined SNR of $L/4$ H-S/MRC receivers using DPSK in a Rayleigh static fading environment for various SNR profiles. The normalized SNR is taken at input mean SNR=30dB.

The normalized SNR is defined as the ratio of the combined output SNR over the mean of the actual branch SNR's, $\tilde{\Gamma}$, defined in (3.61). The SNR is obtained for average input SNR $\tilde{\Gamma} = 30\text{dB}$. Hence the values on the ordinate in Figure 3.17 are given by

$$\text{normalised output SNR} = 10\log\Gamma_h - 30. \tag{3.65}$$

We observe that as the SNR profile decay parameter a decreases, i.e. as the SNR profile becomes more uniform, the average combined SNR is reduced. The exception is when $L=N$, i.e. when the H-S/MRC receiver is reduced to the classical MRC receiver. Because of the convention we use to calculate the average SNR in this section, shown in (3.61), the average SNR of the MRC receiver given by (3.58) is identical for all SNR profiles. This is not true for the H-S/MRC receiver with $L<N$, however, because by selecting the branches with the maximum instantaneous SNR the H-S/MRC receiver takes advantage of the fact that some of the branches in the exponential profile have higher average SNR. Another observation from Figure 3.17, is the monotonically decreasing slope of the SNR curves for all the profiles, indicating the reduced benefit we obtain by selecting more branches.

In Figure 3.18 we plot the SEP curves corresponding to the profiles used in Figure 3.17. It is surprising at first to notice that the receivers providing higher output SNR do not provide the better error performance. We observe in Figure 3.18 that the receiver operating in the uniform SNR profile outperforms the receivers operating in the non-uniform SNR profiles in spite of providing the lowest output SNR. To explain this occurrence it is instructive to consider a receiver without diversity, i.e. a receiver with one branch, having average input SNR equal to $4\tilde{\Gamma}$. This SNR is equal to the sum of the average input SNR's from all four diversity branches. The single branch receiver would, thus, provide output SNR equal to 4Γ, which is equal to the SNR provided by the MRC receiver as shown in Figure 3.17. Of course, the SEP of this single branch receiver is not expected to be lower than the SEP of any diversity receiver and in fact it is calculated as 1.68×10^{-3}, well above the SEP of the receivers shown in Figure 3.18. We could, therefore, conclude that output SNR comparisons of receivers must be done carefully as higher output SNR does not necessarily translate to lower SEP.

Finally, in Figure 3.19 and Figure 3.20 we demonstrate the effect of the parameter t on the tightness of the lower computational complexity SEP bounds derived in (3.40) and (3.41). In Figure 3.19 the exact SEP curve and the bounds for t=0 and t=2 are plotted for a CPSK H-S/MRC receiver with N=4 and L=1 operating in a channel with the exp1 SNR profile. We chose CPSK to avoid any additional effects due to the channel estimation. In Figure 3.20 the corresponding curves are plotted for a channel with exponential profile exp2 and decay parameter a=1. We observe that as the parameter t approaches N-1 the tightness of the bounds improves.

3.5 Conclusions

In this chapter we derived various performance measures for the H-S/MRC receiver which uses MMSE channel estimation for selection and combining of L out of N diversity branches. The final expressions are in a concise, closed-form expression which helps in understanding the factors affecting the performance of the H-S/MRC receiver.

In Section 3.2, the exact expression for the SEP of the H-S/MRC receiver was derived. Due to the consideration of non-uniform SNR profiles the exact expression has a factor of $N!$ increase in complexity over the expression for the uniform SNR profile. The complexity issue could be significant in dense multipath channels with high numbers of diversity branches and is addressed in Section 3.2.1 with the derivation of lower computational complexity bounds. The upper and lower bounds reduce the computational complexity by a factor of $(N-t)!$ over the

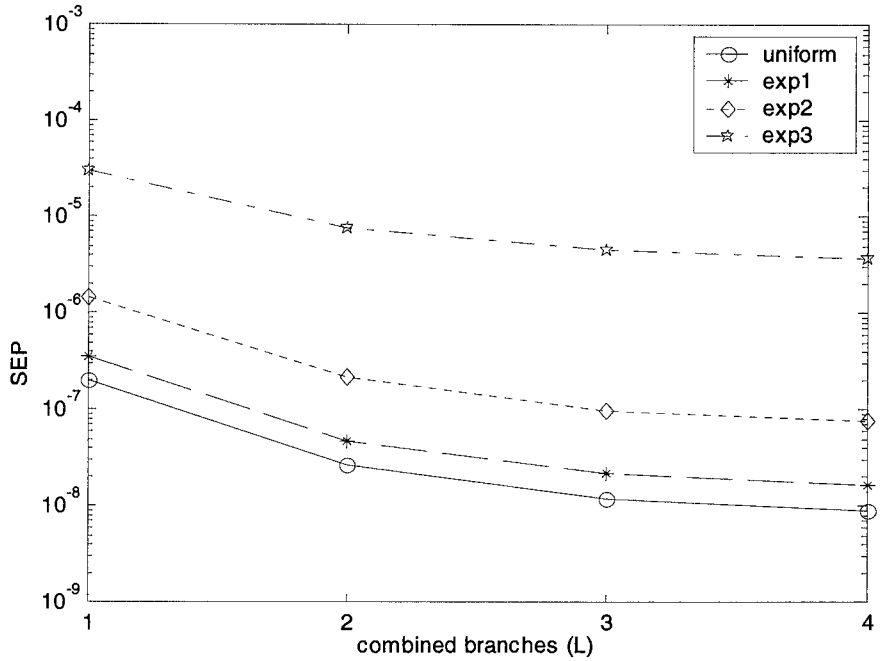

Figure 3.18: SEP of $L/4$ H-S/MRC receivers using DPSK in a Rayleigh static fading environment for various SNR profiles. The SEP is taken at input mean SNR=30dB.

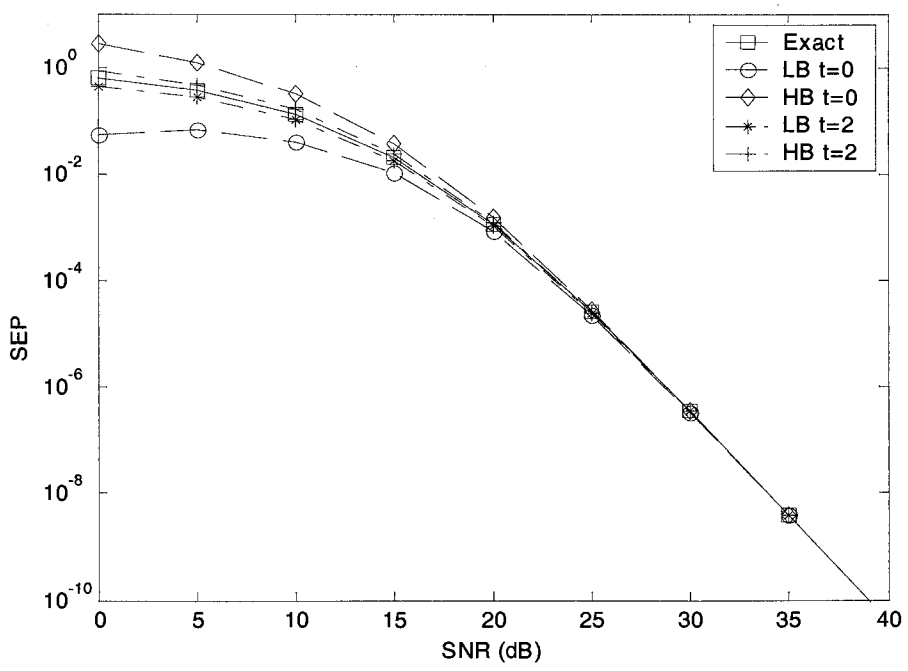

Figure 3.19: SEP of SC CPSK receiver with N=4 diversity branches in profile exp1 with lower and upper bounds calculated for t=0 and t=2.

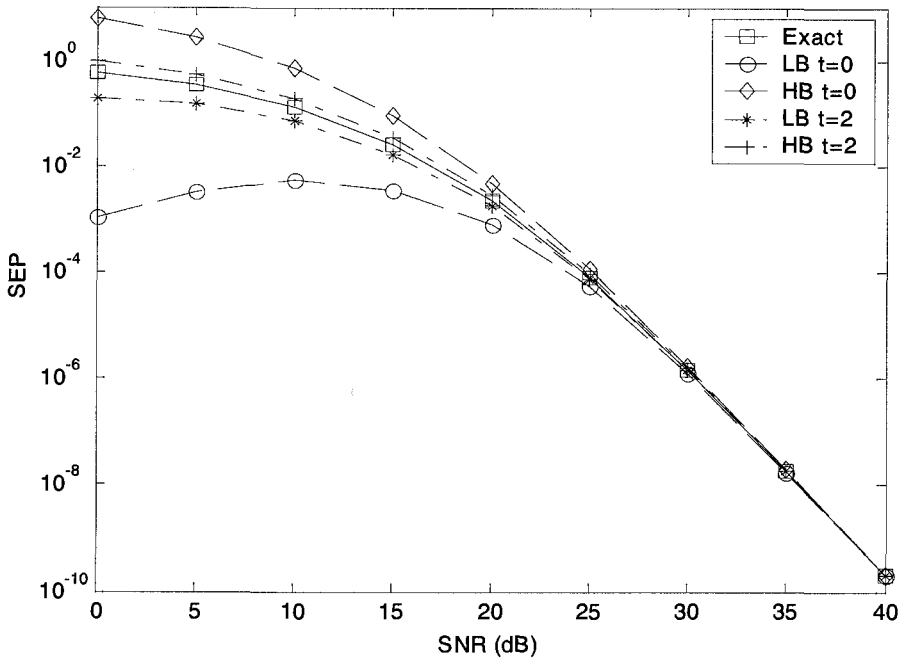

Figure 3.20: SEP of SC CPSK receiver with N=4 diversity branches in profile exp2 with lower and upper bounds calculated for t=0 and t=2.

complexity of the exact expression. In other words the computational complexity of the bounds is $N!/(N-t)!$ higher than the complexity of the uniform SNR profile expression. The value of t can vary from 0, which produces the most crude but least complex approximation, to N-1, which produces the exact value but with $N!$ increase in complexity.

Asymptotic analysis of the SEP at high SNR values was performed in Section 3.2.2 to obtain better understanding of the effect of the SNR profile on the SEP of the H-S/MRC receiver. The asymptotic expression is concise and leads to two conclusions:

a) The asymptotic SEP is inversely proportional to the N th power of the geometric mean of the average branch SNR's. As long as the SNR profile remains the same, the rate of decrease of the SEP with increasing SNR is constant on a logarithmic scale and this rate of decrease is identical for all values of L.

b) The asymptotic SEP is proportional to the function $N!/(L!L^{N-L})$. This function is responsible for the diminishing returns of successively increasing L.

In Section 3.3, we derived a concise expression for the average combined SNR of the H-S/MRC receiver. This expression is a generalization of the expression derived previously by Kong et al in [15] and by Win and Winters in [23] for the coherent H-S/MRC receiver.

The benefit of the H-S/MRC receivers over classical MRC receivers as, for example, in cases where the number of available diversity branches is larger than the capabilities of the receiver was demonstrated in Section 3.4. The L/N H-S/MRC receiver was shown to outperform the classical MRC receiver, which always combines the same L branches but its advantage is reduced in highly unbalanced SNR profiles. In Section 3.4 we showed the effect of the fade rate on the error floor of DPSK and PSAM and identified a possible source of erroneous conclusions when comparing receivers operating in different SNR profiles. A receiver providing higher average output SNR does not necessarily provide lower SEP.

Chapter 4

Selection and Double Selection/Combining Receivers without Channel Statistical Information

In Chapter 3 we analysed the performance of the H-S/MRC receiver operating in a Rayleigh fading channel with the assumption that the channel statistical information (CSI) was available. The CSI was used to design a MMSE channel gain estimator for optimal selection and diversity combining using optimum MRC weights. Absence of CSI on the one hand complicates the detection process, as the optimum MMSE channel estimation cannot be used. The channel uncertainty, manifesting itself as random phase rotation and scaling factor, is especially harmful for PSK because the information for this modulation is carried in the phase of each symbol which the random phase rotation makes harder to detect. On the other hand, absence of CSI forces the use of simpler receivers, such as receivers using plain DPSK, which do not have the channel estimation overhead, but as a consequence their performance is inferior. In addition to combining and detection issues, absence of CSI complicates branch selection in diversity receivers since the optimum criterion of largest instantaneous SNR cannot be used. In many practical receivers the selection is instead based on the signal-plus-noise (SPN) criterion. For example, Neasmith and Beaulieu in [9] provided bit error probability analysis for a SC receiver using binary NFSK and DPSK modulations and employing the SPN criterion.

The performance of receivers which do not use CSI is in general more difficult to analyse than the performance of receivers which use CSI such as the H-S/MRC receiver analysed in Chapter 31. Many of the simplifications used in Chapter 3 arising from the optimum MRC combining can no longer be applied. Consequently, it is very difficult to obtain simple and insightful yet general expressions for this type of hybrid diversity receiver (HDR) except for certain special cases. In the past Brennan [7] used the pdf of the sum of Rayleigh variables to obtain a solution for the EGC receiver and most of the later researchers followed along the same path. In this chapter we use an alternative method to analyse two special cases of HDR's which do not use CSI and are operating in a Rayleigh fading channel with Doppler spread: A receiver which selects a single branch and a receiver which selects and combines the two strongest of the

N available diversity branches, a hybrid of SC and EGC. The former is the classical SC receiver and the latter we call the double selection equal gain combining (2S/EGC) receiver.[1]

Since CSI is not available to the receivers analysed in this chapter, branch selection is based on the received SPN and is, therefore, different from the method used in Chapter 3. The reader may recall that for the H-S/MRC receiver the branch selection was based on the estimated instantaneous branch SNR. Instead, the selection criterion used in this chapter is similar to that considered by Neasmith and Beaulieu in [9] where the authors used the SPN selection criterion in a 2DPSK SC receiver but made the assumption that the channel was invariant over a two-bit interval. This assumption would hold in a static fading channel, i.e. a channel without a Doppler spread, but not in a fast fading channel. Since, in this chapter the received SPN is the selection criterion, which means that a non-optimal, in the MMSE sense, noisy channel estimate is used for the selection, it is not immediately obvious what the best possible selection strategy is. Does selection based on the current received symbol magnitude provide better performance than selection based on the previous symbol magnitude? We prove in Appendix A that the use of the previous instead of the current symbol magnitude for branch selection does indeed provide better performance. While initially this result seems counter-intuitive, when we consider that with DPSK the previous received symbol is used as an estimate of the current value of the fading gain, it is not as surprising. The analysis indicates that selecting the branch with the largest estimated channel gain is more important than selecting the branch with the largest current SPN.

In this chapter we provide exact symbol error probability (SEP) expressions for the SC and 2S/EGC receivers and derive descriptive asymptotic SEP approximations. The asymptotic expressions are derived directly from the final exact SEP expressions. As we show in Chapter 5, it is also possible to obtain *asymptotic* SEP expressions for the general case of a receiver combining an arbitrary number of branches, by applying high SNR approximations in the beginning and throughout the derivation. One of the outcomes of this chapter is the effect of the signal power profile (SPP) and the noise power profile (NPP) on the SEP of the SC and 2S/EGC receivers in contrast to the effect of these profiles on the H-S/MRC receivers from Chapter 3.

Although variations of the SC receiver have been investigated by other authors the specific receiver analysed in this chapter appears to have been missed. The main characteristics of this SC receiver are:

---

[1] Part of the analysis for the SC receiver appeared in [12] and for the 2S/EGC receiver appeared in [13].

1. Modulation is plain DPSK and the receiver uses the raw previous symbol as the channel estimate.
2. The channel is not assumed to be constant over a 2 symbol period and has an autocorrelation function dependent upon the fading rate.
3. Both the average signal power profile (SPP) and the noise power profile (NPP) can be independently non-uniform (unbalanced)
4. We use asymptotic expressions to provide quantitative explanation for the effect of the SPP and NPP on the SEP.

To the best of our knowledge, the double selection equal gain combining (2S/EGC) receiver has not been previously investigated. We provide an exact expression for the SEP of this receiver as well as perform asymptotic analysis to quantify the effect of the non-uniform SPP and NPP on its performance. We contrast the performance of the two receivers analysed in this chapter with the performance of the equivalent SC and double selection maximal ratio combining (2S/MRC) receivers, which are two special cases of the H-S/MRC receiver analysed in Chapter 3. The notation 2S/MRC is chosen to correspond to the notation for the 2S/EGC receiver and refers to a H-S/MRC receiver which selects and combines L=2 branches.

4.1 Selection Combining Receiver

The SC receiver is considered the simplest of the three classical diversity receivers, SC, EGC, MRC, because there is no combining involved [8]. The conceptual receiver model, shown in Figure 4.1, is derived from the diagram of the H-S/MRC receiver shown in Figure 3.1. In contrast to the receiver in Figure 3.1, however, the channel estimators of this receiver do not attempt to produce the optimal MMSE channel estimates.[2] The channel estimate is now the *raw* previous received symbol and the channel estimators are, therefore, nothing more than delay elements. For this SC receiver the penalty in performance when compared to the SC receiver in Chapter 3 is expected to arise from the inability of the sorter in Figure 4.1 to select the branch with the largest instantaneous SNR. This SC receiver at each symbol interval selects the branch with the largest SPN magnitude.

[2] As noted in Section 2.5.2, the optimal estimates are important in channels with non-uniform SNR profiles because they use the statistical information to more optimally compare each branch.

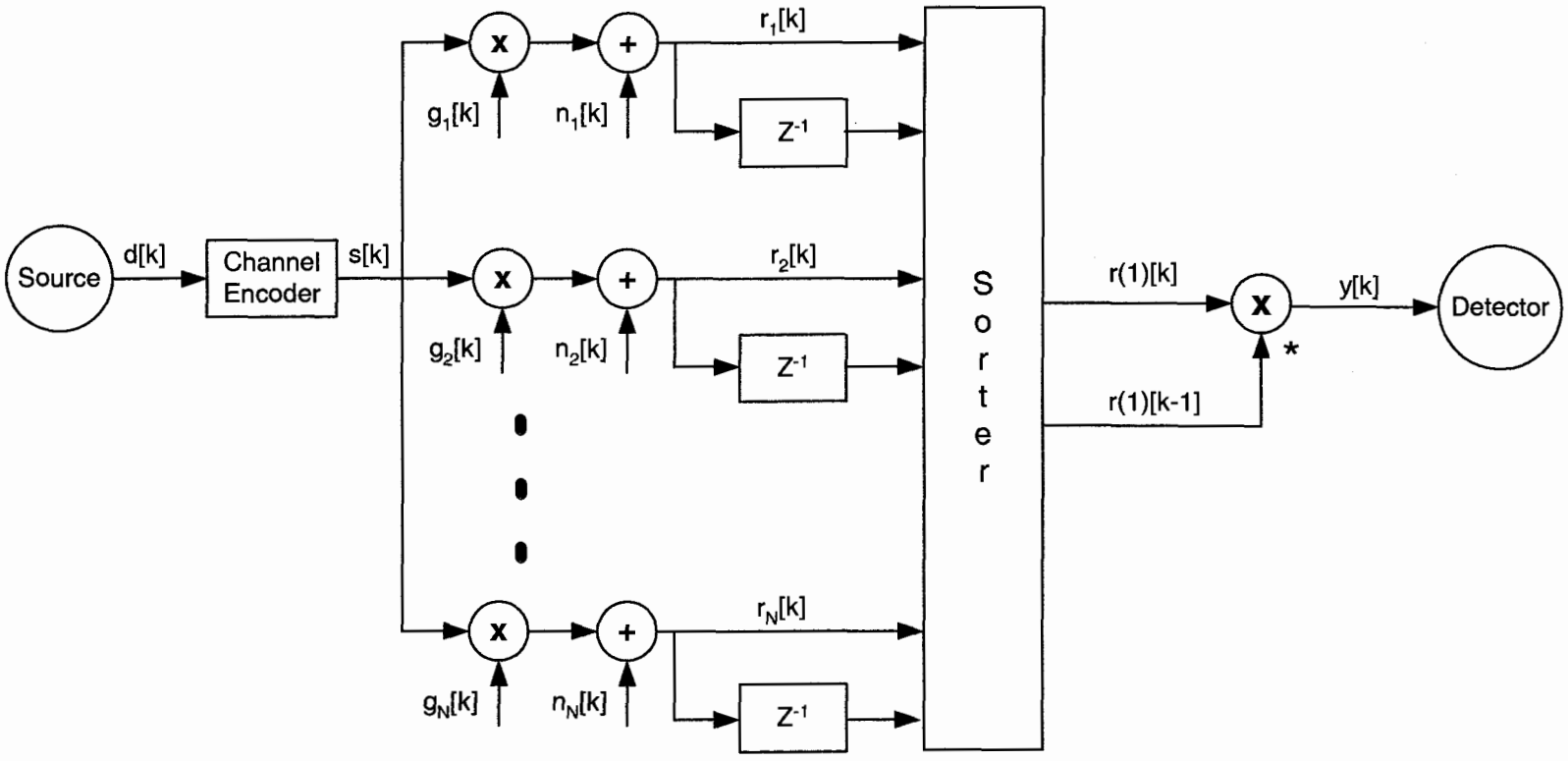

Figure 4.1: System model of the SC diversity receiver with no CSI.

4.1.1 System Description

The signal arriving in the i-th branch of the receiver at time k was shown in (3.1) to be expressed in terms of the fading gain and the AWGN as

$$r_i = g_i + n_i, \tag{4.1}$$

where the time index k was omitted. As already mentioned, for the SC receiver in this section the previous received symbol is used as a crude fading gain estimate. If we use the terminology of Chapter 2, we are now using the observation variable h_i as the fading gain estimate. The observation variable was defined in (2.48) as

$$h_i[k] = r_i[k-1]. \tag{4.2}$$

You may contrast this estimate with the optimum MMSE estimate provided by the H-S/MRC receiver for branch i, shown in (3.8) and repeated below:

$$\hat{g}_i = w_i^* h_i, \tag{4.3}$$

where the variable w_i was defined in (2.17) as

$$w_i = \frac{\sigma_{g_i h_i}}{\sigma_{h_i}^2}. \tag{4.4}$$

The H-S/MRC receiver was able to calculate the optimum channel estimate because it had knowledge of the CSI. Since the SC receiver in this section does not have access to the CSI, it in effect sets w_i to unity for all branches at the cost of reduced accuracy in the selection process, especially at low SNR.[3]

At each symbol interval, the SC receiver selects the branch with the largest estimated signal magnitude. As explained in the previous paragraph the selection is based on the magnitude of the observation variable, that is the metric $|h_i|$, $1 \le i \le N$. Upon selection of the signal with the maximum $|h_i|$, say the signal from branch j, the decision variable at the detector can be written as

$$y = r_j h_j^*. \tag{4.5}$$

From (3.3) we know that the fading gain can be expressed in terms of its MMSE estimate as

$$g_i = \hat{g}_i + e_i, \tag{4.6}$$

---

[3] In the case of the 2S/EGC receiver this inability to calculate w_i also causes reduced accuracy in the combining process.

where, according to the analysis in Section 2.2, e_i represents the MMSE estimation error and it is a zero mean, Gaussian random variable, independent of the estimate $\hat{g}_i$. Observing that the MMSE estimate is related to h_i by the expression in (4.3), it is straightforward to express the actual fading gain as

$$g_i = w_i^* h_i + e_i . \tag{4.7}$$

Note that e_i in this case is also independent of h_i since w_i is just a constant. Finally, the received symbol can be expressed in terms of h_i as

$$r_i = w_i^* h_i + v_i , \tag{4.8}$$

where v_i is the effective noise defined in (2.31) and reproduced below:

$$v_i = e_i + n_i . \tag{4.9}$$

The variance of v_i is denoted by $\mathcal{N}_i$ and was shown in (2.32) to be

$$\mathcal{N}_i \equiv \sigma_{v_i}^2 = \sigma_{e_i}^2 + \sigma_{n_i}^2 . \tag{4.10}$$

Note the presence of w_i in (4.8) as opposed to the equivalent expression for the H-S/MRC receiver in (3.4).

Using (4.8), the decision variable in (4.5) can be written in terms of the observation h_i and the effective noise as

$$y = w_j^* |h_j|^2 + h_j^* v_j . \tag{4.11}$$

The first term on the right hand side is the estimated signal component and the second term is noise. Consequently, the estimated instantaneous SNR at the detector is given by

$$\gamma_s = \frac{\frac{1}{2}\left| w_j^* |h_j|^2 \right|^2}{\frac{1}{2} E\left[\left| h_j^* v_j \right|^2 \right]} = \frac{1}{2} \frac{|w_j|^2}{\mathcal{N}_j} |h_j|^2 . \tag{4.12}$$

It should be stressed at this point that even though the j-th branch may have the largest SPN magnitude, it is not necessarily the branch providing the largest SNR, since γ_s in (4.12) depends not only on $|h_j|$, but also on the branch's effective noise power $\mathcal{N}_j$ and on the channel statistics included in the definition of w_i. In contrast, in a receiver with CSI knowledge as in the case of the H-S/MRC receiver in Chapter 3, all the w_i's and $\mathcal{N}_i$'s are known and, hence, the receiver can normally select the branch with the largest instantaneous branch SNR. We observe that the expression for the instantaneous SNR in (4.12) is the same as the expression (3.20) for the

corresponding SC receiver in Chapter 3. We, therefore, expect that the only factor causing a disparity in the performance of the receiver analysed in this chapter and the special case of the H-S/MRC receiver in Chapter 3 with L=1 will be the selection process.

4.1.2 Symbol Error Probability Analysis

Before deriving the exact SEP expression of this SC receiver we introduce the following random variables:

$$\lambda_i = \frac{1}{2}|h_i|^2. \tag{4.13}$$

The new random variables represent the instantaneous power of the h_i's and are statistically independent and exponentially distributed with pdf given by

$$f_{\lambda_i}(x) = \frac{1}{\Lambda_i} e^{-\frac{x}{\Lambda_i}}, \tag{4.14}$$

where Λ_i represents the average power of h_i and is defined as

$$\Lambda_i = E[\lambda_i] = \frac{1}{2}E[|h_i|^2]. \tag{4.15}$$

Alternatively, Λ_i is the average power of r_i, the received signal plus noise.

By arranging the λ_i's in descending order a new set of random variables $\lambda_{(1)}, \lambda_{(2)}, \ldots, \lambda_{(N)}$ is obtained, where $\lambda_{(1)} > \lambda_{(2)} > \cdots > \lambda_{(N)}$. These ordered random variables, as explained in Section 2.6, are no longer independent and their joint pdf is given by

$$f(\lambda_{(1)}, \lambda_{(2)}, \cdots, \lambda_{(N)}) = \sum_{\mathbf{P}_k} \left(\prod_{i=1}^{N} f_{\lambda_{k_i}}(\lambda_{(i)}) \right), \tag{4.16}$$

where $\mathbf{P}_k$ is the k-th permutation of the branch indices (1,2,...,N). Using the new notation, the detector's SNR defined in (4.12) can be expressed as

$$\gamma_s = \frac{|w_j|^2}{\mathcal{N}_j} \lambda_{(1)}, \tag{4.17}$$

where the largest estimated power, $\lambda_{(1)}$, is assumed to have arrived from the j-th branch and both of the statistics w_j and $\mathcal{N}_j$ are associated with this selected branch.

As explained in Section 3.2, we may use the expression found in [38] to calculate the SEP conditioned on γ_s as

$$P_{e|\gamma_s} = \frac{1}{\pi} \int_0^{\Phi} \exp(-K(\varphi)\gamma_s) d\varphi. \tag{4.18}$$

where $K(\varphi)=\sin^2(\pi/M)/\sin^2(\varphi)$, $\Phi=\pi(M-1)/M$, and M is the constellation size in PSK. Following the approach in Section 3.2, the *unconditional* average SEP can be evaluated from (4.18) by expressing γ_s as a function of $\lambda_{(1)}$. This transformation has the effect of avoiding the calculation of the pdf of γ_s but instead makes use of the pdf of the sorted random variables $\lambda_{(1)},\lambda_{(2)},\ldots,\lambda_{(N)}$ from (4.16). The expression for the average SEP is given by

$$P_e=\frac{1}{\pi}\sum_{\mathbf{P}_k}\int_0^{\Phi}\int_0^{\infty}\int_0^{\lambda_{(1)}}\cdots\int_0^{\lambda_{(N-1)}}\exp\left(-\sum_{i=1}^{N}K(\varphi)a_{k_i}\lambda_{(i)}\right)\left(\prod_{i=1}^{N}f_{\lambda_{k_i}}(\lambda_{(i)})\right)d\lambda_{(N)}\cdots d\lambda_{(2)}d\lambda_{(1)}d\varphi, \tag{4.19}$$

where

$$a_{k_i}=\begin{cases}\dfrac{|w_{k_1}|^2}{\mathcal{N}_{k_1}} & i=1\\ 0 & otherwise\end{cases}. \tag{4.20}$$

The expression in (4.19) can be further manipulated as follows:

$$P_e=\frac{1}{\pi(\Lambda_0)^N}\sum_{\mathbf{P}_k}\int_0^{\Phi}\int_0^{\infty}\int_0^{\lambda_{(1)}}\cdots\int_0^{\lambda_{(N-1)}}\exp\left(-\sum_{i=1}^{N}b_{k_i}\lambda_{(i)}\right)d\lambda_{(N)}\cdots d\lambda_{(2)}d\lambda_{(1)}d\varphi, \tag{4.21}$$

where Λ_0 is the geometric mean of the average powers Λ_i defined as

$$\Lambda_0=\left(\prod_{i=1}^{N}\Lambda_i\right)^{1/N} \tag{4.22}$$

and

$$b_{k_i}=K(\varphi)a_{k_i}+\frac{1}{\Lambda_{k_i}}. \tag{4.23}$$

According to the "virtual branch technique" the dependent variables $\lambda_{(i)}$, $i=1,2,\cdots,N$ can be transformed into the independent variables u_i, $i=1,2,\cdots,N$, using the linear transformation shown in (2.57). The scalar form of the transformation applied to the variables $\lambda_{(i)}$ is given by

$$\lambda_{(i)}=\sum_{n=i}^{N}u_n, \tag{4.24}$$

which is equivalent to the vector equation

$$\boldsymbol{\lambda}=\mathbf{T}\mathbf{u}, \tag{4.25}$$

where $\boldsymbol{\lambda}=\left[\lambda_{(1)},\lambda_{(2)},\cdots,\lambda_{(N)}\right]^T$, $\mathbf{u}=\left[u_1,u_2,\cdots,u_N\right]^T$ and $\mathbf{T}$ is the upper triangular matrix defined in (2.61). Therefore, the expression shown in (4.21) is now transformed into the simple multiple integral with constant limits

$$P_e = \frac{1}{\pi(\Lambda_0)^N} \sum_{\mathbf{P}_k} \int_0^{\Phi} \int_0^{\infty} \int_0^{\infty} \cdots \int_0^{\infty} \exp\left(-\sum_{i=1}^{N} c_{k_i} u_i \right) du_N \cdots du_2 du_1 d\varphi, \tag{4.26}$$

where

$$c_{k_i} = \sum_{n=1}^{i} b_{k_n} . \tag{4.27}$$

The final solution is obtained by direct evaluation of the integrals to obtain the closed form expression

$$P_e = \frac{1}{\pi(\Lambda_0)^N} \sum_{\mathbf{P}_k} \int_0^{\Phi} \prod_{i=1}^{N} \frac{1}{c_{k_i}} d\varphi, \tag{4.28}$$

or, written explicitly

$$P_e = \frac{1}{\pi(\Lambda_0)^N} \sum_{\mathbf{P}_k} \int_0^{\Phi} \prod_{i=1}^{N} \frac{1}{K(\varphi)\left|w_{k_1}\right|^2 / \mathcal{N}_{k_1} + \sum_{n=1}^{i} 1/\Lambda_{k_n}} d\varphi . \tag{4.29}$$

This expression is recognised as being similar to the expression shown in (3.33) which was derived in Chapter 3 for the H-S/MRC receiver.

4.1.3 Average SNR Analysis

We now proceed to derive an expression for the average SNR of the SC receiver. We begin by using the definition of the average SNR, expressed in terms of the instantaneous SNR and its pdf as

$$\Gamma_s = \int_0^{\infty} \gamma_s f_{\gamma_s}(\gamma_s) d\gamma_s, \tag{4.30}$$

where $f_{\gamma_s}(\gamma_s)$ is the pdf of the instantaneous SNR. As in the previous section, the pdf of γ_s is replaced with the joint pdf of the sorted variables $\lambda_{(i)}$, defined in (2.56), and the average SNR in (4.30) can be written as

$$\Gamma_s = \sum_{\mathbf{P}_k} \int_0^{\infty} \int_0^{\lambda_{(1)}} \cdots \int_0^{\lambda_{(N-1)}} a_{k_1} \lambda_{(1)} \left(\prod_{i=1}^{N} f_{k_i}(\lambda_{(i)}) \right) d\lambda_{(N)} \cdots d\lambda_{(2)} d\lambda_{(1)} . \tag{4.31}$$

Using the "virtual branch technique", the expression in (4.31) is transformed into the simpler integral with constant limits

$$\Gamma_s = \frac{1}{(\Lambda_0)^N} \sum_{\mathbf{P}_k} a_{k_1} \int_0^{\infty} \int_0^{\infty} \cdots \int_0^{\infty} \left(\sum_{i=1}^{N} u_i \right) \exp\left(-\sum_{i=1}^{N} d_{k_i} u_i \right) du_N \cdots du_2 du_1, \tag{4.32}$$

where

$$d_{k_i} = \sum_{n=1}^{i} \frac{1}{\Lambda_{k_n}}. \tag{4.33}$$

The multiple integral is easily evaluated by solving each integral independently and the final closed form expression for the SNR is given by

$$\Gamma_s = \frac{1}{(\Lambda_0)^N} \sum_{\mathbf{P}_k} \left(a_{k_1} \left(\sum_{i=1}^{N} \frac{1}{d_{k_i}} \right) \left(\prod_{i=1}^{N} \frac{1}{d_{k_i}} \right) \right). \tag{4.34}$$

The average combined SNR in (4.34) is similar to the corresponding expression for the H-S/MRC receiver shown in (3.55).

4.2 Double Selection Equal Gain Combining Receiver

The analysis of the SC receiver in Section 4.1 benefits from the fact that only a single branch was selected which was then simply used for detection, i.e. no combining was involved. In this section we analyse the performance of the double selection/equal gain combining (2S/EGC) receiver which selects and combines the *two* branches with the maximum estimated SPN magnitude. The analysis of this type of receiver is more complex than both the H-S/MRC and the SC receivers analysed in Chapter 3 and Section 4.1, respectively, since the instantaneous SNR is now a function of the sum of two ordered Rayleigh random variables. The final closed form expression for the average SEP is also in a more complex form than the other expressions we have derived so far.

Before proceeding with the derivation for the SEP of the 2S/EGC receiver, it is necessary to justify the definition of EGC as it is used in this section and later on in Chapters 5 and 6. The EGC receiver according to the classical literature [1]-[2] and research papers as for example [11] and [19] is a receiver which attempts to phase-align the diversity signals and then combines them without applying any additional weights. This contradicts the use of the term by many researchers such as the authors of [44]-[46] where they refer to their receiver as an EGC receiver in spite of using unequal weights (Also see the discussion in [47]). In the references [44]-[46], for example, the combiner output signal consists of the following sum:

$$y = \sum_{i=1}^{N} r_i[k] \cdot r_i[k-1]^* . \tag{4.35}$$

Noting that the magnitudes $|r_i[k-1]|$ are different for each branch we may conclude that the sum in (4.35) is not obtained using equal weights. We name this receiver the "previous symbol gain combining" (PSGC) receiver to stress the application of the unequal magnitudes $|r_i[k-1]|$ of the

previous received symbols. Note that while this is not a standard term it provides a clear distinction from the receivers analysed in this thesis.

In this thesis we follow the traditional approach regarding EGC (also see [46]) in which the EGC receiver simply attempts to phase-align the signals by multiplying them with the phase of the previous received symbol as follows:

$$y = \sum_{i=1}^{N} r_i[k] \cdot e^{j\hat{\theta}_i}, \tag{4.36}$$

where

$$e^{j\hat{\theta}_i} = \frac{r_i[k-1]^*}{|r_i[k-1]|}. \tag{4.37}$$

Obviously, the SC receiver analysed in Section 4.1 is not affected by this distinction since no combining takes place and, thus, the instantaneous SNR in (4.12) is identical for both weighting methods. In contrast, the 2S/EGC receiver analysed in this section and a possible hybrid 2S/PSGC receiver would perform differently since they use different weighting methods for their combined signals. From simulation studies, however, the difference in performance only becomes noticeable for numbers of selected branches higher than two.

Finally, we would like to point out that the term equal gain combining is also used to describe another type of diversity receiver which uses noncoherent square law detection.

4.2.1 System Description

The conceptual model of the 2S/EGC receiver is shown in Figure 4.2, where the sorter selects the *two* branches with the largest estimated SPN magnitude and uses (4.36) to partially remove the fading phase distortion and combine the result.

The received signal in branch i at time k was shown in (4.8) to be

$$r_i = w_i^* h_i + v_i, \tag{4.38}$$

where w_i is a function of the channel statistics and v_i is the effective noise defined in (4.9). The channel estimators shown in Figure 4.2 produce estimates whose instantaneous power determines the branch selection. If $|h_j|$ is the largest and $|h_m|$ is the second largest amongst all the branches (i.e. $|h_j| > |h_m| > |h_i|, i \neq j,m$), then the j-th and m-th branches are selected and the decision

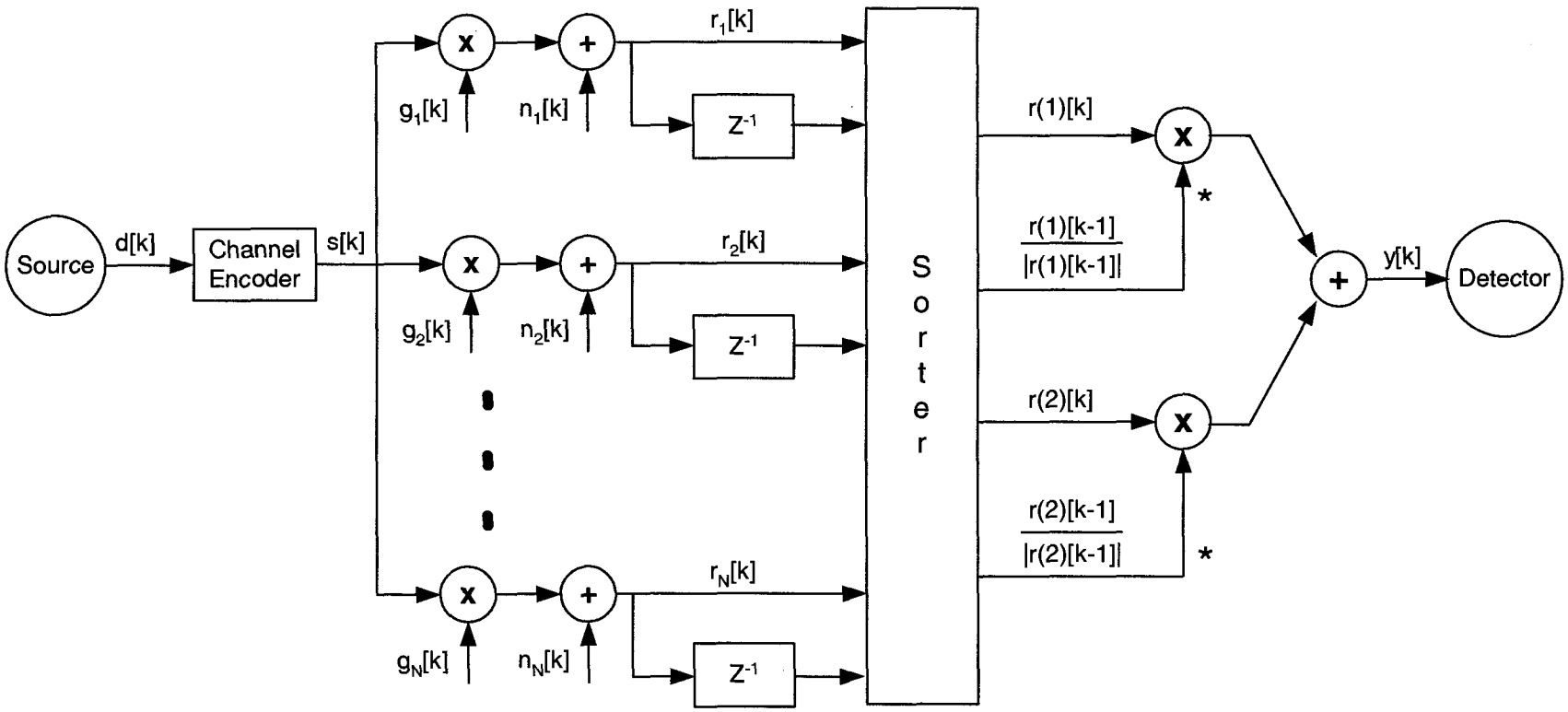

Figure 4.2: System model of the 2S/EGC diversity receiver with no CSI.

variable for the detector can be written as

$$y = r_j \frac{h_j^*}{|h_j^*|} + r_m \frac{h_m^*}{|h_m^*|}. \tag{4.39}$$

To determine the symbol error rate of the 2S/EGC receiver we substitute (4.38) into (4.39) to obtain the following expression for the decision variable:

$$y = \left(w_j^* |h_j| + w_m^* |h_m|\right) s + \left(v_j \frac{h_j^*}{|h_j|} + v_m \frac{h_m^*}{|h_m|} \right). \tag{4.40}$$

The first term in (4.40) is the signal component and the second term is noise. The corresponding instantaneous SNR is defined as

$$\gamma_{2s} = \frac{\frac{1}{2}\left|w_j^* |h_j| + w_m^* |h_m|\right|^2}{\frac{1}{2} E\left[\left|v_j h_j^* / |h_j| + v_m h_m^* / |h_m|\right|^2\right]} = \frac{\frac{1}{2}\left|w_j^* |h_j| + w_m^* |h_m|\right|^2}{\mathcal{N}_j + \mathcal{N}_m}, \tag{4.41}$$

where $\mathcal{N}_i$ is the variance (power) of the effective noise at branch i. It should be noted from (4.40) that, as for the SC receiver in the previous section, even though the j-th and m-th branches may have the largest *SPN magnitudes*, γ_{2s} is not necessarily maximized since it not only depends on $|h_j|$ and $|h_m|$, but also on the branches' effective noise powers $\mathcal{N}_j$, $\mathcal{N}_m$ as well as the channel statistics used to calculate w_j, w_m. We would, therefore, expect that the 2S/EGC would have inferior SEP performance to the H-S/MRC receiver, which has the ability to select the branches with the maximum SNR. This SEP degradation is in addition to the degradation from applying non-optimal weights in the combining as opposed to the optimal weights in the MRC receiver.

4.2.2 Symbol Error Probability Analysis

To derive the exact expression for the SEP of the 2S/EGC diversity receiver we define the random variables

$$l_i = |h_i|, \tag{4.42}$$

which are statistically independent and *Rayleigh* distributed, with probability density functions

$$f_{l_i}(x) = \frac{x}{\Lambda_i} e^{-\frac{x^2}{2\Lambda_i}}, \tag{4.43}$$

where

$$\Lambda_i = \frac{1}{2} E[l_i^2] = \frac{1}{2} E[|h_i|^2], \tag{4.44}$$

Note that while the variables l_i are different from the variables λ_i defined in (4.13) and are related with the expression

$$\lambda_i = \frac{1}{2} l_i^2 . \tag{4.45}$$

The statistic Λ_i, however, is the same quantity as in (4.15) and is defined as the average received SPN power.

Using the new variables and the conditional SEP found in [38], the SEP of the 2S/EGC receiver conditioned on l_j and l_m, can be written as

$$P_{e|(l_j,l_m)} = \frac{1}{\pi} \int_0^{\Phi} \exp\left(-K(\varphi) \frac{\left(w_j^* l_j + w_m^* l_m \right)^2}{2(\mathcal{N}_j + \mathcal{N}_m)} \right) d\varphi , \tag{4.46}$$

where $K(\varphi) = \sin^2(\pi/M)/\sin^2(\varphi)$, $\Phi = \pi(M-1)/M$, and M is the constellation size in PSK. Averaging over all possible permutations of two branches selected from the population of the N available branches we obtain the expression for the average SEP given by

$$P_e = \frac{1}{\pi} \sum_{j=1}^{N} \sum_{\substack{m=1 \\ m \neq j}}^{N} \int_0^{\Phi} \int_0^{\infty} \int_0^{l_j} \exp\left(-K(\varphi) \frac{\left(w_j^* l_j + w_m^* l_m \right)^2}{2(\mathcal{N}_j + \mathcal{N}_m)} \right) \frac{l_j l_m}{\Lambda_j \Lambda_m} \exp\left(-\frac{l_j^2}{2\Lambda_j} - \frac{l_m^2}{2\Lambda_m} \right) \times$$

$$\left(\int_0^{l_m} \cdots \int_0^{l_m} \prod_{\substack{i=1 \\ i \neq j,m}}^{N} \frac{l_i}{\Lambda_i} \exp\left(-\frac{l_i^2}{2\Lambda_i} \right) dl_1 \cdots dl_N \right) dl_m dl_j d\varphi , \tag{4.47}$$

where it should be noted that $dl_1 \cdots dl_N$ does not include dl_j or dl_m. The reason behind this choice of averaging as opposed to the method used in the SC and H-S/MRC cases is the more convenient result of the evaluation of the inner $N-2$ integrals. By choosing the method in (4.47) we obtain the expression consisting of a sum of exponentials shown below:

$$\int_0^{l_m} \cdots \int_0^{l_m} \prod_{\substack{i=1 \\ i \neq j,m}}^{N} \frac{l_i}{\Lambda_i} \exp\left(-\frac{l_i^2}{2\Lambda_i} \right) dl_1 \cdots dl_N = \sum_{i=0}^{N-2} \sum_{n=1}^{Y(i)} (-1)^i \exp\left[-l_m^2 \sum_{k=1}^{i} \mathbf{V}_i^{j,m}(n,k) \right] , \tag{4.48}$$

where

$$Y(i) = \frac{(N-2)!}{i!(N-2-i)!} \tag{4.49}$$

and the definition of $\mathbf{V}_i^{j,m}(n,k)$ is provided below:

Let $\mathbf{v}$ be a vector defined as $\mathbf{v}=(v_1,v_2,\cdots,v_N)^T$. We define the matrix $\mathbf{V}_i^{j,m}$ as a $\frac{(N-2)!}{i!(N-2-i)!}\times i$ matrix consisting of every possible combination of i elements in its rows selected from the vector $\mathbf{v}$ with v_j and v_m removed. We define $\mathbf{V}_0^{j,m}\equiv 0$. $\mathbf{V}_i^{j,m}(n,k)$ is the k-th element in the n-th row of matrix $\mathbf{V}_i^{j,m}$.

The elements of vector $\mathbf{v}$ in (4.48) are assigned the values

$$v_i=\frac{1}{2\Lambda_i}. \tag{4.50}$$

The resulting expression for the SEP only involves the 2 integrals for l_j or l_m and the integral of φ as follows:

$$P_e=\frac{1}{\pi}\sum_{j=1}^{N}\sum_{\substack{m=1\\m\neq j}}^{N}\int_0^{\Phi}\int_0^{\infty}\int_0^{l_j}\frac{l_j l_m}{\Lambda_j\Lambda_m}\exp\left(-\frac{l_j^2}{2\Lambda_j}-\frac{l_m^2}{2\Lambda_m}-K(\varphi)\frac{\left(w_j^* l_j+w_m^* l_m\right)^2}{2(\mathcal{N}_j+\mathcal{N}_m)}\right)\times$$
$$\sum_{i=0}^{N-2}\sum_{n=1}^{Y(i)}(-1)^i\exp\left(-l_m^2\sum_{k=1}^{i}\mathbf{V}_i^{j,m}(n,k)\right)dl_m dl_j d\varphi. \tag{4.51}$$

The triple integral expression for the SEP can be reorganized resulting in

$$P_e=\frac{1}{\pi}\sum_{j=1}^{N}\sum_{\substack{m=1\\m\neq j}}^{N}\frac{1}{\Lambda_j\Lambda_m}\sum_{i=0}^{N-2}(-1)^i\sum_{n=1}^{Y(i)}\int_0^{\Phi}\int_0^{\infty}\int_0^{l_j}l_j l_m\times$$
$$\exp\left(-\frac{l_j^2}{2\Lambda_j}-\frac{l_m^2}{2\Lambda_m}-K(\varphi)\frac{\left(w_j^{\dagger} l_j+w_m^{\dagger} l_m\right)^2}{2(\mathcal{N}_j+\mathcal{N}_m)}-l_m^2\sum_{k=1}^{i}\mathbf{V}_i^{j,m}(n,k)\right)dl_m dl_j d\varphi. \tag{4.52}$$

We now use a two dimensional version of the "virtual branch technique" to convert the 2 inner integrals in (4.52) to a pair of integrals that are independent of the variable l_j. The following linear transformation will ensure that we obtain two integrals with lower and upper limits of 0 and ∞ respectively:

$$\begin{pmatrix}l_j\\l_m\end{pmatrix}=\begin{pmatrix}1&1\\0&1\end{pmatrix}\begin{pmatrix}u\\v\end{pmatrix}. \tag{4.53}$$

After applying the transformation and using the integral tables in [39 eqns 3.322.2 and 3.462.5] we obtain the exact expression for the SEP of the 2S/EGC receiver as

$$P_e = \sum_{j=1}^{N} \sum_{\substack{m=1 \\ m \neq j}}^{N} \sum_{i=0}^{N-2} \sum_{n=1}^{Y(i)} \frac{(-1)^i}{4\pi\Lambda_j\Lambda_m} \left\{ \frac{1}{a_1(\varphi)a_3(\varphi)} + \right.$$

$$\left. \frac{1}{\sqrt{a_1(\varphi)}}\left(1-\frac{a_2(\varphi)}{a_1(\varphi)}\right)\left[\frac{\arcsin\left(\sqrt{1-\frac{a_2(\varphi)^2}{a_1(\varphi)a_3(\varphi)}}\right)}{\left(a_3(\varphi)-\frac{a_2(\varphi)^2}{a_1(\varphi)}\right)^{3/2}} - \frac{a_2(\varphi)}{a_3(\varphi)\sqrt{a_1(\varphi)}\left(a_3(\varphi)-\frac{a_2(\varphi)^2}{a_1(\varphi)}\right)}\right]\right\} \tag{4.54}$$

where the variables $a_1(\varphi)$, $a_2(\varphi)$ and $a_3(\varphi)$ are defined below:

$$a_1(\varphi) = \frac{1}{2\Lambda_j} + K(\varphi)\frac{\left(w_j^*\right)^2}{2(\mathcal{N}_j + \mathcal{N}_m)}, \tag{4.55}$$

$$a_2(\varphi) = \frac{1}{2\Lambda_j} + K(\varphi)\frac{w_j^*(w_j^* + w_m^*)}{2(\mathcal{N}_j + \mathcal{N}_m)}, \tag{4.56}$$

$$a_3(\varphi) = \frac{1}{2\Lambda_j} + \frac{1}{2\Lambda_m} + K(\varphi)\frac{\left(w_j^* + w_m^*\right)^2}{2(\mathcal{N}_j + \mathcal{N}_m)} + \sum_{k=1}^{i} \mathbf{V}_i^{j,m}(n,k). \tag{4.57}$$

We recognise that (4.54) is a complex expression. We, therefore, provide asymptotic analysis in the following section, which results in simpler approximate expressions.

4.3 Asymptotic Analysis of the SC and 2S/EGC Receivers

In this section we provide asymptotic SEP analysis for the SC and 2S/EGC receivers. The SEP expressions we derived in Sections 4.1 and 4.2 depend on statistical parameters such as the average signal and noise powers in each branch, the correlation between the fading gain and its observation etc, which were defined in Chapter 2. It should be stressed at this point that although the SEP expression is a function of the specific channel statistics, the receivers do not use these statistics in their operation.

4.3.1 Asymptotic Analysis of the SC Receiver

The SEP of the DPSK receiver operating in fading channels with Doppler spread is known to be limited by an irreducible error floor, which is caused by the reduced temporal correlation of the fading gain. In other words, since the channel changes randomly between successive symbols, increasing the transmitted signal's power would not improve the SEP beyond a certain level as was shown in Section 3.4. For this reason it is necessary to derive *two* asymptotic expressions for the SEP at high SNR: the *static fading* asymptote and the *error floor* asymptote.

The static fading asymptote is derived under the assumption that fading is static. By static fading we refer to the case where the fading gain remains constant for the period of interest, possibly due to the fact that the receiver and transmitter as well as their environment are stationary. In other words the channel fade rate, f_D, is zero. Furthermore, we assume that for the purpose of our asymptotic analysis the operating range is the high SNR region where, in all the branches, the signal powers are much larger than the noise powers. In mathematical terms, the assumptions for static asymptotic fading are

$$f_D = 0, \tag{4.58}$$

$$\sigma_{g_i}^2 >> \sigma_{n_i}^2, \; i = 1,2,\ldots,N. \tag{4.59}$$

Based on these assumptions the quantities of interest can be approximated by

$$J_0(2\pi f_D) = 1, \tag{4.60}$$

$$\Lambda_i = \sigma_{h_i}^2 = \sigma_{g_i}^2 + \sigma_{n_i}^2 \approx \sigma_{g_i}^2, \tag{4.61}$$

$$\sigma_{g_i h_i} = \sigma_{g_i}^2 J_0(2\pi f_D) = \sigma_{g_i}^2, \tag{4.62}$$

$$w_i = \frac{\sigma_{g_i h_i}}{\sigma_{h_i}^2} \approx 1. \tag{4.63}$$

Another quantity of interest is the average effective noise $\mathcal{N}_i$ defined in (2.32) as

$$\mathcal{N}_i = \sigma_{e_i}^2 + \sigma_{n_i}^2 = \left(\sigma_{g_i}^2 - \frac{\sigma_{g_i h_i}^2}{\sigma_{h_i}^2} \right) + \sigma_{n_i}^2. \tag{4.64}$$

Using (4.59)-(4.62) we can easily show that $\mathcal{N}_i$ can be approximated by $2\sigma_{n_i}^2$ with equality in the limit as $\sigma_{g_i}^2 / \sigma_{n_i}^2 \to \infty$. In other words, the approximation for $\mathcal{N}_i$ is given by

$$\mathcal{N}_i \approx 2\sigma_{n_i}^2. \tag{4.65}$$

It is straightforward to derive a static fading asymptotic approximation to the exact SEP of the SC receiver shown in (4.29). By substituting the high SNR approximations (4.61)-(4.65) into (4.29) the SEP can be approximated by

$$P_e \approx \frac{1}{\pi \left(\prod_{i=1}^{N} \sigma_{g_i}^2 \right)} \sum_{\mathrm{P}_k} \int_0^{\Phi} \prod_{i=1}^{N} \frac{1}{K(\varphi)/2\sigma_{n_{k_1}}^2 + \sum_{n=1}^{i} 1/\sigma_{g_{k_n}}^2} d\varphi. \tag{4.66}$$

Since we are interested in the high SNR region (see assumption (4.59)) the denominator in (4.66) can be approximated by

$$\frac{K(\varphi)}{2\sigma_{n_{k_1}}^2}+\sum_{n=1}^{i}\frac{1}{\sigma_{g_{k_n}}^2}\approx\frac{K(\varphi)}{2\sigma_{n_{k_1}}^2}. \tag{4.67}$$

Hence, the static fading asymptotic approximation to the SEP of the SC receiver is given by the following expression:

$$P_{e\_static}\approx\frac{2^N K_\varphi N!\left(\frac{1}{N}\sum_{i=1}^{N}\left(\sigma_{n_i}^2\right)^N\right)}{\pi\left(\prod_{i=1}^{N}\sigma_{g_i}^2\right)}, \tag{4.68}$$

where K_φ was defined in (3.43) as

$$K_\varphi=\int_0^{\Phi}\frac{d\varphi}{K(\varphi)^N}. \tag{4.69}$$

To show that the asymptotic expression in (4.68) is also an upper bound to the SEP we incorporate $(\Lambda_0)^N$ into the integrand product of the exact SEP expression in (4.29) as follows:

$$P_e=\frac{1}{\pi}\sum_{\mathbf{P}_k}\int_0^{\Phi}\prod_{i=1}^{N}\frac{1}{K(\varphi)\left|w_{k_1}\right|^2\Lambda_{k_i}/\mathcal{N}_{k_1}+\sum_{n=1}^{i}\Lambda_{k_i}/\Lambda_{k_n}}d\varphi. \tag{4.70}$$

The denominator in (4.70) can be shown to be lower bounded by

$$\frac{K(\varphi)\left|w_{k_1}\right|^2\Lambda_{k_i}}{\mathcal{N}_{k_1}}+\sum_{n=1}^{i}\frac{\Lambda_{k_i}}{\Lambda_{k_n}}\geq\frac{K(\varphi)\sigma_{g_{k_i}}^2}{2\sigma_{n_{k_1}}^2}, \tag{4.71}$$

therefore, the asymptotic expression shown in (4.68) also provides an upper bound to the exact SEP expression.

As discussed in Section 3.2.2, for binary DPSK, the integral (4.69) has the simple evaluation shown in (3.45) and reproduced below:

$$K_\varphi=\frac{(2N-1)!!}{(2N)!!}\frac{\pi}{2}, \tag{4.72}$$

where the notation $2k!!$ denotes the product $2\cdot4\cdot6\cdots2k$ and the notation $(2k\text{-}1)!!$ denotes the product $1\cdot3\cdot5\cdots(2k-1)$ where k is any integer. The asymptotic BEP of the SC receiver can therefore be written in a very compact form as

$$P_{e\_static}^{b}\approx\frac{(2N-1)!!}{2}\frac{\left(\frac{1}{N}\sum_{i=1}^{N}\left(\sigma_{n_i}^2\right)^N\right)}{\left(\prod_{i=1}^{N}\sigma_{g_i}^2\right)}. \tag{4.73}$$

For the special case of no diversity, i.e. $N=1$, (4.73) is reduced to the well known asymptotic expression [2]

$$P_e \approx \frac{\sigma_n^2}{2\sigma_g^2} = \frac{1}{2\tilde{\Gamma}}, \tag{4.74}$$

where $\tilde{\Gamma}$ was defined in (3.60) as the input SNR. The expressions in (4.68) and (4.73) demonstrate the significance of the generalized arithmetic mean of the noise powers and of the geometric mean of the signal powers, which are influenced by the NPP and SPP respectively.

The error floor asymptote is defined in the high SNR region where the fading gain uncertainty due to the Doppler spread becomes the dominant factor in the receiver performance and the SEP cannot be improved by further increasing the SNR. In this region the fading gain can no longer be considered constant over time, i.e. the channel fade rate, f_D, cannot be set to 0 as in (4.58). The assumption in (4.59) on the other hand is still valid as the receiver is still operating in the high SNR region. Therefore the following approximation still holds:

$$\Lambda_i = \sigma_{h_i}^2 = \sigma_{g_i}^2 + \sigma_{n_i}^2 \approx \sigma_{g_i}^2, \tag{4.75}$$

The variable w_i can be approximated in this case by

$$w_i = \frac{\sigma_{g_i h_i}}{\sigma_{h_i}^2} \approx J, \tag{4.76}$$

where J is used as a shorter notation to the Bessel function defined as

$$J = J_0(2\pi f_D). \tag{4.77}$$

As in the static fading case, the average effective noise $\mathcal{N}_i$ defined in (4.64) can be shown to be approximated at high SNR by its upper bound as

$$\mathcal{N}_i = (1-J^2)\sigma_{g_i}^2. \tag{4.78}$$

For binary modulation, i.e. differential BPSK, an approximation derived using the technique used for the static fading case provides a very tight and general bound in the sense that it applies to the general SPP. For higher modulations, however, the approximation becomes loose. The difficulty stems from the fact that by applying the approximations in (4.75), (4.76) and (4.78) the denominator of (4.29) becomes

$$K(\varphi)\frac{|w_{k_1}|^2}{\mathcal{N}_{k_1}} + \sum_{n=1}^{i}\frac{1}{\Lambda_{k_n}} \approx \frac{J^2 K(\varphi)}{(1-J^2)\sigma_{g_{k_1}}^2} + \sum_{n=1}^{i}\frac{1}{\sigma_{g_{k_n}}^2}. \tag{4.79}$$

In the case of static fading, it was shown in (4.65) that at high SNR the effective noise power, $\mathcal{N}_i$, was only a function of the AWGN power and, hence, the approximation in (4.67) was easily obtained. In the right hand side of (4.79), however, we observe that both terms are functions of the signal powers. Therefore, eliminating the rightmost term, as done in (4.67), would, in general, produce a loose approximation . There are two exceptions to this issue: At slow fading, for which $J \to 1$, the following holds:

$$\frac{J^2 K(\varphi)}{(1-J^2)\sigma_{g_{k_1}}^2} \gg \sum_{n=1}^{i} \frac{1}{\sigma_{g_{k_n}}^2}. \tag{4.80}$$

Furthermore, for BPSK, for which $M=2$ the factor $K(\varphi)$ attains its maximum value as shown below:

$$K(\varphi) = \frac{\sin^2(\pi/M)}{\sin^2(\varphi)} = \frac{1}{\sin^2(\varphi)}. \tag{4.81}$$

Therefore, based on (4.80) and (4.81), for 2DPSK or for slow fading the error floor can be tightly approximated by

$$P_{e\_floor}^{b} \approx \frac{(1/J^2-1)^N (2N-1)!!}{2^{N+1}} \frac{\left(\frac{1}{N}\sum_{i=1}^{N}\left(\sigma_{g_i}^2\right)^N\right)}{\left(\prod_{i=1}^{N}\sigma_{g_i}^2\right)}. \tag{4.82}$$

Furthermore, for uniform SPP it is possible to derive an approximation to the SEP of the SC receiver for *general M*. With the average effective noise power $\mathcal{N}_i$ given in (4.78), the sum of the inverse branch signal powers on the left hand side of (4.79) cannot be eliminated but we may use the fact that all average signal powers $\sigma_{g_i}^2$ are equal and expand the integrand product in (4.29) to the following:

$$\prod_{i=1}^{N}\left(\frac{K(\varphi)\left|w_{k_1}\right|^2}{\mathcal{N}_{k_1}} + \frac{i}{\Lambda}\right) \approx \left(\frac{K(\varphi)}{(1/J^2-1)}\right)^N \frac{1}{\left(\sigma_g^2\right)^N} + \left(\frac{K(\varphi)}{(1/J^2-1)}\right)^{N-1} \frac{N(N+1)}{2\left(\sigma_g^2\right)^N} + E, \tag{4.83}$$

where E consists of terms with lower powers of $(1/J^2-1)$. The asymptotic expression for the error floor of the SC receiver in a uniform SPP is, thus, given by

$$P_{e\_floor}^{u} \approx \frac{N!}{\pi} K_{\varphi}^{\Diamond}. \tag{4.84}$$

The term $K_{\varphi}^{\Diamond}$ is the integral

$$K_{\varphi}^{\Diamond}=\int_{0}^{\Phi}\frac{d\varphi}{\left(K(\varphi)/(1/J^{2}-1)\right)^{N}+N(N+1)\left(K(\varphi)/(1/J^{2}-1)\right)^{N-1}/2}, \tag{4.85}$$

where the term E in (4.83) is ignored. In (4.84) we observe that for the uniform SPP the error floor is only a function of the total number of branches N and the fade rate f_D.

4.3.2 Asymptotic Analysis of the 2S/EGC Receiver

For the static fading asymptote of the 2S/EGC receiver we apply to the exact expression in (4.54) the approximations in (4.61)-(4.65) as well as the approximation for the "arcsine" function which, for low values of its argument, can be approximated by

$$\arcsin(x)\approx x. \tag{4.86}$$

With algebraic manipulation of the SEP expression in (4.54) and using only the assumption in (4.86) the approximation to the SEP of 2S/EGC can be obtained as

$$P_e=\sum_{j=1}^{N}\sum_{\substack{m=1\\ m\neq j}}^{N}\sum_{i=0}^{N-2}\sum_{l=1}^{Y(i)}\frac{(-1)^{i}}{4\pi\Lambda_j\Lambda_m}\frac{3}{4a_1(\varphi)a_3(\varphi)}. \tag{4.87}$$

This approximation, although compact, is not very enlightening but with the help of the following identity we are able to arrive at more meaningful results:

$$\sum_{j=1}^{N}\sum_{i=0}^{N-1}\sum_{l=1}^{Y(i)}\frac{(-1)^{i}/\Lambda_j}{b_j+\sum_{k=1}^{i}V_i^{j}(l,k)}=\frac{1}{\Lambda_0^{N}}\sum_{\mathbf{P_k}}\left(\prod_{i=1}^{N}1/\left(b_1+\sum_{n=2}^{i}\frac{1}{\Lambda_{k_n}}\right)\right). \tag{4.88}$$

The identity in (4.88) is obtained by deriving the SEP of the SC receiver using the two approaches followed in Sections 4.1 and 4.2. By following the approach of summation over $\mathbf{P}_k$, used in Section 4.1, we obtain the right hand side whereas by following the approach of summation over j, used in Section 4.2, we obtain the left hand side. Using this identity, the sum of terms with alternating positive and negative signs shown in (4.87) is replaced by a sum of products similar to the sum in (4.29) and proves helpful in our derivation of a simple asymptotic expression. Applying the approximations in (4.61)-(4.65) as well as the identity in (4.88) to the intermediate result in (4.87) we obtain the simplified approximate expression

$$P_{e\_static}\approx\frac{3N!K_{\varphi}}{2^{N}\pi}\frac{\left(\frac{1}{N(N-1)}\sum_{j=1}^{N}\sum_{\substack{m=1\\ m\neq j}}^{N}(\sigma_{n_j}^{2}+\sigma_{n_m}^{2})^{N}\right)}{\left(\prod_{i=1}^{N}\sigma_{g_i}^{2}\right)}. \tag{4.89}$$

As discussed in the previous section, when calculating the value of the SEP error floor, the terms $1/\Lambda_{k_i}$ cannot be safely omitted for modulations higher than binary (M=2) or for fast fade rates. We, therefore, provide here only an expression for the binary case. Using the set of approximations in (4.75)-(4.78) we obtain the error floor asymptote as

$$P^{b}_{e\_floor} \approx \frac{3(1/J^2-1)^N(2N-1)!!}{2^{3N+1}} \frac{\left(\frac{1}{N(N-1)} \sum_{j=1}^{N} \sum_{\substack{m=1 \\ m\neq j}}^{N} (\sigma^2_{g_j} + \sigma^2_{g_m})^N \right)}{\left(\prod_{i=1}^{N} \sigma^2_{g_i} \right)}. \tag{4.90}$$

For the SC receiver, we derived in (4.84) a general asymptotic expression for a channel with uniform SPP. We are able to repeat the derivation for the 2S/EGC receiver and obtain the asymptotic expression shown below:

$$P^{u}_{e\_floor} \approx \frac{3N!}{2^N \pi} K^{\Diamond}_{\varphi}, \tag{4.91}$$

where

$$K^{\Diamond}_{\varphi} = \int_0^{\Phi} \frac{d\varphi}{\left(K(\varphi)/(1/J^2-1)\right)^N + N(N+3)/2\left(K(\varphi)/(1/J^2-1)\right)^{N-1}}. \tag{4.92}$$

4.3.3 Selection Metric Issues for the SC and 2S/EGC Receivers

Returning to our earlier discussion in Section 4.1.1 on the effect of the selection metric on the SEP, let us revisit the selection metrics used in the H-S/MRC receiver analysed in Chapter 3 and in the SC and 2S/EGC receivers analysed in this chapter. For the H-S/MRC receiver the selection metric is the variable χ defined as

$$\chi_{mrc} = \gamma_i = \frac{\frac{1}{2}\hat{g}_i^2}{\mathcal{N}_i} \tag{4.93}$$

The metric in (4.93) can be approximated in the static fading case by

$$\chi_{mrc\_static} \approx \frac{\frac{1}{2}|h_i|^2}{2\sigma^2_{n_i}} \tag{4.94}$$

and in the error floor region by

$$\chi_{mrc\_floor} \approx \frac{\frac{1}{2}|h_i|^2}{(1/J^2-1)\sigma^2_{g_i}}. \tag{4.95}$$

In contrast, for the SC and 2S/EGC receivers of this chapter the selection metric χ_{egc} can be expressed as

$$\chi_{egc} = \frac{1}{2}|h_i|^2. \tag{4.96}$$

The absence of the denominator in (4.96) shows that, in effect, the SC and 2S/EGC receivers assume that they are always operating in a channel with a uniform SNR profile. We, therefore, expect that when the channel has a uniform SNR profile their selection decisions would agree with the decisions made by the H-S/MRC receiver. However, contrasting (4.95) with (4.96), we expect that the SC and 2S/EGC receivers would have a higher error floor than the equivalent H-S/MRC receivers when they operate in a channel with a non-uniform SPP. Furthermore, contrasting (4.94) with (4.96) we expect that the SC and 2S/EGC receivers would have a higher asymptotic SEP in the static fading region than the equivalent H-S/MRC receivers when they operate in a channel with non-uniform NPP profile. The reason is the absence of the channel statistics in the receivers of this chapter.

4.4 Results

In this section we use the expressions derived in Sections 4.1-4.3 to compare the performance of the SC and 2S/EGC receivers to the performance of the equivalent H-S/MRC receivers from Chapter 3. To distinguish the two SC receivers we denote the SC receiver from Section 4.1 as "SC noCSI" and the H-S/MRC receiver with L=1 from Chapter 3 as "SC CSI". In this section particular attention is paid to the effect of the SPP and the NPP on the relative performance of the 4 receivers. Further explanation about the divergence in asymptotic performance is also provided in Chapter 5 with the help of the more general asymptotic expressions derived therein.

As in Section 3.4, all systems operate in a Rayleigh fading environment with normalized fade rate f_D and employ differential 8-PSK ($M = 8$) modulation. Contrary to Section 3.4, where the branch SNR's $\tilde{\Gamma}_i = \sigma_{g_i}^2 / \sigma_{n_i}^2$ determined the receiver performance, in this section both the average signal powers, which define the SPP, and the average noise powers, which define the NPP, can influence the SEP of the receivers independently. We, therefore, need to investigate the effect of the SPP and NPP independently of the SNR profile. For all figures in this section we set one of the SPP or NPP as uniform and allow the other to be non-uniform. This helps in isolating the effect of each profile on the SEP of the receivers. The average SNR, $\tilde{\Gamma}$, used in the abscissa of the graphs is calculated in the same way as in Section 3.4, as shown below:

$$\tilde{\Gamma} = \frac{1}{N}\sum_{i=1}^{N}\tilde{\Gamma}_i \,. \tag{4.97}$$

The individual branch SNR's, $\tilde{\Gamma}_i$, are calculated using (3.59) as

$$\tilde{\Gamma}_i = Ge^{-a(i-1)}, \tag{4.98}$$

where a is the profile decay factor, i is the branch index with values $i = 1,2,\ldots,N$ and G is some constant. The tilde (~) over Γ_i indicates that $\tilde{\Gamma}_i$ in (4.97) is the actual input SNR in branch i and not the estimated SNR provided by the channel estimators. Hence, the input SNR is defined as

$$\tilde{\Gamma}_i = \frac{\sigma_{g_i}^2}{\sigma_{n_i}^2} \,. \tag{4.99}$$

In the case of an exponential SNR profile the constant G is defined as

$$G = \frac{N\tilde{\Gamma}(1-e^{-a})}{(1-e^{-aN})}, \tag{4.100}$$

where $\tilde{\Gamma}$ is the mean of the branch SNR's defined in (4.97). With this convention for the SNR, we ensure that the total received SNR is identical for all profiles.

Based on our assumptions and the definition in (4.98) for the average SNR in each branch, we may calculate the values of the signal and noise powers for two cases of non-uniform SNR profiles. When the NPP is uniform and the SPP is exponential, all branch noise powers are set to one as shown below:

$$\sigma_{n_i}^2 = 1 \,. \tag{4.101}$$

The branch signal powers are, therefore, equal to the branch SNR's as follows:

$$\sigma_{g_i}^2 = \frac{N\tilde{\Gamma}(1-e^{-a})}{(1-e^{-aN})}e^{-a(i-1)}, \tag{4.102}$$

When the SPP is uniform and the NPP is exponential, all branch signal powers are set as shown below:

$$\sigma_{g_i}^2 = \tilde{\Gamma} \,. \tag{4.103}$$

The branch noise powers are, therefore, calculated by

$$\sigma_{n_i}^2 = \frac{(1-e^{-aN})}{N(1-e^{-a})}e^{a(i-1)} \,. \tag{4.104}$$

The convention used in (4.104) ensures that the SNR profile is exponential with decay parameter a. The SNR profiles use the same values for the profile decay parameter a as in Section 3.4 but in this case it is also important to specify which of the SPP or NPP is responsible for the exponential

distribution of the profile. In Table 4.1 we reproduce the decay parameter for each of the three SNR profiles we consider in this section.

As discussed in Sections 4.2 and 4.3.3, the two SC receivers, SC noCSI (analysed in Section 4.1) and SC CSI (special case of the H-S/MRC receiver analysed in Chapter 3), are expected to perform identically in a uniform SNR profile. The two double selection receivers, 2S/EGC and 2S/MRC, on the other hand are expected to exhibit a discrepancy even in the uniform SNR profile due to the difference in the weights applied to each of the combined symbols. As stated in Section 4.2, the 2S/EGC receiver simply attempts to phase-align the signals from the two selected branches using the previous symbol's phase. The 2S/MRC receiver, on the other hand, applies

Table 4.1. The three SNR profiles used in Section 4.4 and the corresponding profile decay parameter a.

Profile name	a
uniform	0
exp1	0.5
exp2	1

optimum weights before combining, with a higher weight applied to the symbol with the largest estimated instantaneous SNR.

We first show in Figure 4.3 the SEP of the SC noCSI, SC CSI, 2S/EGC and 2S/MRC receivers when they operate in a uniform SNR profile with both the SPP and the NPP being uniform. All receivers have a total of N=4 diversity branches and the channel has a normalized fade rate $f_D = 0.01$. As expected, we observe in Figure 4.3 that the two SC receivers perform identically whereas the two double selection receivers display a small discrepancy. In Figure 4.4 we plot the SEP of the four receivers operating in a uniform SNR but now the SPP and NPP are identically exponential. This is the only case where both profiles are allowed to be non-uniform. The signal powers are defined as

$$\sigma_{g_i}^2 = \frac{\tilde{\Gamma}(1-e^{-a})}{(1-e^{-aN})} e^{-a(i-1)}, \tag{4.105}$$

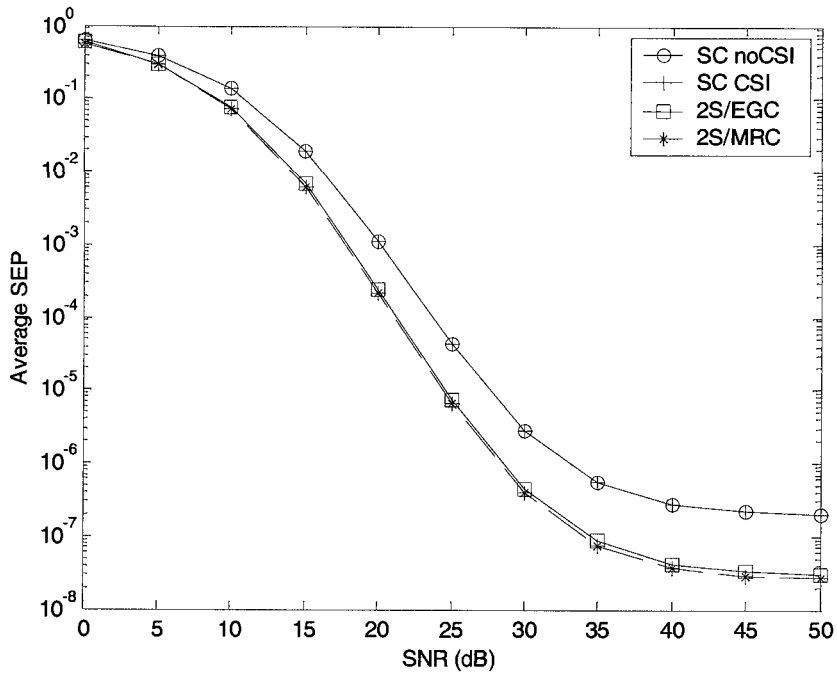

Figure 4.3: SEP of the four hybrid receivers in a channel with uniform SNR profile where both the SPP and the NPP are uniform.

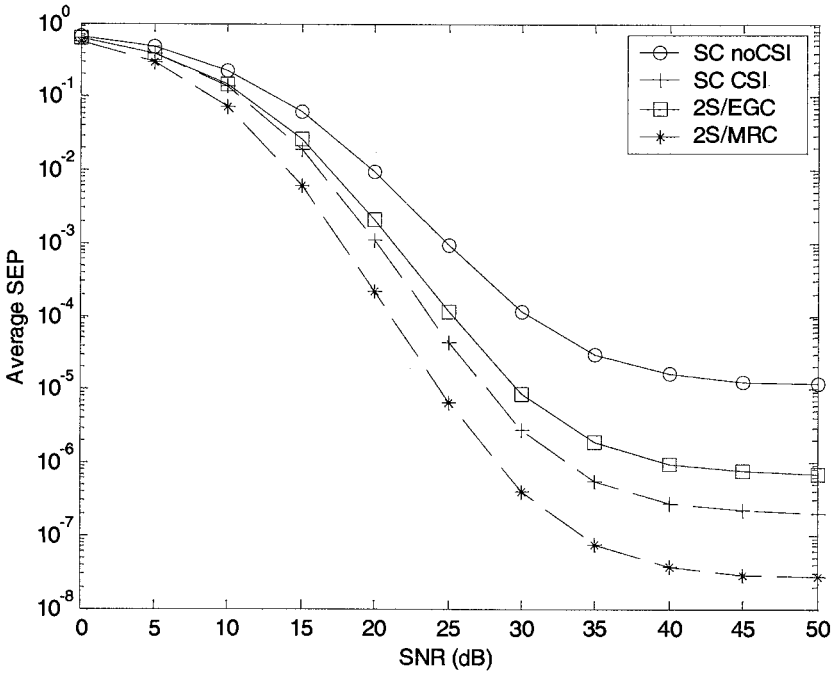

Figure 4.4: SEP of the four hybrid receivers in a channel with uniform SNR profile where the SPP and NPP are identically exponential with profiles defined in (4.105) and (4.106) respectively.

and the noise powers are defined as

$$\sigma_{n_i}^2 = \frac{(1-e^{-a})}{(1-e^{-aN})} e^{-a(i-1)}, \tag{4.106}$$

where the profile decay parameter a=1. The SNR in all branches is, therefore, constant and equal to $\tilde{\Gamma}$. We observe in Figure 4.4 that the H-S/MRC receivers perform identically as in the uniform SNR profile in Figure 4.3. This was expected as the SEP of the H-S/MRC receivers is a function of the average SNR and not the individual SPP and NPP. The SEP of the SC and 2S/EGC receivers, on the other hand, is deteriorated compared to the SEP in Figure 4.3. This indicates the dependence of the SEP of the receivers analysed in this chapter on the individual NPP and SPP instead of the SNR profile.

We, next, investigate the effect of the SPP on the performance of the H-S/EGC receiver in relation to the performance of the H-S/MRC receiver. As explained in Section 4.3 we expect the SPP to affect the *error floor* of the CSI (SC CSI and 2S/MRC) and noCSI (SC noCSI and 2S/EGC) receivers in a different way but would produce no discrepancy in the static fading region above the error floor. We first plot in Figure 4.5 the SEP of the four receivers for a static Rayleigh fading channel with $f_D = 0$ with a uniform NPP and exponential SPP (profile exp2). We observe that the relative performance of the four receivers is identical to the performance shown in Figure 4.3 for the uniform SPP and NPP profile. The exponential SPP has, therefore, no effect on the relative performance of the four receivers. Next we plot in Figure 4.6 and Figure 4.7 the SEP of the four receivers for a channel with a uniform NPP and exponential SPP but with non-static Rayleigh fading with $f_D = 0.01$. The SNR profiles used for the exponential SPP are the exp1 and exp2, respectively, shown in Table 4.1. We observe that the greater unevenness of the signal powers in Figure 4.7 results in a greater disparity between the floors of the noCSI and the CSI receivers. For the moderate profile in Figure 4.6 the 2S/EGC receiver outperforms the SC CSI receiver which is an encouraging sign when operation in channels with no CSI is necessary. We observe that the penalty of operating without CSI is reduced in profiles with moderate imbalance, so that a 2S/EGC receiver could outperform a SC receiver using CSI.

As explained in Section 4.3 we expect the NPP to affect the asymptotic SEP of the CSI and noCSI receivers differently in the *static fading region* whereas it would not affect their error floor. To demonstrate the effect of the NPP, we first plot in Figure 4.8 the SEP of the four receivers operating in a Rayleigh fading channel with $f_D = 0.01$ and an exponential SNR profile

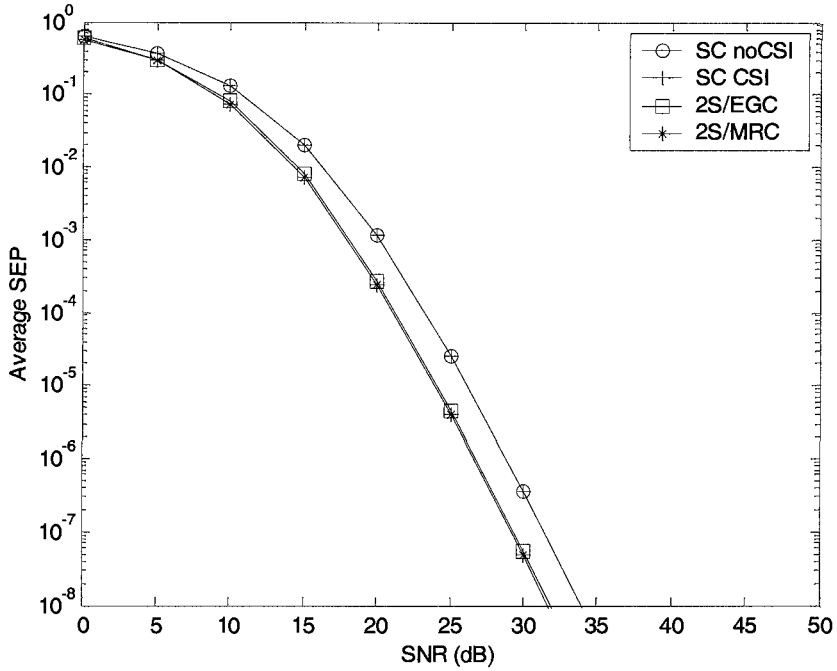

Figure 4.5: SEP of the four hybrid receivers in a static Rayleigh fading channel with the exponential SNR profile exp2 where the NPP is uniform and the SPP is exponential.

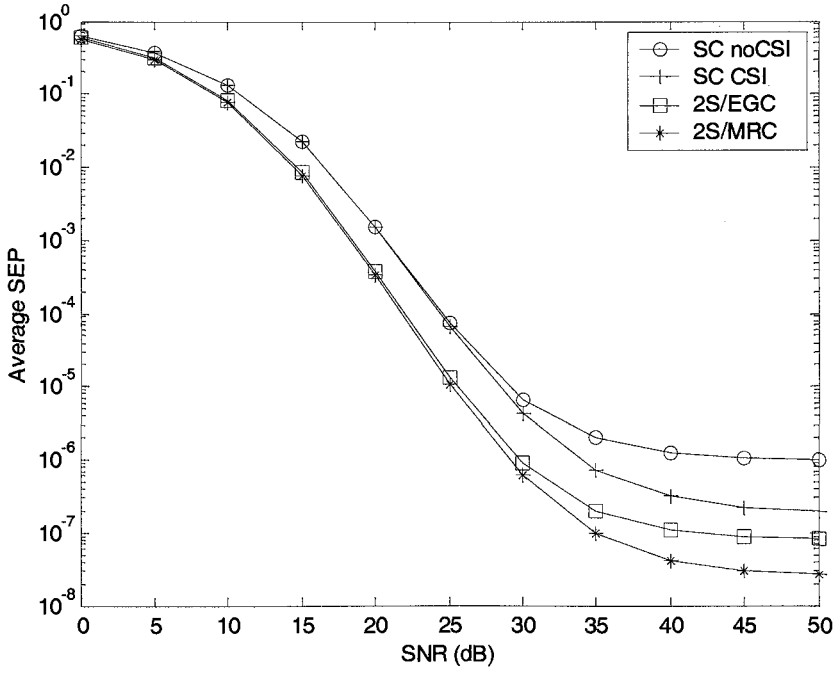

Figure 4.6: SEP of the four hybrid receivers in a Rayleigh channel with normalized fade rate $f_D = 0.01$. The SNR profile is the exp1 profile in Table 4.1 where the NPP is uniform and the SPP is exponential.

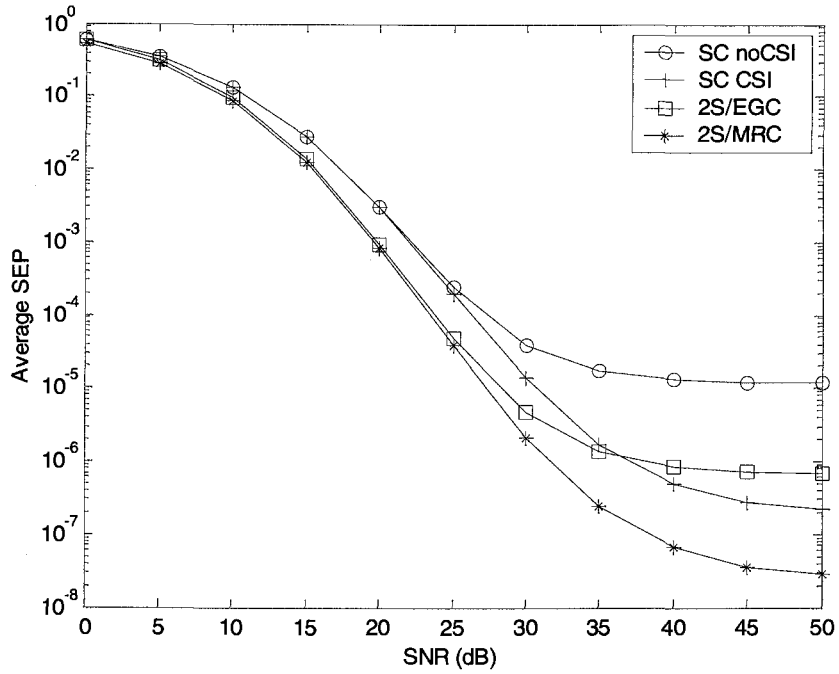

Figure 4.7: SEP of the four hybrid receivers in a Rayleigh channel with normalized fade rate $f_D = 0.01$. The SNR profile is the exp2 profile in Table 4.1 where the NPP is uniform and the SPP is exponential.

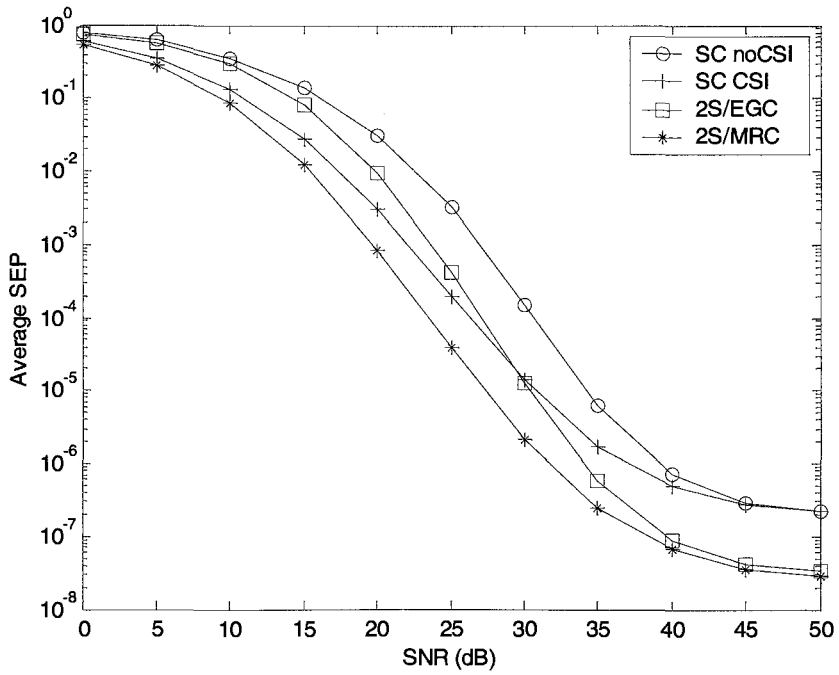

Figure 4.8: SEP of the four hybrid receivers in a Rayleigh channel with normalized fade rate $f_D = 0.01$. The SNR profile is the exp2 profile in Table 4.1 where the SPP is uniform and the NPP is exponential.

with uniform SPP and exponential NPP (profile exp2). We observe that the relative error floors of the four receivers are identical to the error floors shown in Figure 4.3 for the uniform SPP and NPP case and, hence, the NPP has no effect on the relative error floors. We next plot in Figure 4.9 and Figure 4.10 the SEP of the four receivers for a channel with a uniform SPP and exponential NPP but with static Rayleigh fading with $f_D = 0$. The SNR profiles for the exponential SPP are the exp1 and exp2, respectively, shown in Table 4.1. We observe that the greater the unevenness of the NPP, indicated by the larger value of a, the larger the disparity in the static asymptotic SEP of the receivers. At the exp1 profile we observe, that as for the error floor regions in Figure 4.6 and Figure 4.7, the 2S/EGC receiver outperforms the SC CSI receiver in the more moderate exponential SPP.

In Figure 4.11 we plot the exact and asymptotic SEP of the four receivers which use binary DPSK in a Rayleigh fading channel with $f_D = 0.01$. The NPP is uniform and the SPP is exponential with a=1. We observe that the asymptotes match the exact curves in the error floor region. In Figure 4.12 we plot the exact and asymptotic SEP of the four receivers using DPSK with M=8 and operating in a static Rayleigh fading channel. The SPP is uniform and the NPP is exponential with a=1 in this case. We observe that the asymptotes approach the exact curves at high SNR.

4.5 Conclusions

In this chapter we analysed the performance of two receivers which have no CSI knowledge and, therefore, cannot optimally select and combine the selected signals: The SC and the 2S/EGC receivers. We derived exact expressions for the SEP of both of these receivers and for the average SNR of the SC receiver. Furthermore we performed asymptotic analysis on the exact SEP expressions and obtained simple expressions to approximate the SEP at high SNR in the two possible operating regions: The static fading region and the error floor region.

In Section 4.4 we demonstrated that when the SPP and NPP are uniform the SC noCSI and 2S/EGC receivers provide almost identical performance as the equivalent SC CSI and 2S/MRC receivers analysed in Chapter 3. In the case of SC the performance is, in fact, identical whereas in the case of the double selection the 2S/MRC receiver slightly outperforms the 2S/EGC receiver. We also demonstrated that a non-uniform SPP creates a larger disparity between the error floors of the CSI (SC CSI and 2S/MRC) and noCSI (SC noCSI and 2S/EGC) receivers whereas a non-uniform NPP creates a larger disparity in the static fading region.

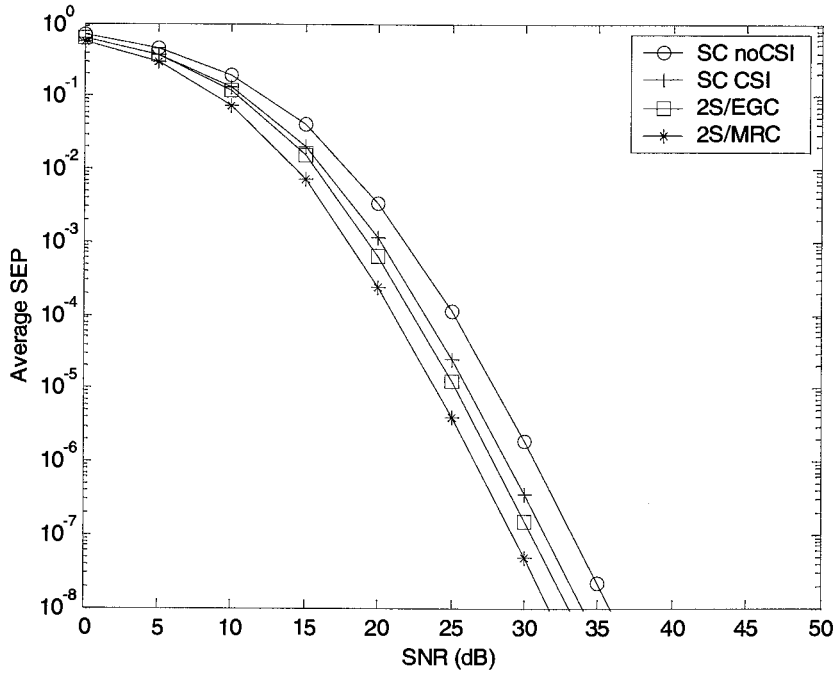

Figure 4.9: SEP of the four hybrid receivers in a static Rayleigh fading channel. The SNR profile is the exp1 profile in Table 4.1 where the SPP is uniform and the NPP is exponential.

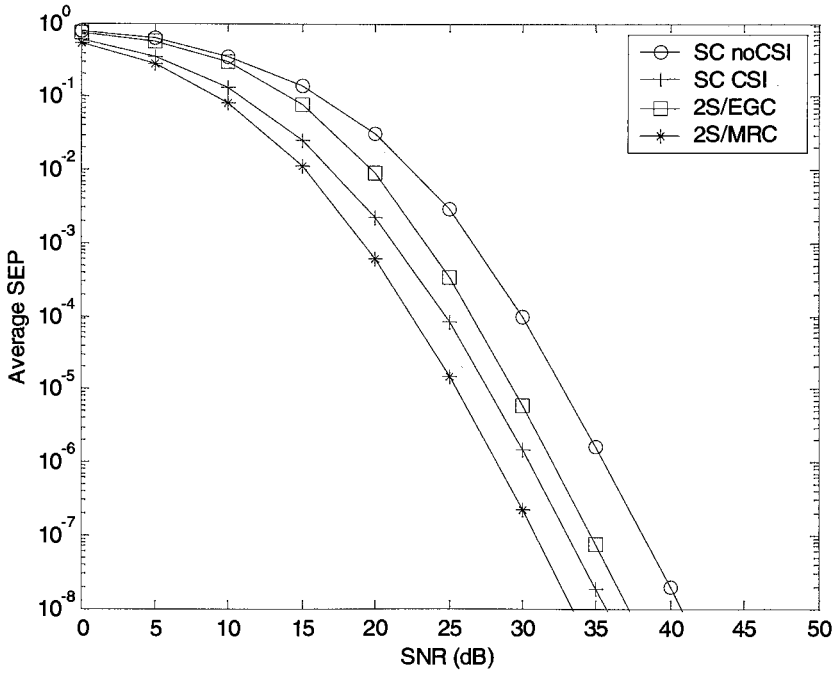

Figure 4.10: SEP of the four hybrid receivers in a static Rayleigh fading channel. The SNR profile is the exp2 profile in Table 4.1 where the SPP is uniform and the NPP is exponential.

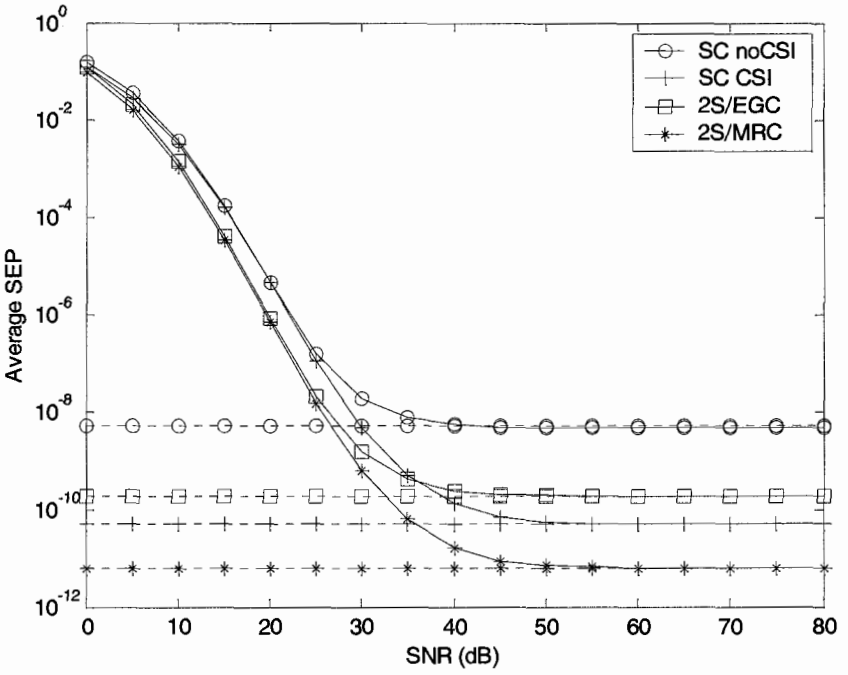

Figure 4.11: SEP of the four hybrid receivers using binary DPSK in a Rayleigh channel with normalized fade rate $f_D = 0.01$. The SNR profile is the exp2 profile in Table 4.1 where the NPP is uniform and the SPP is exponential.

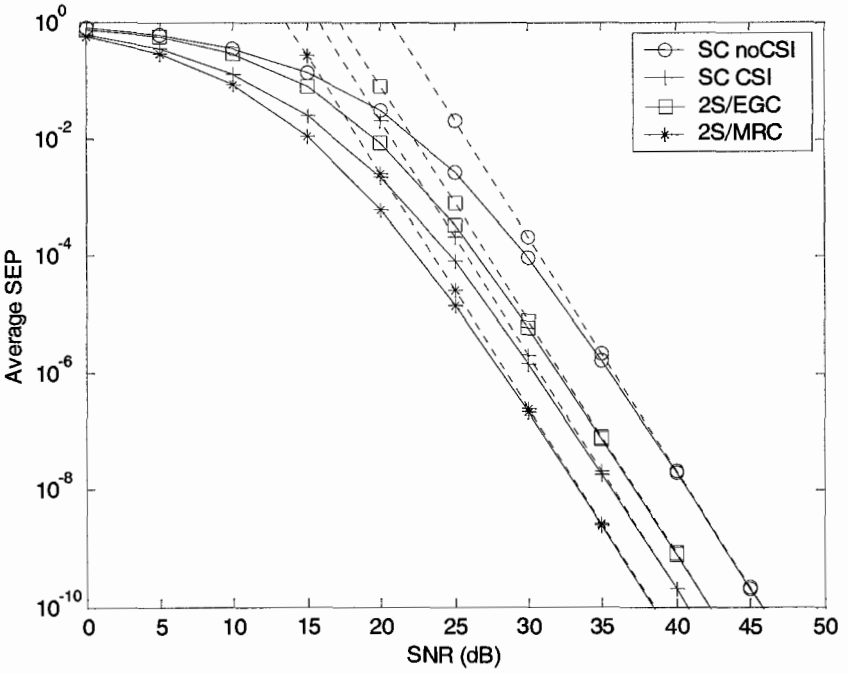

Figure 4.12: SEP of the four hybrid receivers using 8-PSK in a static Rayleigh fading channel. The SNR profile is the exp2 profile in Table 4.1 where the SPP is uniform and the NPP is exponential.

Chapter 5

Unified Asymptotic Analysis of Hybrid Diversity Receivers

In Chapter 3 we derived exact expressions for the SEP of the H-S/MRC receiver, which has access to the channel statistical information (CSI) and employs optimum MMSE channel estimation. Furthermore, in Chapter 4 we derived exact SEP expressions for two special cases of receivers without access to the CSI, which use DPSK modulation; the SC noCSI and the 2S/EGC receivers. It was indicated in Chapter 4 that it is not possible to derive a meaningful, exact SEP expression for the general case of the receiver, which selects L branches and combines them using EGC, due to the presence of a sum of Rayleigh distributed random variables. In this chapter, we follow a unified approach to derive concise, general, closed-form expressions for the SEP of hybrid diversity receivers (HDR) *operating at high SNR's*. We consider the general hybrid selection/equal gain combining (H-S/EGC) receiver but we also revisit the H-S/MRC receiver to better demonstrate our approach to asymptotic analysis as well as to provide a unified framework for the comparison of the two types of receivers. These asymptotic expressions provide insight into the factors affecting the performance of the HDR's as well as into the performance of the classical diversity receivers, SC, EGC and MRC, which are special cases. The expressions derived in this chapter are unique in their simplicity and are derived with the help of a solution to a multiple integral derived in Appendix B. The solution to the integral appears to be unique, at least in the receiver diversity field.

Typically, researchers in the field of receiver diversity derive exact expressions for the SEP of a receiver and then proceed to apply simplifications, which are true under certain conditions, to obtain an approximate expression. This is also the procedure we followed in Chapter 3 for the performance of H-S/MRC and in Chapter 4 for the performance of the SC and the 2S/EGC receivers. The analysis consisted of first deriving exact expressions for the SEP and then obtaining their asymptotic approximations. In this chapter, we deviate from this practice and instead we directly derive asymptotic SEP expressions by applying high SNR approximations in the beginning and throughout the derivation. This approach enables us to derive *general*

expressions for the asymptotic SEP of the H-S/MRC and H-S/EGC receivers and aids in the comparison of the two types of receivers. The results are useful because they provide guidelines into the complexity and performance trade-off considerations of building such systems. As far as it has been possible to determine there is no known analysis in the literature for the H-S/EGC receiver analysed in this chapter.

Asymptotic analysis as a goal in itself has received some attention in the past. Leib and Pasupathy in [48] looked at the asymptotic distribution of the phase of a vector perturbed by Gaussian noise. In [41] Abdel-Ghaffar and Pasupathy derived asymptotic expressions for the SEP of 2 types of MRC and 2 types of EGC receivers and they related the asymptotic expressions to the conditional error rates of the receivers. Furthermore, Brehler and Varanasi in [49] provided general asymptotic error rate analysis of coherent, differentially coherent, and noncoherent MIMO systems in Rayleigh-fading channels.

5.1 Asymptotic Analysis of the H-S/MRC Receiver

In this section, we derive the asymptotic SEP of the H-S/MRC receiver. While the expression derived directly from the exact SEP expression has already been derived in (3.42), this section serves as an introduction to the concept of deriving asymptotic expressions without first obtaining the exact expressions. This section also serves as preparation for the more complex derivation of the asymptotic SEP for the H-S/EGC receiver.

We begin with the expression for calculating the exact SEP of the H-S/MRC receiver shown in (3.25). We amend (3.25) by explicitly showing the joint pdf of the SNR variables and, merging the exponential terms. The resulting expression is shown below:

$$P_e = \frac{1}{\pi(\Gamma_0)^N} \sum_{\mathbf{P}_k} \int_0^{\Phi} \int_0^{\infty} \int_0^{\gamma_{(1)}} \cdots \int_0^{\gamma_{(N-1)}} \exp\left(-\sum_{i=1}^{N} \gamma_{(i)} \left(K(\varphi) a_i + \frac{1}{\Gamma_{k_i}} \right) \right) d\gamma_{(N)} \cdots d\gamma_{(2)} d\gamma_{(1)} d\varphi \,. \tag{5.1}$$

where a_i was defined in (3.22) and is shown below:

$$a_i = \begin{cases} 1 & i = 1,2,\cdots,L \\ 0 & \text{otherwise} \end{cases} . \tag{5.2}$$

We note that when $a_i = 1$, i=1,2,...L, the following inequality holds:

$$K(\varphi) + \frac{1}{\Gamma_{k_i}} = \frac{\sin^2(\pi/M)}{\sin^2(\varphi)} + \frac{1}{\Gamma_{k_i}} \geq \frac{\sin^2(\pi/M)}{\sin^2(\varphi)} . \tag{5.3}$$

At high SNR the right hand side of the inequality in (5.3) is a tight lower bound, therefore, we may use the approximation

$$K(\varphi)+\frac{1}{\Gamma_{k_i}}\approx K(\varphi)\,. \tag{5.4}$$

This can be justified by recalling that $\Gamma_{k_i}\to\infty$ and that $\sin^2\varphi\le 1$, i.e. $\sin^2\varphi$ is upper bounded by 1. Therefore, even at the maximum value of $\sin^2\varphi$ the approximation is valid due to the large value of Γ_{k_i}. The only possible complication might be at very large constellation sizes for which M is large and $\sin^2(\pi/M)\to 0$. For $i>L$, $a_i=0$ and the exponent terms in (5.1) for $i=L+1,L+2,...,N$ are simply $1/\Gamma_{k_i}$. The issue now is the following: Can we ignore the integral

$$I=\int_0^{\gamma_{(L)}}\cdots\int_0^{\gamma_{(N-1)}}\exp\left(-\sum_{i=L+1}^{N}\left(\frac{\gamma_{(i)}}{\Gamma_{k_i}}\right)\right)d\gamma_{(N)}\cdots d\gamma_{(L+1)} \tag{5.5}$$

or must we include the evaluation of the N-L integrals in the solution? To answer this question, let us consider the entire summation in the exponent in (5.1) by replacing a_i with the values given in (3.22). The exponent in (5.1) can be expanded as follows:

$$\sum_{i=1}^{N}\gamma_{(i)}\left(K(\varphi)a_i+\frac{1}{\Gamma_{k_i}}\right)=\sum_{i=1}^{L-1}\gamma_{(i)}\left(K(\varphi)+\frac{1}{\Gamma_{k_i}}\right)+\left[\left(\gamma_{(L)}K(\varphi)+\frac{\gamma_{(L)}}{\Gamma_{k_L}}\right)+\sum_{i=L+1}^{N}\left(\frac{\gamma_{(i)}}{\Gamma_{k_i}}\right)\right]. \tag{5.6}$$

The justification for approximating (5.6) is similar to the justification for (5.3). From the definition of the variables $\gamma_{(i)}$ we know that they are arranged in descending order. We may therefore use the following inequality for the bracketed term in the right hand side of (5.6):

$$\left[\gamma_{(L)}K(\varphi)+\frac{\gamma_{(L)}}{\Gamma_{k_L}}+\sum_{i=L+1}^{N}\left(\frac{\gamma_{(i)}}{\Gamma_{k_i}}\right)\right]=\gamma_{(L)}K(\varphi)+\sum_{i=L}^{N}\left(\frac{\gamma_{(i)}}{\Gamma_{k_i}}\right)\approx\gamma_{(L)}K(\varphi)\,. \tag{5.7}$$

With (5.7) and (5.4) we may simplify (5.1) as follows:

$$P_e\approx\frac{1}{\pi(\Gamma_0)^N}\sum_{\mathbf{P}_k}\int_0^{\Phi}\int_0^{\infty}\int_0^{\gamma_{(1)}}\cdots\int_0^{\gamma_{(N-1)}}\exp\left(-\sum_{i=1}^{L}\gamma_{(i)}K(\varphi)\right)d\gamma_{(N)}\cdots d\gamma_{(2)}d\gamma_{(1)}d\varphi\,. \tag{5.8}$$

Next, we use the "virtual branch technique", as outlined in Section 2.6, to convert the variables $\gamma_{(i)}$ into the new set of independent variables u_i and, thus, the SEP in (5.1) can be expressed as

$$P_e\approx\frac{1}{\pi\Gamma_0^N}\sum_{\mathbf{P}_k}\int_0^{\Phi}\int_0^{\infty}\int_0^{\infty}\cdots\int_0^{\infty}\exp\left(-K(\varphi)\sum_{i=1}^{N}c_iu_i\right)du_N\cdots du_2du_1d\varphi \tag{5.9}$$

where c_i was defined in (3.31) as

$$c_i = \sum_{n=1}^{i} a_n = \begin{cases} i & i \le L \\ L & L < i \le N \end{cases}. \tag{5.10}$$

The integrand in (5.9) is a product of exponentials and the inner N integrals are easily evaluated to produce the expression

$$P_e \approx \frac{N! K_\varphi}{\pi L! L^{N-L}} \left(\frac{1}{\Gamma_0} \right)^N, \tag{5.11}$$

where K_φ was defined in (3.43) as

$$K_\varphi = \int_0^\Phi \frac{d\varphi}{K(\varphi)^N}. \tag{5.12}$$

Comparing (5.11) with (3.42) we observe that they are identical. As a result of using the lower bounds of the quantities in (5.7) and (5.4), the expression in (5.11) provides an upper bound to the SEP.

Up to this point, the quantities used in calculating the approximate SEP expression have been those estimated at the receiver. We now use the high SNR approximations listed in (4.61)-(4.65) to introduce the relevant channel statistical parameters. While, as in Chapter 3, the expression is valid for both PSAM and DPSK (or any other MMSE estimation method), in this chapter we concentrate on DPSK. Consequently, (5.11) may be expressed in terms of the average signal and noise powers that define the SPP and NPP of the channel. Recall the results in Figure 3.2, where, in spite of using optimum MMSE weighting factors to combine the H-S/MRC signal, the receiver using DPSK could not avoid the appearance of the error floor. It is, therefore, necessary, as in Section 4.3, to provide two separate expressions for the static fading and the error floor asymptotes. The two expressions are, respectively,

$$P_{e\_static} \approx \frac{2^N N! K_\varphi}{\pi L! L^{N-L} \left(\prod_{i=1}^{N} \tilde{\Gamma}_i \right)} \tag{5.13}$$

and

$$P_{e\_floor} \approx \frac{(1/J^2 - 1)^N N! K_\varphi}{\pi L! L^{N-L}}, \tag{5.14}$$

where

$$\tilde{\Gamma}_i = \frac{\sigma_{g_i}^2}{\sigma_{n_i}^2} \tag{5.15}$$

is the actual average SNR defined as the ratio of the arriving signal and noise powers. In contrast, Γ_i used throughout this thesis is the average *estimated* SNR defined as the ratio of the *estimated* signal and *effective* noise powers. The error floor is determined by L, N and the fade rate, f_D as can be seen in (5.14). Furthermore, the static fading asymptote, P_{e_static} in (5.13) is determined by L, N and the geometric mean of the average branch SNR's. The quantity of interest in this case is not the individual signal or noise powers but, instead, their ratio.

As noted in Section 3.2.2, the integral K_φ can be evaluated to the exact expression shown in (3.44). For the special case of binary communications the two asymptotic expressions in (5.13) and (5.14) can be simplified even further by means of (3.45) to obtain the asymptotic bit error rate as respectively

$$P_{e\_static} \approx \frac{(2N-1)!!}{2L!L^{N-L}\left(\prod_{i=1}^{N}\tilde{\gamma}_i\right)} \tag{5.16}$$

and

$$P_{e\_floor} \approx \frac{(1/J^2-1)^N(2N-1)!!}{2^{N+1}L!L^{N-L}}, \tag{5.17}$$

where the notation $2k!!$ denotes the product $2\cdot 4\cdot 6\cdots 2k$ and the notation $(2k\text{-}1)!!$ denotes the product $1\cdot 3\cdot 5\cdots(2k-1)$ where k is any integer.

5.2 Asymptotic Analysis of the H-S/EGC Receiver

In this section, we derive an asymptotic approximation for the SEP of the H-S/EGC receiver. We consider the problem of selecting and combining the L strongest diversity branches out of the available N, where $1 \le L \le N$. This receiver is a *generalized* version of the SC and 2S/EGC receivers analysed in Chapter 4, which selected L=1 and L=2 branches out of N. Similarly to the SC and 2S/EGC receivers, the H-S/EGC receiver has N available diversity branches and operates in a Rayleigh fading environment employing DPSK modulation.

The receiver uses the previous received symbol in each branch as the channel estimate and bases the branch selection on the SPN of that symbol as explained in Chapter 4. The decision variable for the demodulator is a generalized form of (4.39) and is given by

$$y = \sum_{i=1}^{L} r_{(i)} \frac{h_{(i)}^*}{|h_{(i)}|}, \tag{5.18}$$

where $1 \le L \le N$. By expressing the received symbol in each branch as

$$r_i = w_i^* h_i + v_i \tag{5.19}$$

we may express the decision variable shown in (5.18) as

$$y = \left(\sum_{i=1}^{L} w_{k_i}^* \left| h_{(i)} \right| \right) + \left(\sum_{i=1}^{L} v_{k_i} \frac{h_{(i)}^*}{\left| h_{(i)} \right|} \right), \tag{5.20}$$

where w_i was defined in (4.4) for DPSK as

$$w_i = \frac{\sigma_{g_i h_i}}{\sigma_{h_i}^2}. \tag{5.21}$$

v_i is the effective noise defined in (4.9) as

$$v_i = e_i + n_i, \tag{5.22}$$

where e_i is a random variable, independent of h_i, defined as

$$e_i = g_i - w_i^* h_i. \tag{5.23}$$

For the decision variable in (5.20) the corresponding instantaneous SNR is defined as

$$\gamma = \frac{\frac{1}{2}\left| \sum_{i=1}^{L} w_{k_i}^* \left| h_{(i)} \right| \right|^2}{\frac{1}{2} E\left[\left| \sum_{i=1}^{L} v_{k_i} \frac{h_{(i)}^*}{\left| h_{(i)} \right|} \right|^2 \right]} = \frac{\frac{1}{2}\left| \sum_{i=1}^{L} w_{k_i}^* \left| h_{(i)} \right| \right|^2}{\sum_{i=1}^{L} \mathcal{N}_{k_i}}, \tag{5.24}$$

where $\mathcal{N}_i$ was defined in (2.32) as $\mathcal{N}_i = \sigma_{v_i}^2 = \sigma_{e_i}^2 + \sigma_{n_i}^2$.

5.2.1 Symbol Error Probability Analysis

To derive the exact expression for the SEP of the H-S/EGC diversity receiver we use the random variables l_i, which were defined in (4.42) as

$$l_i = \left| h_i \right|. \tag{5.25}$$

The l_i's are statistically independent and Rayleigh distributed, with probability density functions defined in (4.43) as

$$f_{l_i}(x) = \frac{x}{\Lambda_i} e^{-\frac{x^2}{2\Lambda_i}}, \tag{5.26}$$

where

$$\Lambda_i = \frac{1}{2} E[l_i^2] = \frac{1}{2} E[\left| h_i \right|^2]. \tag{5.27}$$

As in the previous chapters, we use the SEP expression conditioned on the instantaneous SNR introduced by Pawula et al in [38]. Using the new variables and the ordered variable notation introduced in Section 2.6, the conditional SEP can be expressed in integral form in terms of $\mathbf{l} = \{l_{(1)}, l_{(2)}, ..., l_{(N)}\}$ as

$$P_{e|\mathbf{l}} = \frac{1}{\pi}\int_0^{\Phi} \exp\left(-K(\varphi) \frac{\left|\sum_{i=1}^{L} w_{k_i}^* l_{(i)}\right|^2}{2\left(\sum_{i=1}^{L} \mathcal{N}_{k_i}\right)} \right) d\varphi . \tag{5.28}$$

The expression in (5.28) is a generalization of the average SEP expression shown in (4.46). We obtain the average SEP of the H-S/EGC receiver by averaging over all possible permutations $\mathbf{P}_k$ of the N branches as follows:

$$P_e = \frac{1}{\pi}\sum_{\mathbf{P}_k}\int_0^{\Phi}\int_0^{\infty}\cdots\int_0^{l_{(N-1)}} \exp\left(-K(\varphi) \frac{\left|\sum_{i=1}^{L} w_{k_i}^* l_{(i)}\right|^2}{2\left(\sum_{i=1}^{L} \mathcal{N}_{k_i}\right)} \right) \left(\prod_{i=1}^{N} \frac{l_{(i)}}{\Lambda_{k_i}} \exp\left(-\frac{l_{(i)}^2}{2\Lambda_{k_i}} \right) \right) dl_{(N)} \cdots dl_{(1)} d\varphi . \tag{5.29}$$

By combining the exponential terms, we observe that the following inequality holds:

$$K(\varphi) \frac{\left|\sum_{i=1}^{L} w_{k_i}^* l(i)\right|^2}{2\left(\sum_{i=1}^{L} \mathcal{N}_{k_i}\right)} + \sum_{i=1}^{N} \frac{l(i)^2}{2\Lambda_{k_i}} \geq K(\varphi) \frac{\left|\sum_{i=1}^{L} w_{k_i}^* l(i)\right|^2}{2\left(\sum_{i=1}^{L} \mathcal{N}_{k_i}\right)} . \tag{5.30}$$

The approach for calculating the SEP approximation for the H-S/EGC receiver is conceptually the same as the approach followed for the H-S/MRC receiver. We observe that, as in (5.9), a similar simplification can be performed at high SNR to eliminate the term $\sum_{i=1}^{N} l(i)^2 / 2\Lambda_{k_i}$ which originates from the pdf of the Rayleigh variables. This is possible since at large SNR the term $\sum_{i=1}^{N} l(i)^2 / 2\Lambda_{k_i}$ is much smaller than the first term and the following approximation is tight:

$$K(\varphi) \frac{\left|\sum_{i=1}^{L} w_{k_i}^* l(i)\right|^2}{2\left(\sum_{i=1}^{L} \mathcal{N}_{k_i}\right)} + \sum_{i=1}^{N} \frac{l(i)^2}{2\Lambda_{k_i}} \approx K(\varphi) \frac{\left|\sum_{i=1}^{L} w_{k_i}^* l(i)\right|^2}{2\left(\sum_{i=1}^{L} \mathcal{N}_{k_i}\right)} . \tag{5.31}$$

Furthermore, in static fading w_i and $\mathcal{N}_i$ may be approximated by

$$w_i \approx 1, \tag{5.32}$$

$$\mathcal{N}_i \approx 2\sigma_{n_i}^2 . \tag{5.33}$$

With the approximations in (5.31)-(5.33), the SEP shown in (5.29) can be approximated by

$$P_e \approx \frac{1}{\pi}\sum_{\mathbf{P}_k}\int_0^{\Phi}\int_0^{\infty}\cdots\int_0^{l_{(N-1)}}\left(\prod_{i=1}^{N}\frac{l_{(i)}}{\Lambda_{k_i}}\right)\exp\left(-K(\varphi)\frac{\left(\sum_{i=1}^{L} l_{(i)}\right)^2}{2\left(\sum_{i=1}^{L} 2\sigma_{n_{k_i}}^2\right)}\right) dl_{(N)}\cdots dl_{(1)}d\varphi. \tag{5.34}$$

For clarity the following function is defined:

$$K(\varphi,k) = \frac{K(\varphi)}{4\sum_{i=1}^{L}\sigma_{n_{k_i}}^2}, \tag{5.35}$$

where the variables k and φ indicate the dependence of $K(\varphi,k)$ on the $N!$ branch permutations, as discussed in Section 2.6, as well as on the integration angle φ. Using the definition in (5.35), the asymptotic SEP approximation of (5.34) may be rewritten as

$$P_e \approx \frac{1}{\pi\Lambda_0^N}\sum_{\mathbf{P}_k}\int_0^{\Phi}\int_0^{\infty}\cdots\int_0^{l_{(N-1)}}\left(\prod_{i=1}^{N} l_{(i)}\right)\exp\left(-K(\varphi,k)\left(\sum_{i=1}^{L} l_{(i)}\right)^2\right) dl_{(N)}\cdots dl_{(1)}d\varphi, \tag{5.36}$$

where Λ_0 is the geometric mean of the Λ_i's and was defined in (4.22) as

$$\Lambda_0 = \left(\prod_{i=1}^{N}\Lambda_i\right)^{1/N}. \tag{5.37}$$

The first step in evaluating the integral in (5.36) is to evaluate the $N-L$ innermost integrals as shown below:

$$\int_0^{l_{(L)}}\cdots\int_0^{l_{(N-1)}}\left(\prod_{i=L+1}^{N} l_{(i)}\right) dl_{(N)}\cdots dl_{(L+1)} = \frac{l_{(L)}^{\,2(N-L)}}{2^{N-L}(N-L)!}. \tag{5.38}$$

Substituting (5.38) into (5.36) and separating terms produces the expression

$$P_e \approx \frac{1}{\pi\Lambda_0^N 2^{N-L}(N-L)!}\sum_{\mathbf{P}_k}\int_0^{\Phi}\int_0^{\infty}\cdots\int_0^{l_{(L-1)}} l_{(L)}^{\,2(N-L)}\left(\prod_{i=1}^{L} l_{(i)}\right)\times$$

$$\exp\left(-K(\varphi,k)\left(\sum_{i=1}^{L} l_{(i)}\right)^2\right) dl_{(L)}\cdots dl_{(1)}d\varphi. \tag{5.39}$$

The dependency of the upper limits of each integral in (5.39) to the next largest integration variable may be removed with the familiar "virtual branch technique" described in Section 2.6. The transformation results in the following expression for the asymptotic SEP in terms of the independent variables u_i:

$$P_e \approx \frac{1}{\pi \Lambda_0^N 2^{N-L}(N-L)!} \sum_{\mathbf{P}_k} \int_0^{\Phi} \int_0^{\infty} \cdots \int_0^{\infty} u_L^{2(N-L)} \left(\prod_{i=1}^{L} \sum_{j=i}^{L} u_j \right) \times$$

$$\exp\left(-K(\varphi,k) \left(\sum_{i=1}^{L} i u_i \right)^2 \right) du_1 \cdots du_L d\varphi \,. \tag{5.40}$$

The term $\prod_{i=1}^{L} \sum_{j=i}^{L} u_j$ in (5.40), which is a product of sums of the variables u_i, expands to a sum of $L!$ products of the variables u_i as shown below:

$$\left(\prod_{i=1}^{L} \sum_{j=i}^{L} u_j \right) = \sum_{\mathbf{Q}_n} \left(\prod_{j=1}^{L} u_j^{q(n,j)} \right). \tag{5.41}$$

$\mathbf{Q}$ denotes a matrix with $L!$ rows and L columns containing in each row the exponents of u_j. In other words, the n-th row of this matrix contains the vector $\mathbf{Q}_n = [q(n,1), q(n,2), \ldots, q(n,L)]$, each element of which is the exponent of $[u_1, u_2, \ldots, u_N]$ in the product $\prod_{j=1}^{L} u_j^{q(n,j)}$. The exponents $q(n,j)$ are non-negative integers in the range $[0,L]$ satisfying $\sum_{j=1}^{L} q(n,j) = L$. We use the alternative sum of products form shown in (5.41), to express (5.40) in the more convenient form shown below:

$$P_e \approx \frac{1}{\pi \Lambda_0^N 2^{N-L}(N-L)!} \sum_{\mathbf{P}_k} \sum_{\mathbf{Q}_n} \int_0^{\Phi} \int_0^{\infty} \cdots \int_0^{\infty} u_L^{2(N-L)} \left(\prod_{j=1}^{L} u_{n_j}^{q(n,j)} \right) \times$$

$$\exp\left(-K(\varphi,k) \left(\sum_{i=1}^{L} i u_i \right)^2 \right) du_1 \cdots du_L d\varphi \,. \tag{5.42}$$

In Appendix B we derive the solution to the more general multiple integral shown below:

$$\int_0^{\infty} \cdots \int_0^{\infty} \left(\prod_{i=1}^{N} x_i^{b_i} \right) \exp\left(-K \left(\sum_{i=1}^{N} a_i x_i \right)^2 \right) dx_1 \cdots dx_N = \frac{1}{2^N K^N (2N-1)!!} \left(\prod_{i=1}^{N} a_i^{-b_i-1} \right) \left(\prod_{i=1}^{N} b_i! \right). \tag{5.43}$$

The solution provided in Appendix B and reproduced in (5.43) can be adapted to match the L inner integrals of interest in (5.42) as follows:

$$\int_0^{\infty} \cdots \int_0^{\infty} u_L^{2(N-L)} \left(\prod_{j=1}^{L} u_{n_j}^{q(n,j)} \right) \exp\left(-K(\varphi,k) \left(\sum_{i=1}^{L} i u_i \right)^2 \right) du_1 \cdots du_L =$$

$$\frac{1}{2^N K(\varphi,k)^N (2N-1)!!} \left(\prod_{j=1}^{L} j^{-c(n,j)-1} \right) \left(\prod_{j=1}^{L} c(n,j)! \right), \tag{5.44}$$

where the notation $2k!!$ denotes the product $2\cdot 4\cdot 6\cdots 2k$ and the notation ($2k$-1) denotes the product $1\cdot 3\cdot 5\cdots(2k-1)$ where k is any integer and

$$c(n,j)=\begin{cases} q(n,j) & j=1,2,\cdots,L-1 \\ q(n,L)+2(N-L) & j=L \end{cases}. \tag{5.45}$$

We incorporate the integral evaluation shown in (5.44) into (5.42) to obtain the asymptotic SEP expression

$$P_e \approx \frac{1}{\pi\Lambda_0^N 2^{2N-L}L!(N-L)!(2N-1)!!}\sum_{\mathbf{Q}_n}\left(\prod_{j=1}^{L}\frac{c(n,j)!}{j^{c(n,j)}}\right)\sum_{\mathbf{P}_k}\int_0^{\Phi}\frac{1}{K(\varphi,k)^N}d\varphi. \tag{5.46}$$

We obtain the final form by substituting (5.35) back in (5.46) as follows:

$$P_e \approx \frac{2^N C(L,N)K_\varphi}{\pi}\frac{\left(\frac{1}{N!}\sum_{\mathbf{P}_k}\left(\sum_{i=1}^{L}\sigma_{n_{ki}}^2\right)^N\right)}{\left(\prod_{i=1}^{N}\Lambda_i\right)}, \tag{5.47}$$

where

$$C(L,N)=\frac{\binom{N}{L}\sum_{\mathbf{Q}_n}\left(\prod_{j=1}^{L}\frac{c(n,j)!}{j^{c(n,j)}}\right)}{2^{N-L}(2N-1)!!}. \tag{5.48}$$

An alternative form of (5.48) may be obtained with the help of the following axiom[1]:

$$\sum_{\mathbf{Q}_n}\left(\prod_{j=1}^{L}\frac{c(n,j)!}{i^{c(n,j)}}\right)=\sum_{i=0}^{L-1}\binom{L-1}{i}\frac{(2(N-L)+1+i)!}{L^{2(N-L)+1+i}}. \tag{5.49}$$

Consequently, $C(L,N)$ can be written in the following form which can be calculated more conveniently than (5.48):

$$C(L,N)=\frac{\binom{N}{L}\left(\sum_{i=0}^{L-1}\binom{L-1}{i}\frac{(2(N-L)+1+i)!}{L^{2(N-L)+1+i}}\right)}{2^{N-L}(2N-1)!!}. \tag{5.50}$$

In Figure 5.1 we plot the function $C(L,N)$ versus L. Recall that N refers to the total number of available branches and L refers to the number of selected branches. We set the value of N to 4, 6

[1] This axiom may be verified using numerical methods.

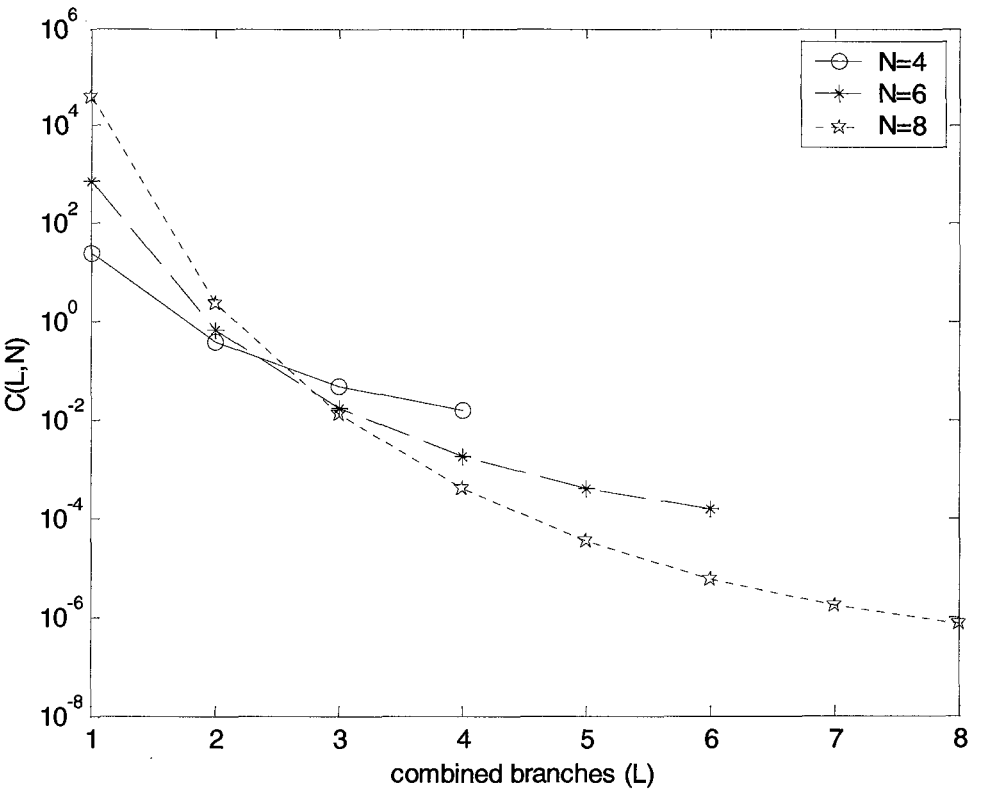

Figure 5.1: Three plots of the function $C(L,N)$ versus L obtained by setting N to the values 4, 6 and 8.

and 8 and for each N we plot the value of $C(L,N)$ for $1 \le L \le N$. We observe that the function $C(L,N)$ is monotonically decreasing for a fixed N but its slope decreases as L increases.

We can draw two conclusions from the expression in (5.47):

1. The asymptotic SEP depends on a function of the general arithmetic mean of the effective noise powers over the geometric mean of the SPN powers of the N branches as shown below:

$$r_h = \frac{\left(\frac{1}{N!} \sum_{\mathbf{P}_k} \left(\sum_{i=1}^{L} \sigma^2_{n_{k_i}} \right)^N \right)}{\left(\prod_{i=1}^{N} \Lambda_i \right)}. \tag{5.51}$$

2. The asymptotic SEP depends on $C(L,N)$, a function of L and N which is monotonically decreasing for a fixed N and increasing L as shown in Figure 5.1

In static fading we may use the approximations shown in (4.61)-(4.65) to produce the asymptotic SEP expression of the H-S/EGC receiver as follows:

$$\tilde{P}_{e\_static} \approx \frac{2^N C(L,N) K_\varphi}{\pi} \frac{\left(\frac{1}{N!} \sum_{\mathbf{P_k}} \left(\sum_{i=1}^{L} \sigma_{n_{ki}}^2 \right)^N \right)}{\left(\prod_{i=1}^{N} \sigma_{g_i}^2 \right)}. \tag{5.52}$$

In (5.52) we observe a deviation from the expression derived for the H-S/MRC receiver in (5.16). Comparing (5.16) and (5.52) it is interesting to note that while in (5.16) only the *ratio* of the branch signal and noise powers is affecting the asymptotic SEP, in (5.52) the two sets of signal and noise powers affect the asymptotic SEP in a different way.

In this section we derived the asymptotic SEP expression for the H-S/EGC receiver operating in the Rayleigh channel. The final expression is concise and helps in identifying the factors affecting the asymptotic performance of the H-S/EGC receiver. Even though the Rayleigh model is used for this analysis, it is straightforward to expand the analysis to provide an expression for the Nakagami channel. The Nakagami pdf was shown in (2.40) and is reproduced below for the variables l_i:

$$f_{l_i}(x) = \frac{2}{\Gamma(m)} \left(\frac{m}{2\Lambda_i} \right)^m x^{2m-1} \exp\left(-\frac{mx^2}{2\Lambda_i} \right), \tag{5.53}$$

The main possible obstacles arising from (5.53) are the power ($2m$-1) of the variable x and the constant m inside the exponential. However, the first obstacle can be accommodated by the integral evaluation in Appendix B, since the derivation solves a more general integral, and the second obstacle is eliminated by the approximation in (5.31).

5.3 Special Cases

In this section we provide asymptotic SEP expressions for certain important special cases. The analysis, so far, considered receivers with generally non-uniform signal or noise power profiles. It is worthwhile to investigate if any simplifications can be applied to the asymptotic SEP when the receiver is operating in a uniform SNR profile. Furthermore, the special cases analysed in Chapter 4, the SC and 2S/EGC receivers, are considered here and an adjustment to the asymptotic approximation to the SEP of the 2S/EGC receiver is presented. Finally, the classical EGC, which combines all N available branches, is another important special case for which we provide a simple asymptotic expression.

5.3.1 Uniform Noise and Signal Power Profiles

When the diversity branches of the H-S/EGC receiver are affected by iid AWGN variables, the receiver is operating in a uniform NPP. This is the case most often analysed in the literature and the analysis is usually simpler than when a general profile is assumed. In [41] and [4] the analysis was general enough to include non-uniform NPP but no meaningful conclusions could be reached from the expressions derived therein. Of the few exceptions, is a comment in [41] that for the uniform NPP the SEP depends only on the $\tilde{\Gamma}_i$ which can also be verified by our analysis.

The special case of uniform NPP may be obtained from (5.52) by setting $\sigma_{n_i}^2 = \sigma_n^2$. The asymptotic static fading expression is shown below:

$$\tilde{P}_{e\_static} \approx \frac{2^N L^N K_\varphi C(L,N)}{\pi\left(\prod_{i=1}^{N} \tilde{\Gamma}_i\right)}, \tag{5.54}$$

where $\tilde{\Gamma}_i$ was defined in (5.15) as the actual received SNR. When the SPP is also uniform, the static fading asymptotic SEP of (5.52) is simplified even further as shown below:

$$\tilde{P}_{e\_static} \approx \frac{2^N L^N K_\varphi C(L,N)}{\pi \tilde{\Gamma}^N}. \tag{5.55}$$

5.3.2 SEP Approximation of the SC Receiver

As mentioned in Section 5.3.1, it is not common to find analysis of the performance of diversity receivers with non-uniform NPP. The SC receiver with general SPP and NPP was analysed in Chapter 4 where we derived asymptotic expressions from the exact expression of the SEP in (4.68) and (4.79). It is straightforward to verify that (5.52) reduces to (4.68) for the special case of $L=1$.

5.3.3 SEP Approximation of the 2S/EGC Receiver

The asymptotic expression for the SEP of the 2S/EGC receiver is obtained from (5.52) by substituting $L=2$ as

$$\tilde{P}_{e\_static} \approx \frac{NN!K_\varphi}{\pi 2^{N-2}(2N-1)} \frac{\left(\frac{1}{N!}\sum_{\mathbf{P}_k}\left(\sigma_{n_{k_1}}^2 + \sigma_{n_{k_2}}^2\right)^N\right)}{\left(\prod_{i=1}^{N}\sigma_{g_i}^2\right)}. \tag{5.56}$$

Comparing (5.56) with (4.89) we observe a discrepancy. The ratio of (5.56) over (4.89) shows a discrepancy equal to

$$\varepsilon = \frac{4N}{3(2N-1)}. \tag{5.57}$$

The explanation is that the exact SEP expression for the 2S/EGC receiver in Chapter 4 was very complex and in order to arrive at a simple expression various simplifications were made, resulting in a less tight approximation. Therefore, the merit of the asymptotic analysis in this chapter cannot be overemphasized.

5.3.4 SEP Approximation of the Classical EGC Receiver

For the special case of the classical EGC receiver it is more convenient to obtain the asymptotic SEP for the static fading case by returning to the conditional SEP expression shown in (5.28) instead of attempting to simplify (5.52) by setting L=N. Since for the classical EGC receiver no selection is performed, i.e. L=N, the asymptotic SEP derivation is simplified. Based on the general H-S/EGC derivation the instantaneous SNR of the EGC combiner is given by

$$\gamma(\mathbf{l}) = \frac{\left|\sum_{i=1}^{N} w_i^* l_i\right|^2}{2\sum_{i=1}^{N} \mathcal{N}_i} \tag{5.58}$$

and the exact expression for the SEP is

$$P_e = \frac{1}{\pi}\int_0^{\Phi}\int_0^{\infty}\cdots\int_0^{\infty}\left(\prod_{i=1}^{N}\frac{l_i}{\Lambda_i}\right)\exp\left(-\sum_{i=1}^{N}\frac{l_i^2}{2\Lambda_i} - K(\varphi)\frac{\left|\sum_{i=1}^{N} w_i^* l_i\right|^2}{2\sum_{i=1}^{N}\mathcal{N}_i}\right) dl_1\cdots dl_N d\varphi. \tag{5.59}$$

By making the same assumptions as we did to obtain (5.34) we arrive at the approximate expression

$$P_{e\_static} \approx \frac{1}{\pi}\int_0^{\Phi}\int_0^{\infty}\cdots\int_0^{\infty}\left(\prod_{i=1}^{N}\frac{l_i}{\Lambda_i}\right)\exp\left(-K(\varphi,k)\left(\sum_{i=1}^{N} l_i\right)^2\right) dl_N\cdots dl_1 d\varphi. \tag{5.60}$$

This is a special case of (5.44) with L=N and $c_i = 1$. It is straightforward to show that based on the solution to the general integral shown in (B.16), the inner integrals evaluate to

$$\int_0^{\infty}\cdots\int_0^{\infty}\left(\prod_{i=1}^{N} l_i\right)\exp\left(-K\left(\sum_{i=1}^{N} l_i\right)^2\right) dl_N\cdots dl_1 = \frac{1}{2^N K^N (2N-1)!!}. \tag{5.61}$$

Substituting (5.61) into (5.60) the SEP approximation becomes

$$P_{e\_static} \approx \frac{2^N K_\varphi}{\pi(2N-1)!!} \frac{\left(\sum_{i=1}^{N} \sigma_{n_i}^2\right)^N}{\left(\prod_{i=1}^{N} \Lambda_i\right)}. \tag{5.62}$$

We use the approximation to the Λ_i's shown in (4.61) to obtain the final form of the asymptotic SEP of the EGC receiver as

$$P_{e\_static} \approx \frac{2^N K_\varphi}{\pi(2N-1)!!} \frac{\left(\sum_{i=1}^{N} \sigma_{n_i}^2\right)^N}{\left(\prod_{i=1}^{N} \sigma_{g_i}^2\right)}. \tag{5.63}$$

It can be verified using numerical methods that the general expression in (5.52) is reduced to (5.63) by setting L=N.

5.4 Results

In this section we use the asymptotic expressions derived in Sections 5.1-5.3 to show the effect of combining additional branches has on the SEP of the H-S/EGC and H-S/MRC receivers. Furthermore, we demonstrate the influence of the SPP and the NPP on the asymptotic SEP of the 2 receivers types.

The receivers we analyse in this section, as in Sections 3.4 and 4.4, operate in a Rayleigh fading environment with possible Doppler spread and employ differential 8-PSK (M=8) modulation. The convention we use to define the SNR profile of the channel as well as to define the SPP and NPP was explained in Section 4.4. In essence, we set either the SPP or the NPP to be uniform and allow the other profile to vary in an exponential decay fashion. The exponential SPP or NPP defines the SNR profile. We reproduce in Table 5.1 the three profiles shown in Table 4.1 and their profiles decay parameters.

To illustrate the value of the asymptotic expressions derived in this chapter, we study the effect of having different numbers of combined branches L on the asymptotic SEP of the H-S/EGC receiver. In Figure 5.2 we plot the normalized SEP of the H-S/EGC receiver versus the number of selected branches L for a total number of available branches N=8. The SEP is normalized by setting the SEP for L=1 (SC noCSI receiver) to be equal to 1. Hence, we plot the ratio of the SEP for various L over the SEP of the SC receiver. In the plot we assume a slow fade rate and high SNR so that the receiver operates above the error floor and in the static asymptotic

Table 5.1. The two SNR profiles used in Section 5.4 and the corresponding profile decay parameter a.

Profile name	a
uniform	0
exp2	1

region. The normalization provides results which are independent of the specific SNR as long as the receiver operates in its asymptotic static region. We observe that as the number of selected branches increases from 1 to 6 the SEP monotonically decreases although with gradually decreasing steps. As the number of selected branches increases to 7 and 8, however, we observe that the SEP begins to increase. We actually observe something odd, an increase in the SEP when we use more diversity branches. A similar observation was made by Eng et al in [4] where they derived the bit error probability (BEP) of special cases of the "non-coherent" hybrid diversity receivers SC, SC2 (selects and combines 2 branches) and SC3 (selects and combines 3 branches) operating in static fading. They compared the BEP of the three receivers to the BEP of the EGC receiver and noted that in some cases the SEP of the EGC receiver was inferior to the SEP of the SC3. We also note in Figure 5.2 that when the number of selected branches increases above L=4 we do not get as substantial a SEP improvement as at the lower values. Considering the higher overhead of combining more branches it may not be efficient to combine more than 4 branches for the receiver having N=8 available diversity branches.

To provide a quantitative measure of the change in the SEP with the selection of additional branches, we define the *selection gain* function as follows:

$$Sg = 10\log\left(\frac{P_e(L-1)}{P_e(L)}\right). \tag{5.64}$$

For the receiver of Figure 5.2 the corresponding selection gain is plotted in Figure 5.3. We observe that the selection gain for this receiver becomes negative for L=7 and L=8. This is an indication that the SEP actually increases with increasing number of selected branches as we also observed in Figure 5.2.

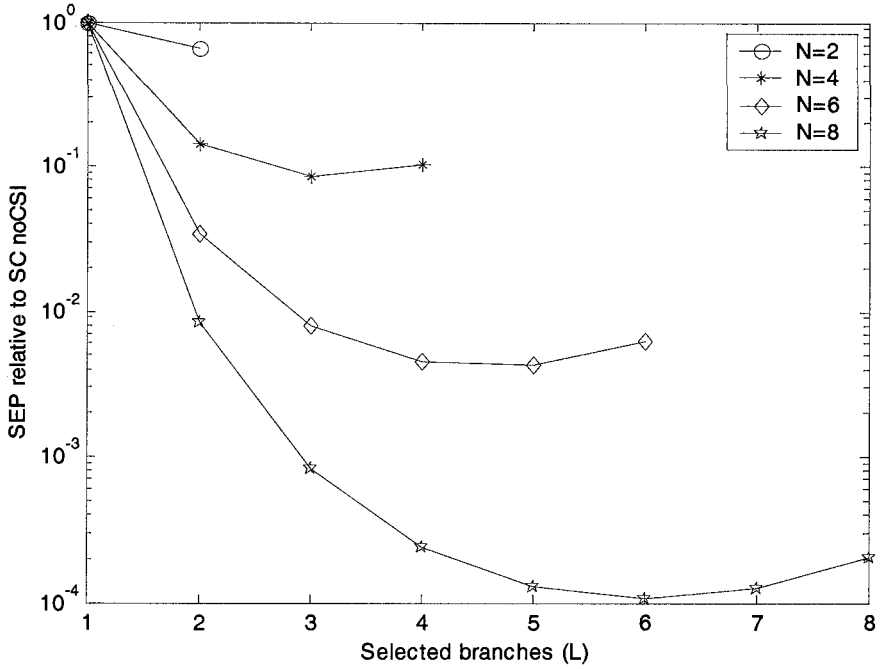

Figure 5.2: SEP ratio of the H-S/EGC receiver versus L for total branches N=2,4,6,8. The receiver is operating in a static Rayleigh fading channel with uniform SPP and NPP.

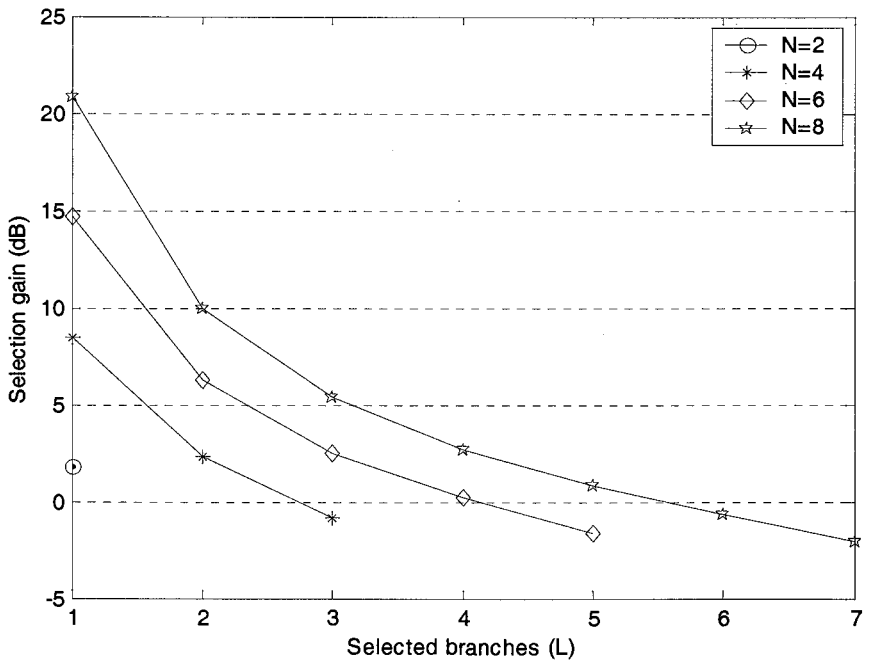

Figure 5.3: The selection gain of the H-S/EGC receiver versus L for total branches N=2,4,6,8. The receiver is operating in a static Rayleigh fading channel with uniform SPP and NPP.

We, next, study the effect of selecting additional branches in a non-uniform NPP. In Figure 5.4 and Figure 5.5 we plot the SEP and selection gain respectively for the uniform SPP and exponential NPP profile with decay parameter a=1. We observe that the SEP no longer increases as the number of selected branches increases but we still observe the diminishing returns seen in the uniform profile. Similar plots of the corresponding SEP and selection gain for an exponential SPP and uniform NPP would produce results identical to Figure 5.2 and Figure 5.3 and are omitted. The justification is obtained by observing in (5.47) that the factor involving the signal powers is not influenced by the value of L and thus the relative asymptotic SEP and the selection gain are independent of the SPP.

For the H-S/MRC receiver the corresponding relative SEP and selection gain plots are not affected by the SPP or NPP and are shown in Figure 5.6 and Figure 5.7 for a uniform SNR profile. We observe that, unlike the plots of the H-S/EGC receiver shown in Figure 5.2 and Figure 5.3, the SEP is a monotonically decreasing function of L or, in other words, the selection gain is positive for all L. This conclusion can also be reached by evaluating the selection gain function, defined in (5.64), to obtain the expression

$$Sg = 10(N - L + 1)\log\left(\frac{L}{L-1}\right). \tag{5.65}$$

We observe in (5.65) that the selection gain only depends on L and N and, furthermore, it is always a positive number. We therefore do not expect to see any variation in the selection gain of the H-S/MRC receiver for different SNR profiles.

5.5 Conclusions

In this chapter we derived asymptotic expressions for the SEP of the general H-S/MRC and H-S/EGC receivers which operate in a Rayleigh fading channel affected by Doppler spread and use DPSK. The analysis avoided the difficulties that exist in the exact derivation of the SEP and used a new integral solution from Appendix B to arrive at the final expressions.

Using the asymptotic expressions we demonstrated in Section 5.4 that the SEP of the H-S/EGC receiver is not guaranteed to improve as we increase the number of combined branches. Specifically we showed that for a H-S/EGC receiver operating in a Rayleigh fading channel with 8 available diversity branches having uniform SPP and NPP we obtain the best SEP by combining the 6 branches with the maximum instantaneous signal plus noise magnitude. Combining 7 or 8 increases the SEP. When the H-S/EGC operates in an exponential NPP with

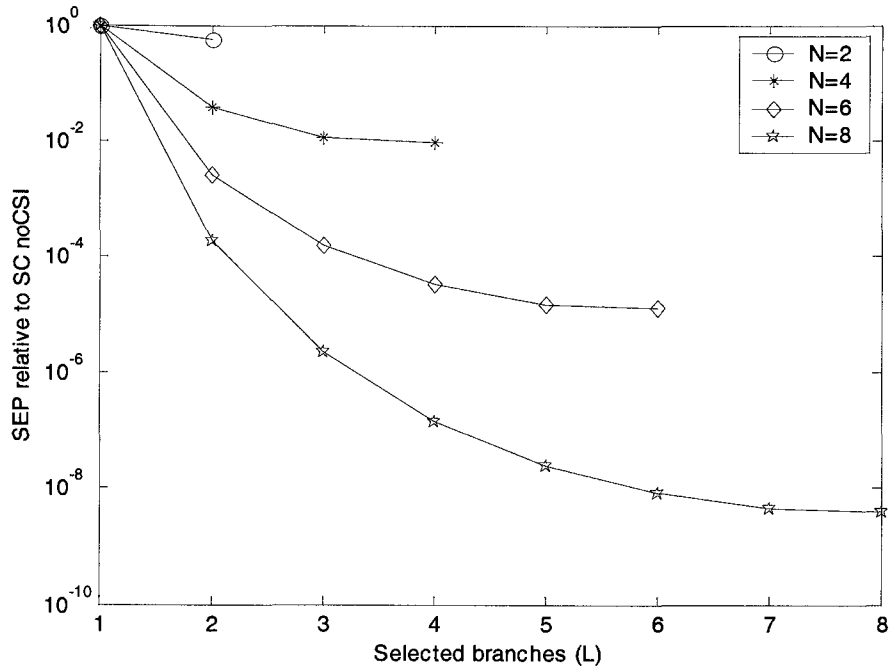

Figure 5.4: SEP ratio of the H-S/EGC receiver versus L for total branches N=2,4,6,8. The receiver is operating in a static Rayleigh fading channel with uniform SPP and exponential NPP with profile decay parameter a=1.

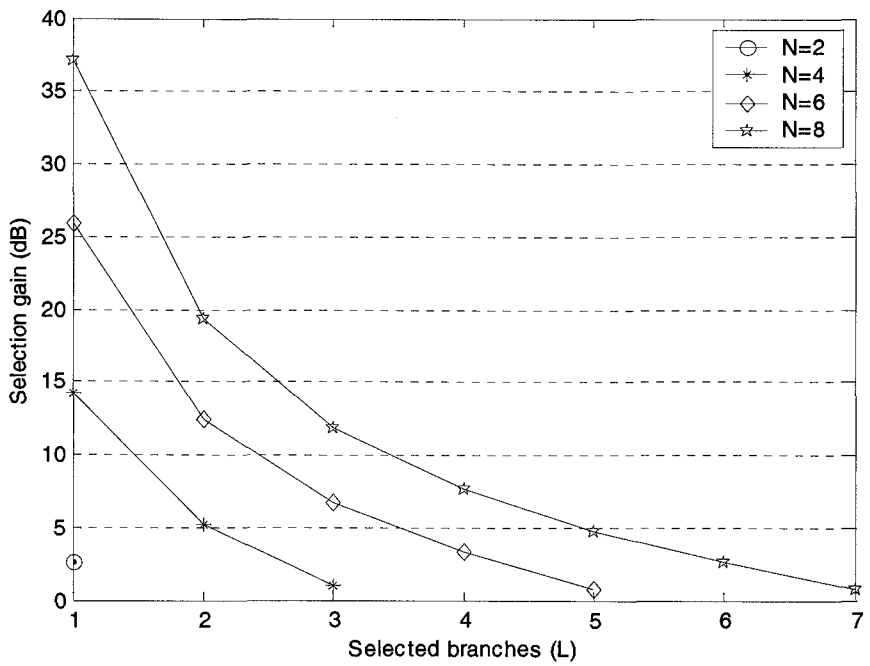

Figure 5.5: The selection gain of the H-S/EGC receiver versus L for total branches N=2,4,6,8. The receiver is operating in a static Rayleigh fading channel with uniform SPP and exponential NPP with profile decay parameter a=1.

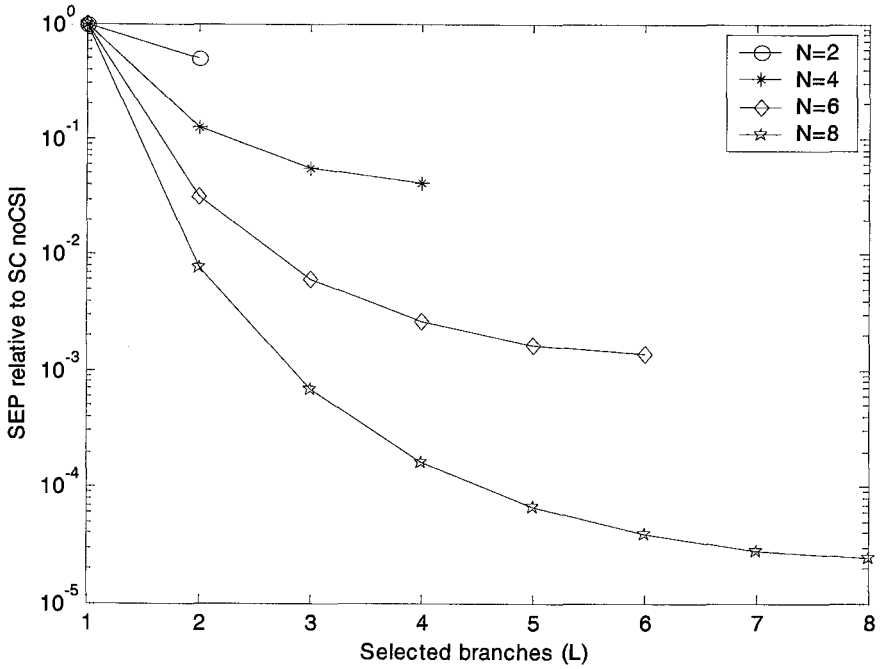

Figure 5.6: SEP ratio of the H-S/MRC receiver versus L for total numbers of branches N=2,4,6,8. The receiver is operating in a static Rayleigh fading channel.

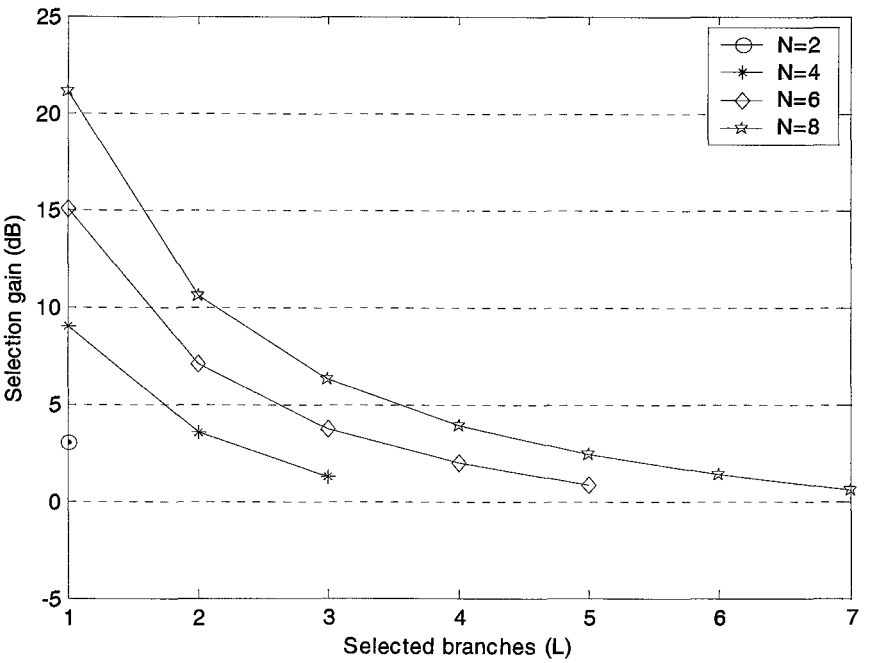

Figure 5.7: The selection gain of the H-S/MRC receiver versus L for total branches N=2,4,6,8. The receiver is operating in a static Rayleigh fading channel.

profile decay parameter a=1 we found that the increase in the SEP at large numbers of combined branches does not occur. The H-S/MRC receiver on the other hand will always benefit by the combining of additional branches but with diminishing although the benefit diminishes as $L \to N$. This was also proven by evaluating the selection gain function for the H-S/MRC receiver.

Chapter 6

A Reduced-Complexity Hybrid Diversity Receiver

So far we have investigated postdetection hybrid diversity receivers which perform symbol by symbol selection and combining. Implicit in the description of these receivers is the availability of the baseband signals from all the branches both for the current and for the previous symbol intervals. The previous symbol is needed for differential detection. Consider the H-S/MRC and H-S/EGC receivers with DPSK modulation analysed in Chapters 3 and 5 respectively. These receivers have N available diversity branches and, *at each symbol interval,* select for combining the L ($1 \le L \le N$) branches with the largest SNR and SPN respectively. A reasonable question would be: What if at two consecutive symbol intervals different sets of L branches were selected? In that case, a receiver with a fixed number of L demodulators[1] would lose the phase reference from the previous symbol, required for differential detection, causing unacceptable error rates [47]. It is, therefore, necessary for proper symbol-by-symbol operation of the receivers analysed in Chapters 3-5 to use a higher number of demodulators than L. Consider the two possible scenarios: $0 < L \le N/2$ and $N/2 < L \le N$. In the former, the HDR requires $2L$ demodulators, all of which may be necessary in rapidly varying fading channels with rapid reordering of the instantaneous branch powers. In the latter scenario, the HDR requires the maximum number of N demodulators. This indicates that the general HDR's studied thus far require, in addition to the minimum number of L demodulators, a number of demodulators equal to

$$L_a = \min(N - L, L). \tag{6.1}$$

The scenarios just described require the signals from $L + L_a$ diversity branches to be demodulated at every symbol interval. For the H–S/EGC receiver, however, only the L strongest

---

[1] The term demodulator is sometimes used loosely in the literature so we need to explain its usage in this chapter. We refer to demodulation as the recovery of the baseband pulse. Thus a demodulator performs frequency down-conversion and includes receive filters such as a matched filter and an equalizer. The output of the demodulator is the discrete-time variable $r_i[k]$, defined in (2.21), obtained by sampling the matched filter output at the end of each symbol interval [50].

of these signals are combined and the demodulation of the $L+L_a$ branches gives rise to higher complexity and higher power consumption [3][4]. Furthermore, the simplicity of combining fewer diversity branches is lost. In fact, classical EGC applied on all the branches could instead be used with negligible additional complexity. In spite of this issue, there is an abundance of published works dealing with the postdetection SC and HDR type of receivers. For example the receivers in [4], [24] and [51] even assume perfect knowledge of the channel state. It is, however, understood that the analysis of the coherent receivers provides a lower bound for the SEP of more realistic receivers. The H-S/MRC receiver analysed in Chapter 3, for example, uses channel statistical information (CSI) for MMSE channel estimation to provide performance close to the equivalent coherent HDR. The switch diversity receiver [51]-[53] is another example of a more practical, suboptimal (compared to SC) receiver which only switches to a different branch if the power of the currently selected branch falls below a certain threshold, irrespective of the instantaneous relative power of the branches. Of course, a receiver using DPSK in switch diversity would also suffer from the same problem described in the previous paragraph; specifically the differential phase reference would be lost at the switching time. Although switching between branches occurs less frequently in switch diversity than in classical SC diversity, the loss of phase reference is still an issue. Alternatively, predetection combining could be used to perform cophasing and combining of the signals at IF but this technique also faces problems with switching transient noise due to phase or amplitude differences between the branches and additional analog circuitry complexity [47] [51].

At this point it would appear that using DPSK in combination with any form of selection or switch diversity is problematic. This fact could explain the scarcity of analyses of DPSK used in conjunction with any form of selective diversity. In this chapter we develop a reduced-complexity hybrid diversity receiver (RHDR) to demonstrate a more plausible way of taking advantage of the simplicity of DPSK and the power of hybrid diversity. The RHDR at each symbol interval only requires two branches to be demodulated yet it achieves diversity performance which is superior to the performance of the SC receiver, analysed in Chapter 4. In this chapter we describe the operation of this RHDR and provide performance statistics obtained by Monte Carlo simulation.

6.1 System Model and Operation

As already discussed the combination of DPSK and selection diversity is problematic unless $L+L_a$ diversity branches are demodulated and available to the selector and the combiner. We, therefore, describe in this section the operation of the RHDR, a receiver which monitors N

diversity branches but only uses two demodulators. The RHDR is able to maintain differential phase reference for at least one branch at all times. Contrast the two baseband demodulators needed for the RHDR to the $L+L_a$ demodulators necessary for the HDR's analysed in Chapters 3-5 and the reduction in complexity becomes apparent.

The system model for the RHDR is a modified version of the 2S/EGC receiver model described in Chapter 4 and shown in Figure 4.2. The modification occurs in the branch sorter/selector which is placed at the IF stage of the receiver. The conceptual diagram of the RHDR receiver is shown in Figure 6.1. The "Power Comparator and Selection Logic" block compares the envelopes of the N branches and selects two of them based both on their instantaneous magnitude as well as on the decisions made at the previous symbol interval. The two selected branches are demodulated and their sampled versions r_1 and r_2 become available to the combining logic. Depending on certain conditions one or both of the branches may then be used to provide the decision variable y. It is therefore expected that the performance of the RHDR will be bounded by the SC and the 2S/EGC receivers analysed in Chapter 4.

6.1.1 RHDR Operation

The symbol by symbol operation of the RHDR is described by the algorithm shown in Figure 6.2. The notation used in this figure is defined as follows:

j_1, j_2: The indices of the two branches with the maximum and second maximum respectively signal magnitudes in the current symbol interval.

b_1, b_2: The indices of the two *selected* branches. The indices are stored in memory and are used in the following symbol interval to aid in the selection of the next two branches.

$r(j_1)$, $r(j_2)$: The received symbols from branches j_1 and j_2 respectively.

r_1, r_2: The two *selected* symbols stored in memory to be used in the following symbol interval for differential phase reference. Note that, as will be clarified shortly, r_1, r_2 are not necessarily the same as $r(j_1)$, $r(j_2)$.

The instantaneous signal strength measurement and sorting is performed at IF in each symbol interval.

The receiver is initialized by selecting the two branches with the maximum signal magnitude, j_1 and j_2. The signals are demodulated and the two baseband symbols $r(j_1)$ and $r(j_2)$ as well as the indices of the two branches from which they arrived, j_1 and j_2, are saved in memory as follows:

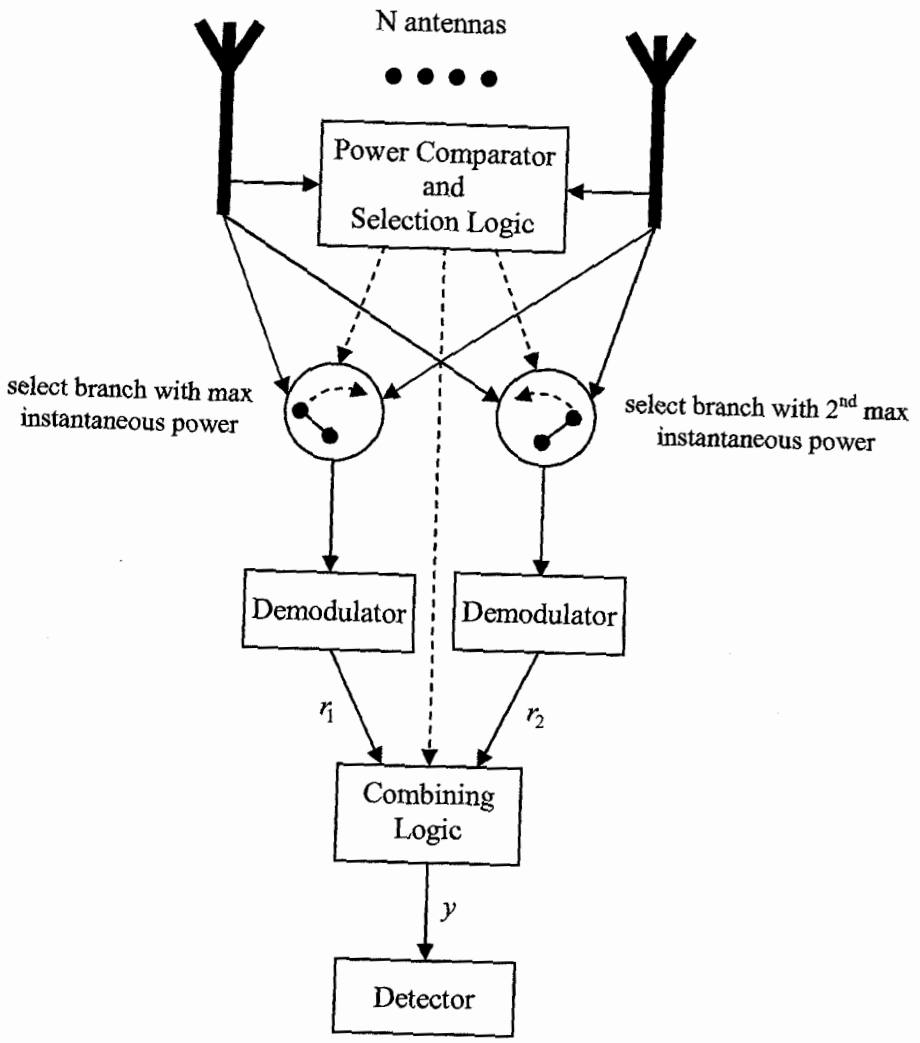

Figure 6.1: Conceptual diagram of the RHDR.

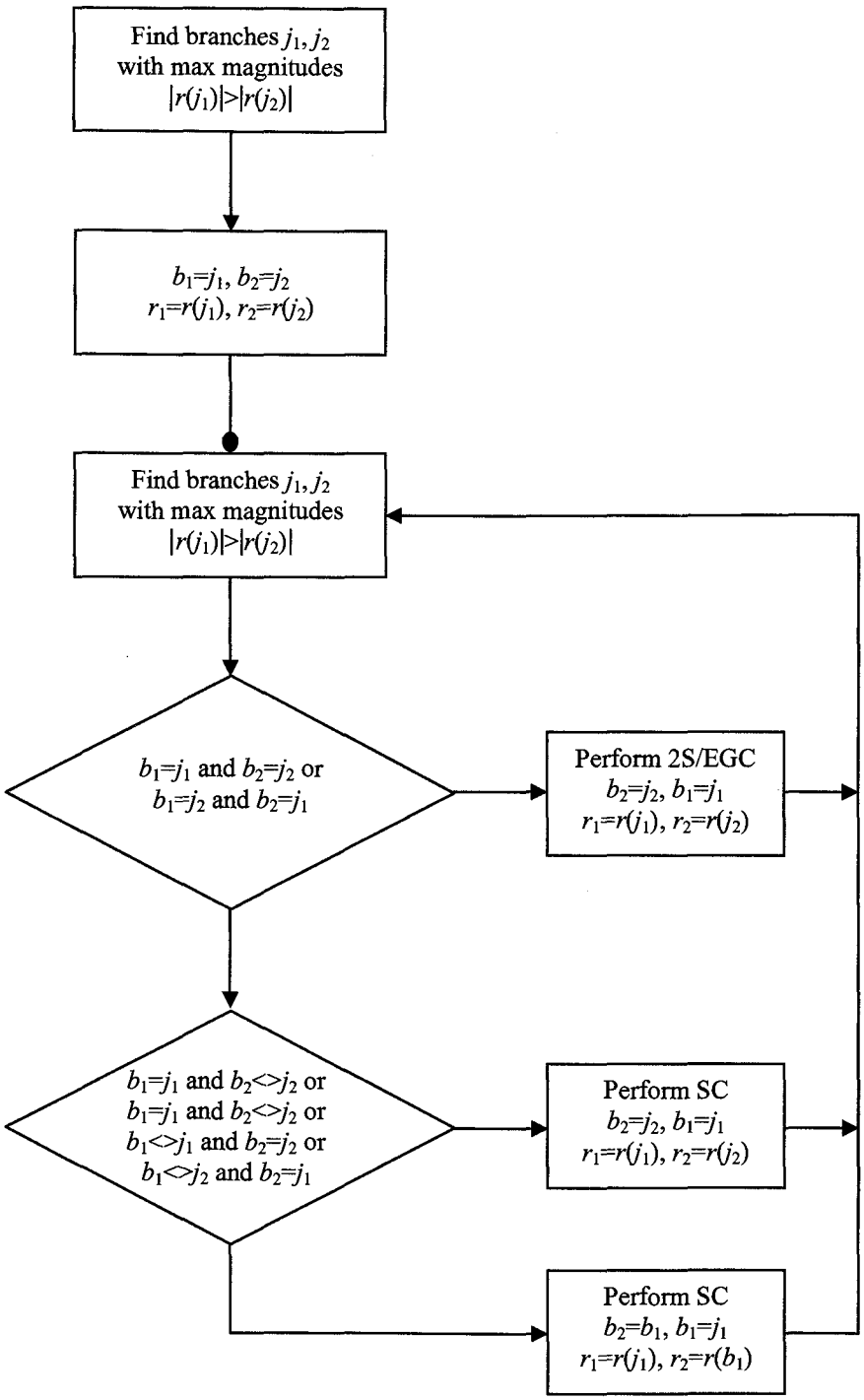

Figure 6.2: The algorithm for the RHDR.

$$b_1 = j_1,\ b_2 = j_2, \tag{6.2}$$

$$r_1 = r(j_1),\ r_2 = r(j_2). \tag{6.3}$$

For this algorithm to operate properly, the four variables in (6.2) and (6.3) must be stored in memory because this would ensure that the receiver would select at least one of these branches in the following interval. Failure to do so, that is selecting two different pairs of branches in two consecutive symbol intervals, would result in a loss of differential phase reference and almost certainly result in an erroneous detection as discussed earlier.

At the next symbol interval, the two branches with the largest instantaneous power, j_1 and j_2, are identified. The indices of these two branches as well as the indices of the two selected branches from the previous symbol interval, b_1 and b_2, are considered and a decision is made on which branches will then be selected. At this point it should be stressed that if the two pairs of indices, b_1, b_2 and j_1, j_2, are different there is danger of loosing differential phase reference. Therefore, special provisions must be taken to ensure that at least one of the two previously selected branches is also selected in the current interval in spite of not having one of the two largest magnitudes. To explain how the RHDR avoids loosing the differential phase reference we describe below the three modes in which the RHDR is operating based on the algorithm shown in Figure 6.2:

Operation mode 1

Condition: The two branches with the currently maximum signal magnitudes are the same as the previous two branches, that is

$$b_1 = j_1 \ and \ b_2 = j_2 \text{ or} \tag{6.4}$$

$$b_1 = j_2 \ and \ b_2 = j_1. \tag{6.5}$$

Action: Demodulate both branches (j_1 and j_2) and perform equal gain combining. Assuming the condition in (6.4) was satisfied, the following operations would be performed:

$$y = \frac{r_1^*}{|r_1|} r(j_1) + \frac{r_2^*}{|r_2|} r(j_2), \tag{6.6}$$

$$b_1 = j_1 \ and \ b_2 = j_2, \tag{6.7}$$

where y is the decision variable at the detector. In this case the RHDR behaves like the 2S/EGC receiver.

Operation mode 2

Condition: Only one of the two branches with the currently maximum signal magnitudes was in the previously selected pair, that is

$$b_1 = j_1 \text{ and } b_2 <> j_2 \text{ or} \tag{6.8}$$

$$b_1 = j_2 \text{ and } b_2 <> j_1 \text{ or} \tag{6.9}$$

$$b_1 <> j_2 \text{ and } b_2 = j_1 \text{ or} \tag{6.10}$$

$$b_1 <> j_1 \text{ and } b_2 = j_2 . \tag{6.11}$$

Action: Demodulate both branches (j_1 and j_2). However, only the branch which was selected in both symbol intervals is used for detection. The reason is the absence of the phase reference for the other branch. Assuming the condition in (6.8) was satisfied, the following operations would be performed:

$$y = \frac{r_1^*}{|r_1|} r(j_1)$$

$$b_1 = j_1 \text{ and } b_2 = j_2 \tag{6.12}$$

The RHDR receiver behaves like the SC receiver described in Section 4.1 and uses a branch which in both the previous and the current symbol intervals belongs to the pair of branches with maximum instantaneous signal strength.

Operation mode 3

Condition: Neither of the two branches with the currently maximum signal magnitudes was in the previously selected pair, that is

$$b_1 <> j_1 \text{ and } b_1 <> j_2 \text{ and } b_2 <> j_1 \text{ and } b_2 <> j_2 . \tag{6.13}$$

Action: Demodulate the one branch with the current maximum signal strength, j_1, as well as the branch which had the maximum signal strength in the previous symbol interval, b_1. The selection of the branch with the maximum signal strength in the previous interval ensures the presence of a differential phase reference for detection whereas the selection of the branch with the maximum power in the current interval ensures that in the following interval there will be a differential phase reference from the branch with the maximum signal strength. Use only the signal from branch b_1 for detection. The following operations would be performed:

$$y = \frac{r_1^*}{|r_1|} r(b_1)$$

$$b_1 = j_1 \text{ and } b_2 = b_1 \tag{6.14}$$

Even in this case, the RHDR receiver behaves like the SC receiver described in Section 4.1, where it was explained that the selection is based on the strength of the previous received symbols.

It should be apparent from this description that the best case scenario occurs when the same two branches have the maximum signal strength in two consecutive symbol intervals. A situation when this best case scenario applies for the majority of the time, could arise at slow fade rates and high SNR where the temporal correlation of the fading gain is high and the random noise effect is insignificant. In this case, the RHDR performs like the 2S/EGC described in Section 4.2. In the worst case scenario, due to abrupt redistributions of the instantaneous branch powers both of the selected branches at one symbol interval would be different from the two branches selected in the following symbol interval. In this case, a decision is made to demodulate the branch with the previously maximum signal strength as well as the branch with the currently maximum signal strength. This decision ensures that one branch maintains the differential phase reference and the branch with currently the maximum signal strength will provide differential phase reference in the next symbol interval. The reader may recognise that even in the worst case scenario, the RHDR is equivalent to the SC receiver analysed in Section 4.1.

6.2 Monte Carlo Simulation

To evaluate the performance of an RHDR with N=4 diversity branches and to compare it with the HDR's considered in Chapter 4 we used Monte Carlo simulation.

6.2.1 Model Description

The transmitter generates random MPSK symbols which it differentially encodes and transmits through the channel. The channel is modelled as four independent, Rayleigh fading, AWGN branches where the fading is affected by Doppler spread with normalized maximum fade rate f_D. The fading gain generation is based on the Jakes model [51].

The branch signals at the receiver are sorted in each symbol interval according to their magnitude and their indices are considered for the decision on which branches to select and which branches to combine. For the purposes of this chapter the following receivers were simulated:

1. *SC receiver*: This receiver was analysed in Section 4.1.
2. *SC limited receiver*: This receiver only demodulates the strongest branch at each symbol interval. Since it only obtains the symbol with the maximum SPN magnitude at each symbol interval it cannot guarantee differential phase continuity when conditions require switching to a different branch.

3. *2S/EGC receiver*: This receiver was analysed in Section 4.2.

4. *2S/EGC limited receiver*: This receiver operates similarly to the SC limited receiver except that it demodulates two branches. This receiver still cannot guarantee differential phase continuity between switches.

5. *2EGC receiver*: This is the classical EGC receiver with a total of two diversity branches (N=2). The 2EGC receiver represents classes of receivers which due to complexity or power limitations are limited to only two branches in spite of the potential of exploiting a larger number of diversity branches. To provide a fair comparison with the other receivers we assume that the 2EGC receiver is able in the beginning of communications to choose the two branches with the largest average SPN. This decision does not change for the duration of the communication session. While in uniform SPP and NPP the branches have identical SNR, in non-uniform SPP and/or NPP the choice of branches is important.

6. *RHDR receiver:* The receiver described in Section 6.1.

The RHDR is using more intelligence than the other five receivers to perform the conditional tests shown in the algorithm of Figure 6.2 and described in Section 6.1. Based on which one of the conditions listed in Section 6.1.1 is satisfied, the RHDR combines the appropriate branches and collects statistics on which condition was satisfied. The SC limited and 2S/EGC limited receivers are included merely to demonstrate the need for the creativity found in the RHDR in situations where only one or two branches can be demodulated.

6.3 Simulation Results

To evaluate the performance of the RHDR and to compare it to the five other receivers listed in the previous section we performed simulations under various operating scenarios. In all simulations we used four independent diversity branches affected by AWGN and multiplicative Rayleigh fading. The receivers we consider in this section operate in a Rayleigh fading environment with possible Doppler spread and employ differential 8-PSK (M=8) modulation. The convention we use to define the branch SNR profile as well as to define the SPP and NPP was explained in more detail in Section 4.4. In essence, the general SNR profile is exponential and to observe the effect of the SPP and the NPP independently we set either the SPP or the NPP to be uniform and allow the other profile to vary exponentially. The exponential SPP or NPP, then also define the SNR profile. We reproduce in Table 6.1 the three profiles used in this section and their profile decay parameters.

Table 6.1. The two SNR profiles used in Section 6.3 and the corresponding profile decay parameter a.

Profile name	a
Uniform	0
exp2	1

In Figure 6.3, Figure 6.4 and Figure 6.5 we compare the SEP of the six receivers described in Section 6.2.1 which are operating in a static Rayleigh fading channel. In Figure 6.3, the SPP and NPP are uniform, in Figure 6.4 the NPP is uniform and the SPP is exponential with profile decay parameter a=1, and in Figure 6.5 the SPP is uniform and the NPP is exponential with profile decay parameter a=1. As explained in Section 6.2.1, in the case of uniform SPP and NPP the 2EGC receiver may use any two branches. In Figure 6.4 and Figure 6.5, where the SPP and NPP respectively are exponential, the 2EGC receiver uses the two branches with the largest average SNR for the duration of communications. For example, consider an exponential SNR profile defined by

$$\tilde{\Gamma}_i = Ge^{-a(i-1)}, \tag{6.15}$$

The 2EGC receiver would use the two branches with indices i=1,2 as we assume that it can correctly identify the branches with the largest average SNR. We observe, in all three figures that the receivers SC limited and 2S/EGC limited do not provide acceptable performance. This observation reinforces the argument of this chapter that the H-S/EGC receivers using DPSK must demodulate the signals from all diversity branches in order to operate properly. In Figure 6.3 and Figure 6.4 we observe that the 2EGC receiver is outperformed by the higher diversity order hybrid receivers at almost all SNR levels with a larger performance disparity shown in the uniform profile of Figure 6.3. Recall that when the average SPP and NPP is uniform all branches have identical average signal and noise powers. The 2EGC receiver selects two of the branches in the beginning of communications and for the duration of the communications ignores the other two, which are potentially equally good. On the other hand, in the non-uniform SPP used for Figure 6.4, the 2EGC receiver uses for the duration of the communications the two branches with the highest average branch SNR and ignores the two weakest branches. Since the branches with higher average SNR are also more likely to have higher instantaneous SNR, it is understandable that the 2EGC receiver is not overly penalized by ignoring the two weaker branches.

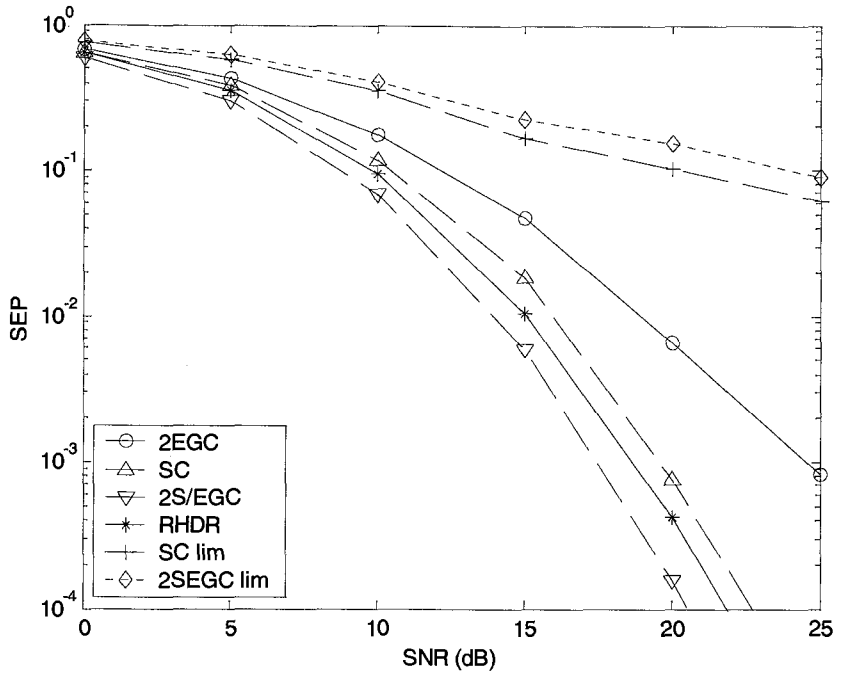

Figure 6.3: SEP comparison for the 1 and 2 branch combining receivers for uniform SPP and NPP.

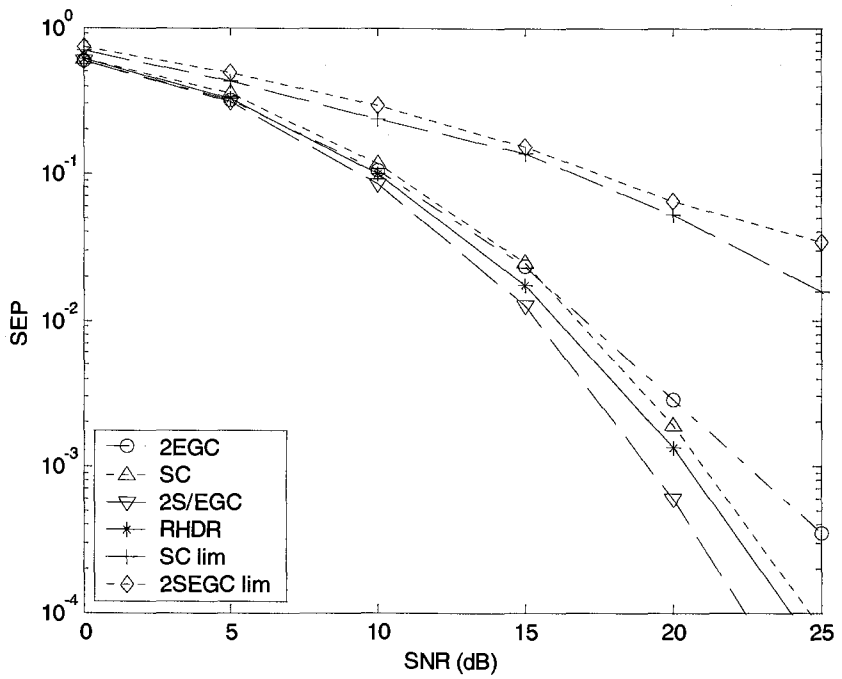

Figure 6.4: SEP comparison for the 1 and 2 branch combining receivers for uniform NPP and exponential SPP.

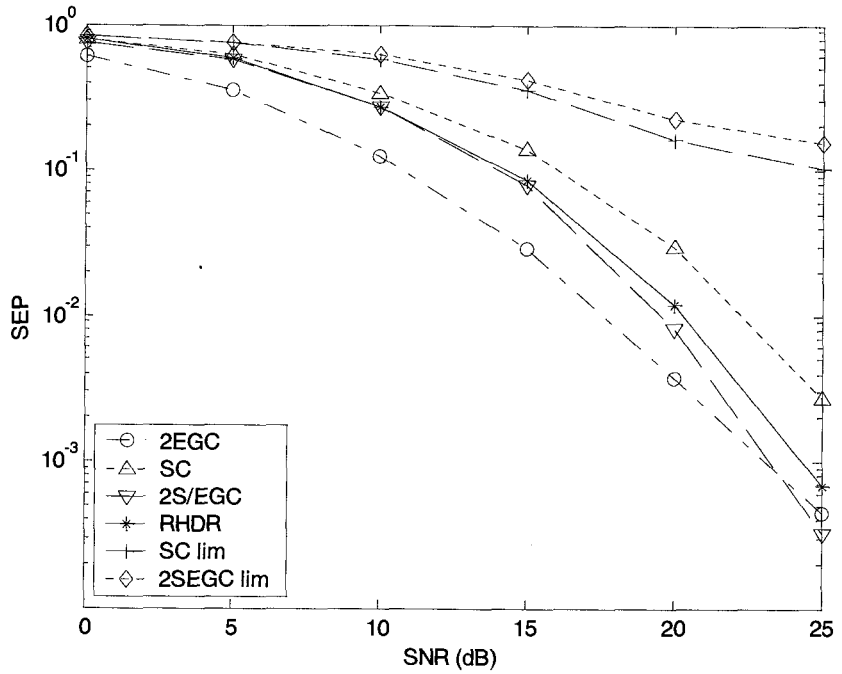

Figure 6.5: SEP comparison for the 1 and 2 branch combining receivers for uniform SPP and exponential NPP.

Contrary to the results shown in Figure 6.3 and Figure 6.4 we observe in Figure 6.5 that in a non-uniform NPP the 2EGC receiver outperforms the hybrid receivers at low SNR. It is not immediately obvious why this occurs but comparing Figure 6.5 with Figure 6.3 and Figure 6.4 we observe that the 2EGC receiver's performance does not change significantly between the three profiles whereas the performance of the hybrid receivers deteriorates considerably in Figure 6.5. Recall that the average power of the received signal in the i-th branch was shown in (4.61) to be

$$\Lambda_i = \sigma_{g_i}^2 + \sigma_{n_i}^2 . \tag{6.16}$$

Based on the assumption of uniform SPP and exponential NPP, we may deduce that at low SNR, where the noise power is significant compared to the signal power, the branches with higher noise power would be more likely to exhibit higher SPN magnitudes. Therefore, by incorrectly selecting the branches with higher noise powers the SEP of the HDR's suffers. This situation changes at high SNR (above 25dB) where the signal power becomes more dominant and the effects of the noise on the selection process diminish. One could therefore conclude that receivers operating at low SNR in fading environments with non-uniform NPP should choose the simpler 2EGC combining instead of the more complex 2S/EGC, assuming of course that the 2EGC receiver can correctly identify the branches with the largest average SNR. The selection accuracy

of the HDR's would improve in the case of antenna diversity, by adjusting the gains in the all the branches to obtain equal noise powers as suggested by Barrow [54].

In Section 6.1.1 we described the operation of the RHDR in each of the three operation modes. The RHDR behaves like a 2S/EGC receiver in operation mode 1 and like a SC receiver in operation modes 2 and 3. The difference between conditions 2 and 3 is that in condition 2 the selected branch in both the previous and the current symbol intervals belongs to the set of the two strongest branches whereas in condition 3 the selected branch had the largest magnitude in the previous interval but it no longer has one of the two maximum magnitudes. We, therefore, expect that the RHDR would perform better while it operates in mode 1 than for the other two modes. The percentage of time that the RHDR operates in one of the three operation modes is shown in Figure 6.6 and Figure 6.7 for a slow fade rate with $f_D = 0.002$ and a fast fade rate with $f_D = 0.01$ respectively. The solid lines in Figures 6.6-6.7 correspond to the uniform SPP and NPP channel, the dashed lines correspond to the exponential SPP (a=1) and uniform NPP channel and the dotted lines correspond to the exponential NPP (a=1) and uniform SPP channel. As should be expected, at low SNR the RHDR operates as a SC receiver for most of the time whereas at high SNR the situation is reversed and the RHDR operates as a 2S/EGC receiver for most of the time. This can be explained by considering the reasons which would lead to a redistribution of the instantaneous branch powers. At low SNR, noise is a major factor in the received SPN magnitude and, thus, the instantaneous branch power distribution among branches changes in a more random fashion. We observe that for the SNR interval shown in Figures 6.6-6.7 the exponential SPP enables the RHDR to operate in the 2S/EGC mode for a higher percentage of time than the other profiles and the exponential NPP forces the RHDR to operate in the 2S/EGC mode for the lowest percentage of time. By comparing Figures 6.6 and 6.7 we also observe that in this SNR range the fading rate does not influence the time that the RHDR spends in each of the modes of operation significantly.

While symbol-by-symbol branch selection is desirable, it is not always feasible. For example, it was suggested in [55] and [56] that for TDMA the selection could be performed more conveniently on a frame-by-frame basis instead of a symbol-by-symbol basis. We, thus, investigate the effect of a less frequent branch selection on the SEP of the RHDR. In Figures 6.8-6.10 we observe the effects of reducing the frequency of the branch power comparison process, where the receivers operate in a Rayleigh fading environment with fade rate $f_D = 0.01$. Under normal operation the RHDR performs the branch power comparison on a symbol-by-symbol

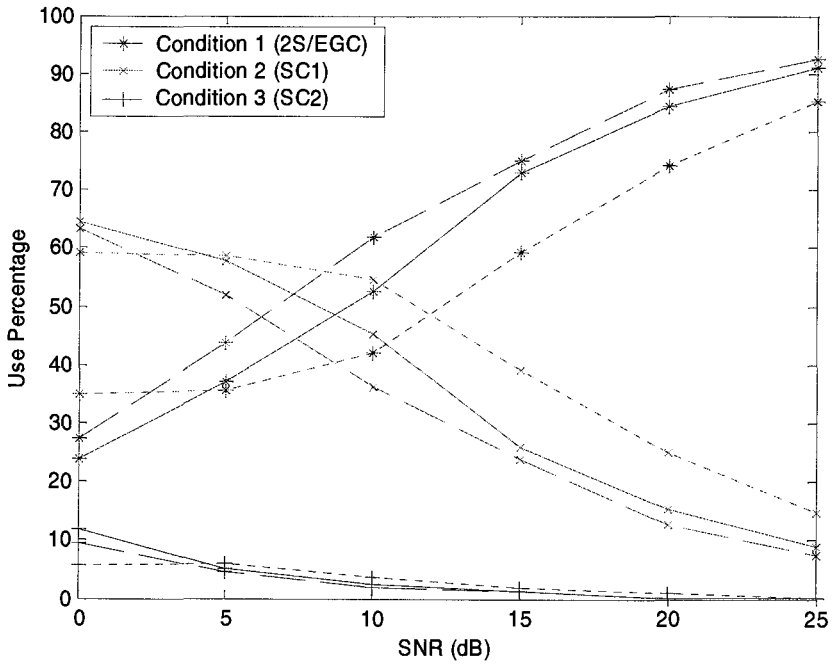

Figure 6.6: Mode of operation for the RHDR in a slow fading environment with $f_D = 0.002$ for the three power profiles used for Figures 6.3-6.5.

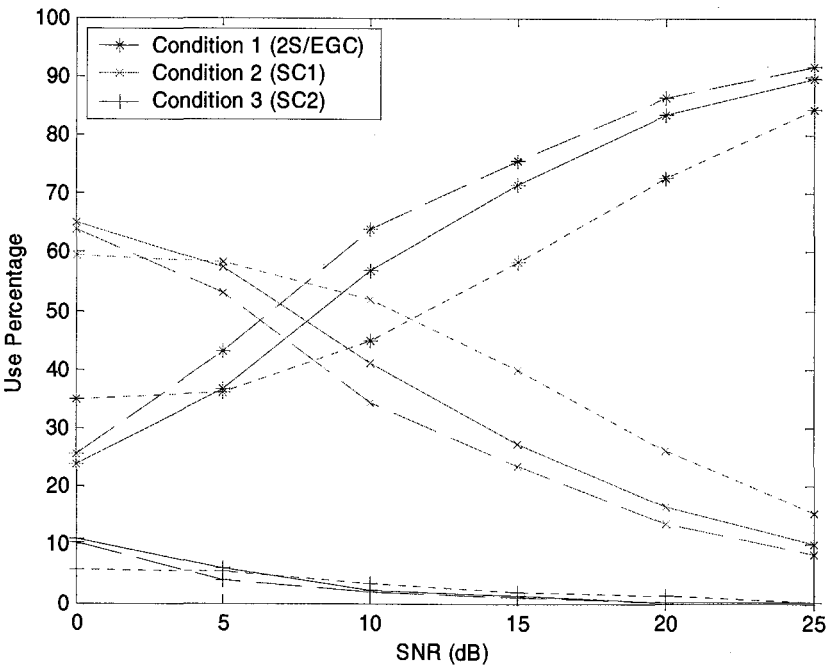

Figure 6.7: Mode of operation for the RHDR in a slow fading environment with $f_D = 0.01$ for the three power profiles used for Figures 6.3-6.5.

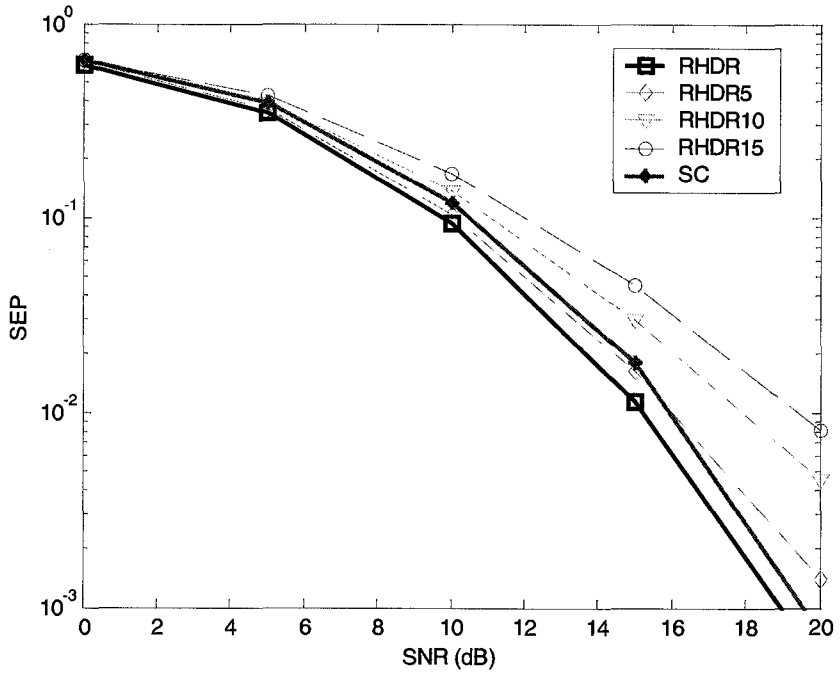

Figure 6.8: SEP comparison for the SC, RHDR and slower branch comparison algorithms for uniform SPP and NPP.

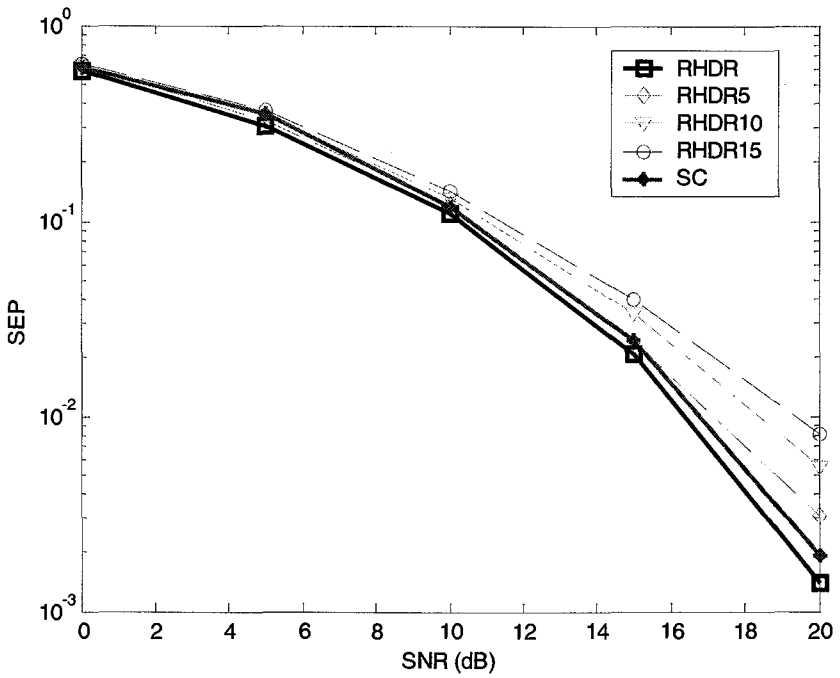

Figure 6.9: SEP comparison for the SC, RHDR and slower branch comparison algorithms for uniform NPP and exponential SPP.

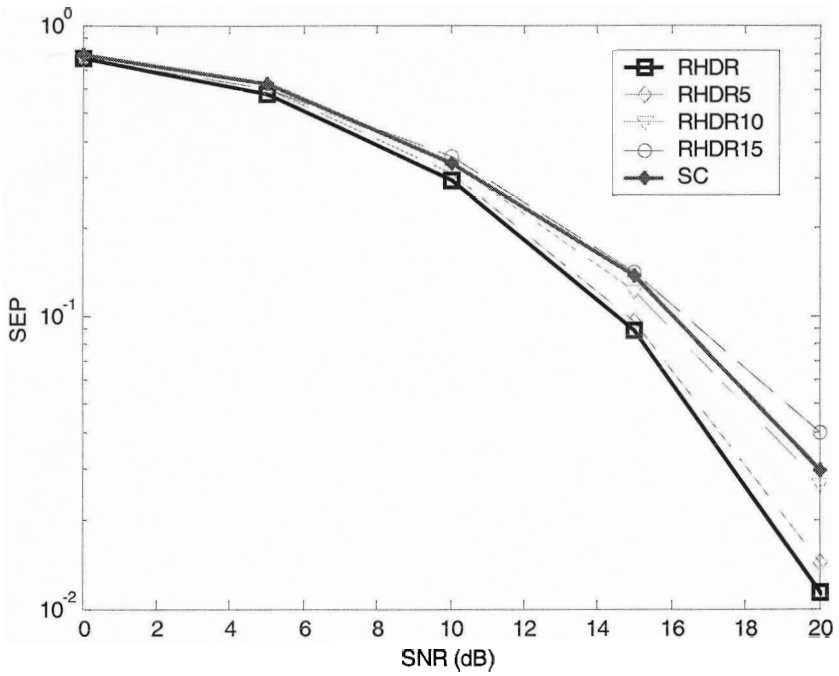

Figure 6.10: SEP comparison for the SC, RHDR and slower branch comparison algorithms for uniform SPP and exponential NPP.

basis. Less frequent power comparison may be done every k symbols in which case the receiver would operate according to the algorithm shown in Figure 6.2 at every k symbols and as a 2EGC receiver in the $k-1$ symbols in between. You may consider the selection being performed on a frame by frame basis as opposed to the symbol by symbol basis of the RHDR. The plots for the uniform SNR profile, the uniform NPP and exponential SPP (a=1) and the uniform SPP and exponential NPP (a=1) are shown in Figures 6.8-6.10 respectively. The branch power comparison is performed every 5, 10 and 15 symbols. We observe in all three figures that by decreasing the selection frequency the SEP increases. In Figures 6.11-6.13 we show the effect of the comparison frequency in a Rayleigh fading environment with a slower fade rate $f_D = 0.002$ and power profiles equivalent to the profiles used in Figures 6.8-6.10 respectively. The values used for k in this case are 5, 10 and 20. As should be expected, in this environment the suboptimal receivers perform better than in the faster fading environment but we also observe that in some cases they outperform the symbol-by-symbol RHDR. Considering that the suboptimal receivers operate as RHDR receivers every k symbols, that is for $1/k$ proportion of the time, and as 2EGC receivers for $(k\text{-}1)/k$ proportion of the time, the results indicate that the benefit of combining two branches outweigh the benefits of the continuous monitoring of all the branches by the RHDR.

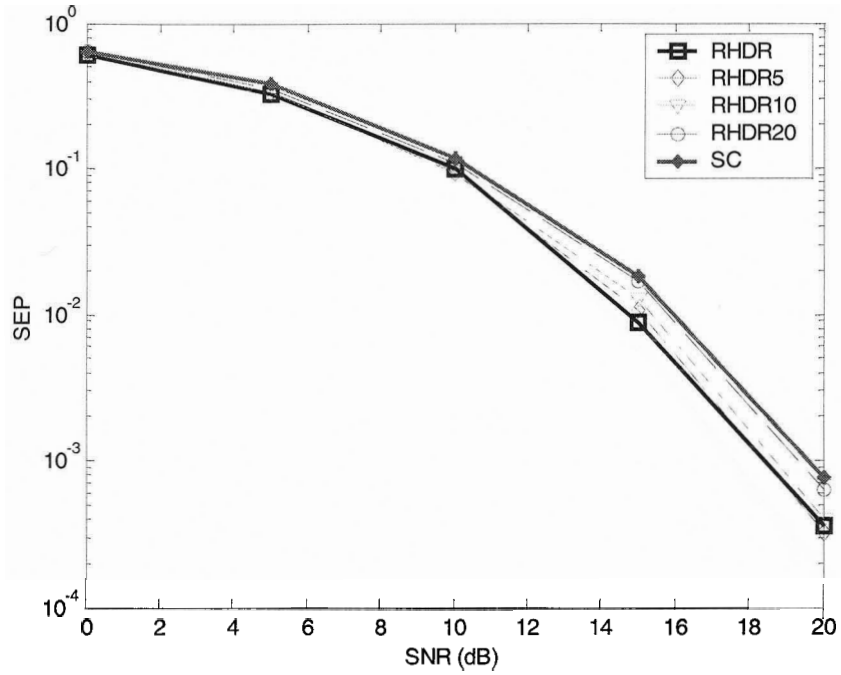

Figure 6.11: SEP comparison for the SC, RHDR and slower branch comparison algorithms for uniform SPP and NPP.

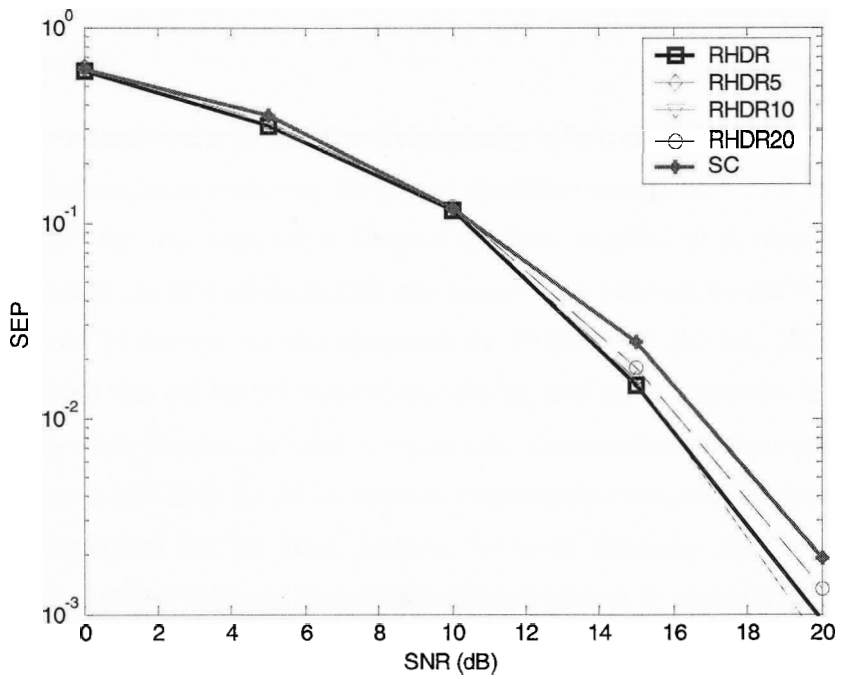

Figure 6.12: SEP comparison for the SC, RHDR and slower branch comparison algorithms for uniform NPP and exponential SPP.

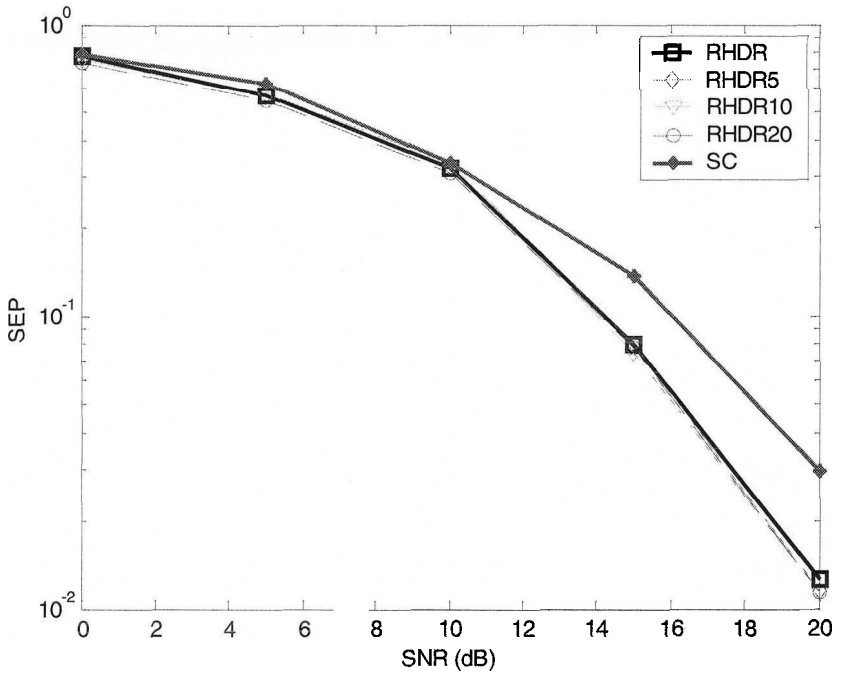

Figure 6.13: SEP comparison for the SC, RHDR and slower branch comparison algorithms for uniform SPP and exponential NPP.

6.4 Conclusion

In this chapter we described a new, reduced-complexity hybrid diversity receiver, which reduces the number of demodulators necessary for proper operation to only two. This receiver performs better than the SC receiver analysed in Chapter 4, which requires all available branches to be demodulated. In fact, the SEP of the RHDR was shown to be bounded by the SEP of the SC and 2S/EGC receivers. In Section 6.3 we compared the RHDR with the SC, 2S/EGC and 2EGC receivers and found that the RHDR outperforms the SC and 2EGC receivers in most scenarios. One exception is when the average noise powers in the diversity branches are not equal. We saw in Section 6.3 that at low SNR the 2EGC receiver outperforms the hybrid receivers in this profile. We, therefore, concluded that the 2EGC receiver due to its simplicity may be preferred when a system is operating at low SNR and has unequal noise powers in its diversity branches. However, the relatively high error rates of 0.002 in this SNR range may not be desirable in many applications. In Section 6.3 we also performed tests to examine the performance of the RHDR under even simpler configurations, in which the receiver performs less frequent branch power comparisons, say every k symbols, rather than on a symbol-by-symbol basis. A practical application would be a TDMA a receiver with two antennas which may scan each branch during

its idle periods and select the two branches with maximum power for the duration of the frame. This receiver was called the burst demodulator in [55] and [56].

Chapter 7

Conclusions

In this thesis we analysed the performance of the hybrid diversity receivers (HDR), a fairly new breed of diversity receivers, which use a hybrid of two of the classical diversity techniques, i.e. SC and EGC or SC and MRC. We considered receivers with available channel statistical information (CSI) as well as receivers which do not have CSI available. We derived closed form expressions for their average symbol error probability (SEP) and in some cases for their average output signal to noise ratio (SNR). For the derivations we assumed a Rayleigh fading channel with Doppler spread and diversity branches with generally non-identical branch powers at the receiver. The derived SEP expressions were in the form of an integral with constant limits which can be very easily evaluated. Furthermore, we gained insight into the factors affecting the SEP of the hybrid receivers by deriving asymptotic expressions which apply at high SNR's. The recurring influencing factors for all the receivers are the geometric mean of the branch signal powers and the general arithmetic mean of either the signal or the noise powers.

7.1 Major Results and Contributions

1. Analysis of the H-S/MRC Receiver

We analysed the H-S/MRC receiver which uses MMSE channel estimation for selection and combining of L out of N diversity branches. Our analysis produced the following results:

- Exact expression for the average SEP of the H-S/MRC receiver in the form of a single integral with finite limits.
- Lower computational complexity bounds to the SEP, which can be adjusted by making different complexity-tightness compromises.
- Simple asymptotic approximation to the SEP at high SNR. This expression provides insight into the effect of the branch SNR profile on the SEP of the H-S/MRC receiver.
- Exact expression for the average SNR of the H-S/MRC receiver.

We showed that the SEP of the H-S/MRC receiver deteriorates in non-uniform branch SNR profiles. We also showed that using the average output SNR as an indication of the SEP

performance of H-S/MRC receivers operating in different branch SNR profiles might lead to erroneous conclusions.

2. Analysis of the SC and 2S/EGC Receivers

We analysed the performance of the SC and the 2S/EGC receivers which have no CSI knowledge and, therefore, cannot optimally select and combine the selected diversity signals. For the two receivers we derived the following:

- Exact expressions for the SEP of both of these receivers. As for the H-S/MRC receiver, we derived exact, closed-form expressions in the form of a single integral with constant limits.
- Asymptotic approximations to the SEP of the two receivers for the static and the error floor operating regions. We separated the asymptotic analysis for the two receivers to account for the error floor and the static fading regions which occur at high SNR.
- Exact expression for the average SNR of the SC receiver.

Furthermore, we observed that in the absence of CSI, the receivers operating with equal average signal and noise branch powers exhibit virtually no deterioration in performance compared to the performance of the equivalent, more complex, H-S/MRC receivers. We also observed that a non-uniform SPP affects the relative error floor value of the SC and 2S/EGC receivers compared to the error floor of the two H-S/MRC receivers, whereas a non-uniform NPP affects the relative SEP in the static fading region.

3. Unified Asymptotic Analysis of Hybrid Diversity Receivers

We derived asymptotic expressions for the SEP of the H-S/MRC and H-S/EGC receivers which combine an arbitrary number of branches. Using high SNR approximations from the outset of the derivation we were able to obtain the following expressions:

- Asymptotic SEP expression of the H-S/MRC receiver. This expression is identical to that derived directly from the exact expression in Chapter 3.
- Asymptotic SEP expression of the H-S/EGC receiver. We were able to obtain an asymptotic expression by performing high SNR approximations in spite of the existing difficulties in obtaining an exact SEP expression for the general H-S/EGC receiver. These expressions enabled observation of the behaviour of the H-S/EGC receivers at high SNR and provided a correction to the asymptotic SEP of the 2S/EGC receiver derived in Chapter 4. In the process of deriving the asymptotic SEP, we also derived the solution to a multiple integral which appears to be new in the receiver diversity field.

Furthermore, the asymptotic expressions helped us to demonstrate that while the SEP of the H-S/MRC receiver can always be improved by the combining of additional branches, the SEP of the H-S/EGC receiver is not guaranteed to improve.

4. A Reduced Complexity HDR

We described and simulated the operation of a new, reduced-complexity hybrid diversity receiver (RHDR), which only uses two demodulators. The RHDR's performance is bounded by the SEP of the SC and 2S/EGC receivers. We showed that if complexity is an issue, the RHDR is a more attractive receiver than even the SC receiver analysed in Chapter 4, since the SC receiver requires N demodulators in order to operate properly. Furthermore, we found that at most situations the RHDR takes advantage of the higher number of available diversity branches and outperforms the classical EGC receiver with two branches (2EGC). In situations where complexity is an issue and the average noise powers in the diversity branches are not equal, however, the classical EGC receiver with two branches (2EGC) is shown to be a more attractive option than the RHDR, especially at low SNR. For an even simpler configuration we showed that a version of the RHDR which only performs branch comparison every k symbols provides reasonable performance.

7.2 Research Extensions

There are still some issues in the general area of this thesis that could be investigated in the future:

- Expansion of the asymptotic SEP expressions derived in Chapter 5 to account for the more general Nakagami channel. As mentioned in Chapter 5 this expansion would take advantage of the multiple integral derived in Appendix B to produce the corresponding expressions for the Nakagami channel.
- The asymptotic approximations may be adjusted to provide tighter fit even at low SNR.
- In this thesis we analysed receivers which do not have CSI available and use DPSK as a means of obtaining a form of a channel fading estimate to aid in the selection and combining. A better channel estimation, which would still not use CSI, could be obtained by using pilot symbol assisted modulation and non MMSE channel estimation. A possible estimation strategy would be linear interpolation of the pilot symbols but more sophisticated interpolation may also be used.

- As explained in chapters 4 and 5, the exact expression for the H-S/EGC receiver is, at this point, very difficult to obtain. More effort may be expended to obtain a concise, closed-form expression for the H-S/EGC receiver.
- The H-S/MRC receivers use CSI to obtain MMSE channel estimates. It is possible that in certain situations the CSI at the H-S/MRC may not be accurate. It would be interesting to derive the effect of such an inaccuracy on the SEP of the H-S/MRC receiver and then contrast this SEP to the SEP of the H-S/EGC receivers with the correct values.
- In Chapter 4, we made the distinction between the EGC combining weights and the weights used by the PSGC receiver. This receiver is called, incorrectly in our opinion, by some researchers an EGC receiver. While the PSGC receiver has already been studied, the hybrid version of this receiver has not. It would be interesting to analyse the H-S/PSGC receiver and compare its performance to that of the H-S/EGC and H-S/MRC receivers.
- Finally, to gain more insight into the practical aspects of the receivers analysed in this thesis, it would be very beneficial to implement them using software defined radio (SDR) architecture.

Appendix A

Branch Selection Issues in Selection Diversity Receivers Using DPSK

In our analysis of receivers operating in channels with unknown CSI, the instantaneous signal plus noise (SPN) of each branch is used as the selection criterion. Since the previous received symbol is used as a noisy phase reference it can also be considered as a crude channel estimate along the same lines that the MMSE estimates were used in Chapter 3. One question that naturally arises from this consideration is which SPN to use for the branch selection; the current symbol instant SPN or the previous instant SPN which is also the channel estimate? It is, in fact, tempting to use the current SPN as the selection criterion since it indicates that the magnitude of the SPN at the current interval is the largest. The analysis in this appendix, however, shows that using the previous symbol SPN for the selection criterion in a SC receiver actually produces larger output SNR.

Let the current symbol instant be denoted by k, and the signal from branch i be defined as

$$r_i = r_i[k], \tag{A.1}$$

where $r_i[k]$ is the received symbol from branch i and it is defined in terms of the fading gain and the AWGN as

$$r_i[k] = g_i[k] + n_i[k]. \tag{A.2}$$

In (A.2) we assume that the transmitted symbol is 1, therefore the received symbol is the sum of the fading gain $g_i[k]$ and the AWGN $n_i[k]$. At time k-1 (previous symbol instant) the signal received from branch i is defined as

$$h_i = r_i[k-1]. \tag{A.3}$$

As described in Section 2.2, r_i may be written in terms of h_i as

$$r_i = w_i^* h_i + e_i + n_i, \tag{A.4}$$

where the variables w_i and e_i were introduced in Section 2.2 and are defined as

$$w_i = \frac{\sigma_{g_i h_i}}{\sigma_{h_i}^2}, \tag{A.5}$$

$$e_i = g_i - w_i^* h_i \tag{A.6}$$

and n_i is the AWGN variable with variance $\sigma_{n_i}^2$. The variance of e_i was shown in Section 2.2 to be

$$\sigma_{e_i}^2 = \sigma_{g_i}^2 - \frac{\sigma_{g_i h_i}^2}{\sigma_{h_i}^2}. \tag{A.7}$$

Furthermore, when the variables r_i and h_i are sorted according to their magnitudes they are denoted as $r_{(i)}$ and $h_{(i)}$ as described in (2.55), Section 2.6 with $r_{(1)}$ and $h_{(1)}$ having the largest magnitude amongst the branches.

We begin with the case of a channel having uniform signal and noise power profiles (uniform SPP and NPP). Uniform SPP and NPP imply that all the branches have identical statistics. For the trivial case no change in the strongest branch over two consecutive symbol instants there is obviously no difference in the output SNR by the two scenarios. For the non-trivial case in which the strongest branch changes over the two consecutive time instants $k-1$ and k, the ordering of the variables r_i and h_i also changes. In other words $r_{(1)}$ and $h_{(1)}$ arrive from two different branches. In this case we contrast scenario 1 in which the branch with maximum $|h_{(i)}|$ is selected with scenario 2 in which the branch with maximum $|r_{(i)}|$ is selected by comparing their respective output SNR's. Let the decision variable for scenario 1 be defined as

$$y_h = h_{(1)}^* r_{(i)}, \tag{A.8}$$

where $i>1$. The index i cannot be equal to 1 since we assume that the branch with the maximum SPN in the current instant is different from the branch in the previous instant. Let the decision variable for scenario 2 be defined as

$$y_r = h_{(j)}^* r_{(1)}, \tag{A.9}$$

where $j>1$. Let us now calculate the instantaneous SNR of the two decision variables. Using (A.4) the decision variables can be written as

$$y_h = h_{(1)}^* [w^* h_{(1)} + e_{(i)} + n_{(i)}], \tag{A.10}$$

$$y_r = h_{(j)}^* [w^* h_{(j)} + e_{(1)} + n_{(1)}]. \tag{A.11}$$

The instantaneous SNR's at the output of the SC receiver for the two decision variables in (A.10) and (A.11) are, respectively,

$$\gamma_h = \frac{|w|^2 |h_{(1)}|^2}{2(\sigma_e^2 + \sigma_n^2)}, \tag{A.12}$$

$$\gamma_r = \frac{|w|^2 |h_{(j)}|^2}{2(\sigma_e^2 + \sigma_n^2)}. \tag{A.13}$$

It is apparent from (A.12) and (A.13) that scenario 1 always produces higher SNR for the SC receiver in the case of uniform SPP and NPP.

In order to verify the validity of our selection criterion for the general case of the SC receiver operating in a non-uniform SPP and/or NPP channel we now compare the average output SNR for the two scenarios. The average output SNR of the receiver in scenario 1 was found in (4.34) to be

$$\Gamma_h = \frac{1}{(\Lambda_0)^N} \sum_{\mathbf{P_k}} \left[a_{k_1} \left(\sum_{i=1}^{N} \frac{1}{d_{k_i}} \right) \left(\prod_{i=1}^{N} \frac{1}{d_{k_i}} \right) \right], \tag{A.14}$$

where

$$\Lambda_0 = \left(\prod_{i=1}^{N} \Lambda_i \right)^{1/N}, \tag{A.15}$$

$$\Lambda_i = \frac{1}{2} E\left[|h_{(i)}|^2 \right], \tag{A.16}$$

$$a_{k_i} = \begin{cases} \dfrac{|w_{k_1}|^2}{\mathcal{N}_{k_1}} & i = 1 \\ 0 & otherwise \end{cases} \tag{A.17}$$

and

$$d_{k_i} = \sum_{n=1}^{i} \frac{1}{\Lambda_{k_n}}. \tag{A.18}$$

Following the approach followed in Section 4.1.3, the average output SNR for the receiver in scenario 2 is defined as

$$\Gamma_r = \int_0^{\infty} \gamma_r f_{\gamma_r}(\gamma_r) d\gamma_r, \tag{A.19}$$

where γ_r is defined in (A.13) and $f_{\gamma_r}(\gamma_r)$ is its exponential pdf. Following the approach of Section 4.1.3, (A.19)can be written as

$$\Gamma_r = \sum_{\mathbf{P_k}} \int_0^{\infty} \int_0^{\lambda_{(1)}} \cdots \int_0^{\lambda_{(N-1)}} a_{k_j} \lambda_{(j)} \left(\prod_{i=1}^{N} f_{k_i}(\lambda_{(i)}) \right) d\lambda_{(N)} \cdots \lambda_{(2)} \lambda_{(1)}. \tag{A.20}$$

Using the virtual branch transformation described in Section 2.6, the expression in (A.20) is transformed into the simpler integral with constant limits

$$\Gamma_r = \frac{1}{(\Lambda_0)^N} \sum_{\mathbf{P_k}} a_{k_j} \int_0^\infty \int_0^\infty \cdots \int_0^\infty \left(\sum_{i=j}^{N} u_i \right) \exp\left(-\sum_{i=1}^{N} d_{k_i} u_i \right) du_N \cdots du_2 du_1 , \tag{A.21}$$

where d_{k_i} is defined in (A.18). Performing the multiple integration the final closed form expression for the SNR is obtained as

$$\Gamma_r = \frac{1}{(\Lambda_0)^N} \sum_{\mathbf{P_k}} \left[a_{k_j} \left(\sum_{i=j}^{N} \frac{1}{d_{k_i}} \right) \left(\prod_{i=1}^{N} \frac{1}{d_{k_i}} \right) \right]. \tag{A.22}$$

Comparing (A.22) and (4.34) it is clear that $\Gamma_h \geq \Gamma_r$ since a_{k_1} is a positive quantity in all cases of interest.

To try to explain intuitively this important result, we must consider how a receiver detecting DPSK modulation operates. Using the previous received symbol as a reference the receiver attempts to detect the current symbol. In other words, the receiver uses the previous symbol as a known quantity and attempts to see how the current symbol deviates from the known quantity.

Appendix B

Multiple Integral Evaluation to Assist in the Asymptotic SEP Derivation of the H-S/EGC Receiver

B.1 The Integral

In this section we derive the solution to the following integral:

$$I=\int_0^{\infty}\cdots\int_0^{\infty}\left(\prod_{i=1}^{N}\lambda_i^{b_i}\right)\exp\left(-K\left(\sum_{i=1}^{N}a_i\lambda_i\right)^2\right)d\lambda_1\cdots d\lambda_N\,. \tag{B.1}$$

This integral is reduced to (5.42) when $a_i=i$. Let us, first, define the vectors

$$\boldsymbol{\lambda}=[\lambda(1),\lambda(2),\ldots,\lambda(N)]\,, \tag{B.2}$$

$$\mathbf{u}=[u_1,u_2,\ldots,u_N] \tag{B.3}$$

and the following transformation:

$$\boldsymbol{\lambda}=\mathbf{T}\mathbf{v}\,. \tag{B.4}$$

The transformation matrix $\mathbf{T}$ is defined as

$$\mathbf{T}=\begin{bmatrix} a_1 & 0 & 0 & \cdots & 0 & 0\\ 0 & a_2 & 0 & \cdots & 0 & 0\\ 0 & 0 & a_3 & \cdots & 0 & 0\\ \vdots & \vdots & \vdots & \ddots & \vdots & \vdots\\ 0 & 0 & 0 & \cdots & a_{N-1} & 0\\ a_1 & a_2 & a_3 & \cdots & a_{N-1} & a_N \end{bmatrix}. \tag{B.5}$$

The effect of this transformation is that the sum in the exponent inside the integral is reduced to the single variable, v_N. After applying the transformation the integral in (B.1) becomes

$$I=\int_0^{\infty}\exp\left(-Kv_N^2\right)\int_0^{v_N}\cdots\int_0^{\left(v_N-\sum_{i=3}^{N-1}v_i\right)}\int_0^{\left(v_N-\sum_{i=2}^{N-1}v_i\right)}J(\mathbf{T})\left(\prod_{i=1}^{N-1}\left(\frac{v_i}{a_i}\right)^{b_i}\right)\left(\frac{\left(v_N-\sum_{i=2}^{N-1}v_i\right)-v_1}{a_N}\right)^{b_N}dv_1dv_2\cdots dv_{N-1}dv_N\,, \tag{B.6}$$

where $J(\mathbf{T})$ is the Jacobian of the transformation shown below:

$$J(\mathbf{T}) = |\mathbf{T}|^{-1} = \left(\prod_{i=1}^{N} a_i \right)^{-1}. \tag{B.7}$$

Using the binomial expansion

$$\left(\left(v_N - \sum_{i=2}^{N-1} v_i \right) - v_1 \right)^{b_N} = \sum_{j=0}^{b_N} \binom{b_N}{j} (-1)^j v_1^j \left(v_N - \sum_{i=2}^{N-1} v_i \right)^{b_N - j} \tag{B.8}$$

in (B.6) we obtain the expression

$$I = \left(\prod_{i=1}^{N} a_i^{-b_i - 1} \right) \int_0^{\infty} \exp\left(-K v_N^2\right) \int_0^{v_N} \cdots \int_0^{\left(v_N - \sum_{i=3}^{N-1} v_i\right)} \int_0^{\left(v_N - \sum_{i=2}^{N-1} v_i\right)} \left(\prod_{i=1}^{N-1} v_i^{b_i} \right) \times$$

$$\left(\sum_{j=0}^{b_N} \binom{b_N}{j} (-1)^j v_1^j \left(v_N - \sum_{i=2}^{N-1} v_i \right)^{b_N - j} \right) dv_1 dv_2 \cdots dv_{N-1} dv_N . \tag{B.9}$$

This expression may be solved iteratively by successively moving the product terms in the binomial expansion and integrating. The first two steps for integrating with respect to v_1 are illustrated below:

$$I = \left(\prod_{i=1}^{N} a_i^{-b_i - 1} \right) \int_0^{\infty} \exp\left(-K v_N^2\right) \int_0^{v_N} \cdots \int_0^{\left(v_N - \sum_{i=3}^{N-1} v_i\right)} \int_0^{\left(v_N - \sum_{i=2}^{N-1} v_i\right)} \left(\prod_{i=2}^{N-1} v_i^{b_i} \right) \times$$

$$\left(\sum_{j=0}^{b_N} \binom{b_N}{j} (-1)^j v_1^{b_1 + j} \left(v_N - \sum_{i=2}^{N-1} v_i \right)^{b_N - j} \right) dv_1 dv_2 \cdots dv_{N-1} dv_N , \tag{B.10}$$

$$I = \left(\prod_{i=1}^{N} a_i^{-b_i - 1} \right) \int_0^{\infty} \exp\left(-K v_N^2\right) \int_0^{v_N} \cdots \int_0^{\left(v_N - \sum_{i=4}^{N-1} v_i\right)} \int_0^{\left(v_N - \sum_{i=3}^{N-1} v_i\right)} \left(\prod_{i=2}^{N-1} v_i^{b_i} \right)$$

$$\left(\sum_{j=0}^{b_N} \binom{b_N}{j} \frac{(-1)^j}{b_1 + j + 1} \left(v_N - \sum_{i=2}^{N-1} v_i \right)^{b_N + b_1 + 1} \right) dv_2 dv_3 \cdots dv_{N-1} dv_N . \tag{B.11}$$

This procedure is repeated $N-2$ times until (B.11) becomes

$$I = \left(\prod_{i=1}^{N} a_i^{-b_i - 1} \right) \left(\prod_{i=1}^{N-1} A(i) \right) \int_0^{\infty} (v_N)^{\sum_{k=1}^{N} b_k + (N-1)} \exp\left(-K v_N^2\right) dv_N \tag{B.12}$$

where

$$A(i) = \sum_{j=0}^{b_N + \sum_{k=1}^{i-1} b_k + (i-1)} \binom{b_N + \sum_{k=1}^{i-1} b_k + (i-1)}{j} \frac{(-1)^j}{b_i + j + 1} . \tag{B.13}$$

It is proven in Section B.2 that

$$\sum_{j=0}^{b_N+\sum_{k=1}^{i-1}b_k+(i-1)}\binom{b_N+\sum_{k=1}^{i-1}b_k+(i-1)}{j}\frac{(-1)^j}{b_i+j+1}=\frac{1}{(b_i+1)}\Big/\binom{b_N+\sum_{k=1}^{i}b_k+i}{b_i+1} \tag{B.14}$$

and the solution of the integral can be simplified to

$$I=\left(\prod_{i=1}^{N}a_i^{-b_i-1}\right)\left(\prod_{i=1}^{N-1}\frac{1}{(b_i+1)}\Big/\binom{b_N+\sum_{k=1}^{i}b_k+i}{b_i+1}\right)\frac{(M-1)!}{2K^M}. \tag{B.15}$$

Note that in (B.15) we assume that $\sum_{k=1}^{N}b_k=2M-N$, where $M\geq N$, which is true for the purpose of this thesis. Finally, the integral is simplified as follows:

$$\begin{aligned}
I&=\left(\prod_{i=1}^{N}a_i^{-b_i-1}\right)\frac{\left(\prod_{i=1}^{N}b_i!\right)}{(2M-1)!}\frac{(M-1)!}{2K^M}\\
&=\frac{(M-1)!}{2(2M-1)!K^M}\left(\prod_{i=1}^{N}a_i^{-b_i-1}\right)\left(\prod_{i=1}^{N}b_i!\right)\\
&=\frac{(M-1)!}{2(2M-1)!!(2M-2)!!K^M}\left(\prod_{i=1}^{N}a_i^{-b_i-1}\right)\left(\prod_{i=1}^{N}b_i!\right)\\
&=\frac{1}{2^M K^M(2M-1)!!}\left(\prod_{i=1}^{N}a_i^{-b_i-1}\right)\left(\prod_{i=1}^{N}b_i!\right).
\end{aligned} \tag{B.16}$$

B.2 Combinatorics

To simplify the sum in (B.14) we use the help of Combinatorics theory [57]. Using simplified notation, we need to prove the following:

$$C=\sum_{j=0}^{K}\binom{K}{j}\frac{(-1)^j}{j+k}=\frac{1}{k}\Big/\binom{K+k}{k} \tag{B.17}$$

We make use of the following identity [57]:

$$\binom{n-1}{k-1}=\frac{k}{n}\binom{n}{k} \tag{B.18}$$

We apply identity (B.18) k times to the left hand side of (B.17) and successively simplify the result as shown below:

$$C=\sum_{j=0}^{K}\binom{K}{j}\frac{(-1)^j}{j+k}=\sum_{j=0}^{K}\binom{K+k}{j+k}(-1)^j\frac{\left(\prod_{i=1}^{k-1}j+i\right)}{\left(\prod_{i=1}^{k}K+i\right)}$$

$$=\frac{1}{\left(\prod_{i=1}^{k}K+i\right)}\sum_{j=0}^{K}\binom{K+k}{j+k}(-1)^j\left(\prod_{i=1}^{k-1}j+i\right)$$

$$=\frac{1}{\left(\prod_{i=1}^{k}K+i\right)}\sum_{j=k}^{K+k}\binom{K+k}{j}(-1)^{j-k}\left(\prod_{i=1}^{k-1}j+i-k\right)$$

$$=\frac{(-1)^{-k}}{\left(\prod_{i=1}^{k}K+i\right)}\sum_{j=k}^{K+k}\binom{K+k}{j}(-1)^j\left(\prod_{i=1}^{k-1}j+i-k\right)$$

$$=\frac{(-1)^{-k}}{\left(\prod_{i=1}^{k}K+i\right)}\left[\sum_{j=0}^{K+k}\binom{K+k}{j}(-1)^j\left(\prod_{i=1}^{k-1}j+i-k\right)-\sum_{j=0}^{k-1}\binom{K+k}{j}(-1)^j\left(\prod_{i=1}^{k-1}j+i-k\right)\right]. \quad \text{(B.19)}$$

We know (for example from [42]) that since the maximum power of j is always less than $K+k+1$, the following is true:

$$\sum_{j=0}^{K+k}\binom{K+k}{j}(-1)^j\left(\prod_{i=1}^{k-1}j+i-k\right)=0. \quad \text{(B.20)}$$

Therefore, (B.19) becomes

$$C=\frac{(-1)^{-k-1}}{\left(\prod_{i=1}^{k}K+i\right)}\left[\sum_{j=0}^{k-1}\binom{K+k}{j}(-1)^j\left(\prod_{i=1}^{k-1}j+i-k\right)\right]. \quad \text{(B.21)}$$

By observing that

$$\prod_{i=1}^{k-1}(j+i-k)=0 \ \textit{for}\ 1\le j\le k-1 \quad \text{(B.22)}$$

we are able to eliminate the k-1 terms of the sum in (B.21) and the expression is simplified as follows:

$$C=\frac{(-1)^{-k-1}}{\left(\prod_{i=1}^{k}K+i\right)}\left[(-1)^0\left(\prod_{i=1}^{k-1}0+i-k\right)\right]=\frac{(-1)^{-k-1}}{\left(\prod_{i=1}^{k}K+i\right)}\left[\prod_{i=1}^{k-1}(i-k)\right]$$

$$= \frac{(-1)^{-k-1}}{\left(\prod_{i=1}^{k} K+i\right)}\left[(-1)^{k-1}\prod_{i=1}^{k-1}(k-i)\right] = \frac{(-1)^{-2}}{\left(\prod_{i=1}^{k} K+i\right)}\left[\prod_{i=1}^{k-1}(k-i)\right] \tag{B.23}$$

By changing the variable in the product using the transformation $n = k - i$ we obtain

$$C = \frac{1}{\left(\prod_{i=1}^{k} K+i\right)}\left[\prod_{n=k-1}^{1}(k-k+n)\right] = \frac{1}{\left(\prod_{i=1}^{k} K+i\right)}\left[\prod_{n=k-1}^{1} n\right] = \frac{(k-1)!}{\left(\prod_{i=1}^{k} K+i\right)} \tag{B.24}$$

Finally, using combinatory notation the end result in (B.24) can be written as

$$C = \frac{(k-1)!}{\left(\prod_{i=1}^{k} K+i\right)} = \frac{1}{k\binom{K+k}{k}}, \tag{B.25}$$

which is the right hand side of (B.17) as required.

Bibliography

[1] M. Schwartz, W.R. Bennett and S. Stein, *Communications Systems and Techniques*, New York: McGraw-Hill, 1966.

[2] J.G. Proakis, *Digital Communications*, New York: McGraw-Hill, 1995.

[3] M.Z. Win and R.A. Scholtz, "On the energy capture of ultrawide bandwidth signals in dense multipath environments", *IEEE Commun. Letters*, vol. 2, pp. 245-247, Sept. 1998.

[4] T. Eng, N. Kong and L.B. Milstein, "Comparison of Diversity Combining Techniques for Rayleigh-Fading Channels", *IEEE Trans. Commun.*, Vol. 44, pp. 1117-1129, Sept. 1996.

[5] S.H. Van Wambeck and A.H. Ross, "Performance of diversity receiving systems", *Proc. IRE* vol 39, pp. 256-264, Mar. 1951.

[6] L. Kahn, "Radio squarer", *Proc. IRE* vol 42, p. 1704, Nov. 1954.

[7] D.G. Brennan, "Linear diversity combining techniques", *Proc. IRE* vol 47, pp. 1075-1102, Jun. 1959.

[8] M.D. Yacoub, *Foundations of mobile radio engineering*, CRC Press, 1993.

[9] E.A. Neasmith and N.C. Beaulieu, "New Results on Selection Diversity", *IEEE Trans. Commun.*, Vol. 46, pp. 695-704, May 1998.

[10] Q.T. Zhang,, "Maximal-Ratio Combining over Nakagami Fading Channels with an Arbitrary Branch Covariance Matrix", IEEE Trans. Veh. Technol., Vol. 48, pp. 1141-1150, July 1999.

[11] Q.T. Zhang, "A Simple Approach to Probability of Error for Equal Gain Combiners over Rayleigh Channels", IEEE Trans. Veh. Technol., Vol. 48, pp. 1151-1154, July 1999.

[12] P. Lombardo, G. Fedele and M.M. Rao, "MRC Performance for Binary Signals in Nakagami Fading with General Branch Correlation", IEEE Trans. Commun., Vol. 47, pp. 44-52, Jan. 1999.

[13] H. Erben, S. Zeisberg, and H. Nuszkowski, "BER Performance of a Hybrid SC/MRC 2DPSK RAKE Receiver in Realistic Mobile Channels", in *Proc. IEEE Veh. Technol. Conf. VTC'94*, Stockholm, Sweden, June 1994, pp.738-741.

[14] N. Kong, T. Eng and L.B. Milstein, "A Selection Combining Scheme For Rake Receivers", in *Proc. IEEE Conf. Iniv. Personal Commun. ICUPC'95*, Tokyo, Japan, Nov. 1995, pp. 426-429.

[15] N. Kong and L.B. Milstein, "SNR of generalized diversity selection combining with nonidentical Rayleigh fading statistics", *IEEE Trans. Commun.*, vol. 48, pp. 1266 -1271, Aug. 2000.

[16] N. Kong, "Average signal-to-interference-plus-noise ratio of a generalized optimum selection combiner for non-identical independent Rayleigh fading channels in the presence of co-channel interference", in *Proc. IEEE Int. Conf. Commun. ICC'01*, pp. 990-994.

[17] M.-S. Alouini and M.K. Simon, "Performance analysis of coherent equal gain combining over Nakagami-m fading channels", *IEEE Trans. Veh. Technol.*, vol. 50, Nov. 2001, pp. 1449-1463.

[18] M.-S. Alouini and M.K. Simon, "Error rate analysis of M-PSK with equal gain combining over Nakagami fading channels", in *Proc. IEEE Veh. Technol. Conf. VTC'99*, Jul. 1999, vol. 3, pp. 2378-2382.

[19] M.-S. Alouini and M.K. Simon, "Performance of Coherent Receivers with Hybrid SC/MRC over Nakagami-m Fading Channels", *IEEE Trans. Veh. Technol.*, July 1999, pp. 1155-1164.

[20] A. Annamalai, C. Tellambura and V.K. Bhargava, "Equal-gain diversity receiver performance in wireless channels", *IEEE Trans. Commun.*, vol. 48, pp. 1732-1745, Oct. 2000.

[21] A. Annamalai and C. Tellambura, "The effects of Gaussian weighting errors in hybrid SC/MRC combiners", in *Proc. IEEE Wireless Commun. and Networking Conf., WCNC'2000*, Sep. 2000, pp. 211 -215.

[22] A. Annamalai and C. Tellambura, "Analysis of hybrid selection/maximal-ratio diversity combiners with Gaussian errors", *IEEE Trans. Wireless Commun.*, Vol. 1, pp. 498-511, Jul. 2002.

[23] M.Z. Win and J.H. Winters, "Analysis of Hybrid Selection/Maximal-Ratio Combining in Rayleigh Fading", in *Proc. IEEE Int. Conf. Commun. ICC'99*, Vancouver, BC, Canada, June 1999, pp. 6-10.

[24] M.Z. Win and J.H. Winters, "Virtual branch analysis of symbol error probability for hybrid selection/maximal-ratio combining in Rayleigh fading", *IEEE Trans. Commun.*, vol. 49, pp. 1926-1934, Nov. 2001.

[25] M.Z. Win and J.H. Winters, "Exact error probability expressions for MRC in correlated Nakagami channels with unequal fading parameters and branch powers", in *Proc. IEEE Global Telecomm. Conf., GLOBECOM '99*, Dec. 1999, pp. 2331-2335.

[26] P. Polydorou and P. Ho, "Error Performance of MPSK with Diversity Combining in Non-Uniform Rayleigh Fading and Non-Ideal Channel Estimation", in *Proc. IEEE Veh. Technol. Conf. VTC'2000*, Tokyo, Japan, May 2000, pp. 627-631.

[27] P. Polydorou and P. Ho, "The effect of channel information on the symbol error probability of selection diversity combining receivers in fading channels", in *Proc. IEEE Int. Conf. On Commun. Syst. ICCS'2000*, Singapore, Nov. 2000.

[28] P. Polydorou and P. Ho, "Symbol Error Probability for Double Selection/Equal Gain Combining of Branches in A Rayleigh Fading environment without Channel Statistical Information", in *Proc. IEEE Global Telecomm. Conf., GLOBECOM '01*, San Antonio, TX, Nov. 2001, pp. 3343 –3347.

[29] S. Haykin, *Adaptive filter theory*, New Jersey, Prent. Hall, 1996.

[30] J.K. Cavers, "An analysis of pilot symbol assisted modulation for Rayleigh fading channels [mobile radio]", *IEEE Trans. Veh. Technol.*, vol. 40, Nov. 1991, pp. 686-693.

[31] M.Z. Win and Z.A. Kostic, "Impact of spreading bandwidth on RAKE reception in dense multipath channels", *IEEE Journal Sel. Areas Commun.*, vol. 17, pp. 1794-1806, Oct. 1999.

[32] M.Z. Win and J.H. Winters, "Analysis of hybrid selection/maximal-ratio combining in Rayleigh fading", *IEEE Trans. Commun.*, vol. COM-47, pp. 1773-1776, Dec. 1999.

[33] P. Bello and B. Nelin, "Predetection Diversity Combining with Selectively Fading Channels", *IEEE Trans. Commun.*, vol. 10, Mar. 1962, pp. 32-42.

[34] M. Gans, "The Effect of Gaussian Error in Maximal Ratio Combiners", *IEEE Trans. Commun.*, vol. 19, Aug. 1971, pp. 492-500.

[35] M.-S. Alouini, W.K. Sang, A.Goldsmith, "RAKE reception with maximal-ratio and equal-gain combining for DS-CDMA systems in Nakagami fading", in *Proc. IEEE 6th Int. Conf. on Univ. Pers. Commun.*, Oct. 1997, pp. 708-712.

[36] B.R. Tomiuk and N.C. Beaulieu, "A new look at maximal ratio combining", in *Proc. IEEE Global Telecomm. Conf., GLOBECOM '00*, Nov.-Dec. 2000, pp. 943-948.

[37] X.D. Dong and N.C. Beaulieu, "Optimal maximal ratio combining with correlated diversity branches", *IEEE Commun. Letters*, vol. 6, Jan. 2002, pp. 22-24.

[38] R.F. Pawula, S.O. Rice, and J.H. Roberts, "Distribution of the phase angle between two vectors perturbed by Gaussian noise", *IEEE Trans. Commun.*, vol. COM-30, pp. 1828-1841, Aug. 1982.

[39] M.-S. Alouini and A.J. Goldsmith, "A unified approach for calculating error rates of linearly modulated signals over generalized fading channels", *IEEE Trans. Commun.*, vol. 47, pp. 1324-1334, Sep. 1999.

[40] S. Haghani, N.C. Beaulieu and M.Z. "Win, Bounds to the error probability of hybrid diversity two-dimensional signalling", in *Proc. IEEE Global Telecomm. Conf., GLOBECOM '02*, Nov. 2002, pp. 1408-1414.

[41] H.S. Abdel-Ghaffar and S. Pasupathy, "Asymptotical performance of M-ary and binary signals over multipath/multichannel Rayleigh and Rician fading", *IEEE Trans. Commun.*, vol. 43, pp. 2721-2731, Nov. 1995.

[42] I.S. Gradshteyn and I.M. Ryzhik, *Table of Integrals Series and Products*, New York, Academic Press, 1980.

[43] N. Kong and L.B. Milstein, "Average SNR of a Generalized Diversity Selection Combining Scheme", *IEEE Commun. Letters*, Vol. 3, pp. 57-59, Mar. 1999.

[44] M. Stojanovic and Z. Zvonar, "Differentially coherent diversity combining techniques for DPSK over fast Rayleigh fading channels", *IEEE Trans. Veh. Technol.*, Vol. 49, pp. 1928-1933, Sep. 2000.

[45] R.K. Mallik and M.Z. Win, "Error probability of binary NFSK and DPSK with postdetection combining over correlated Rician channels", *IEEE Trans. Commun.*, Vol. 48, pp. 1975-1978, Dec. 2000.

[46] F. Adachi and K. Ohno, "BER performance of QDPSK with postdetection diversity reception in mobile radio channels", *IEEE Trans. Veh. Technol.*, Vol. 40, pp. 237-249, Feb. 1991.

[47] M. Ikura and F. Adachi, "Postdetection phase combining diversity", *IEEE Trans. Veh. Technol.*, Vol. 43, pp. 298-303, May 1994.

[48] H. Leib and S. Pasupathy, "The phase of a vector perturbed by Gaussian noise and differentially coherent receivers", *IEEE Trans. Inf. Theory*, Vol. 47, pp. 1491-1501, Nov. 1988.

[49] M. Brehler and M.K. Varanasi, "Asymptotic error probability analysis of quadratic receivers in Rayleigh-fading channels with applications to a unified analysis of coherent and noncoherent space-time receivers", *IEEE Trans. Inf. Theory*, Vol. 47, pp. 2383-2399, Sep. 2001.

[50] B. Sklar, *Digital Communications*, New Jersey: Prentice Hall PTR, 2001

[51] W.C. Jakes, *Microwave mobile communications*, New York: IEEE Press, 1993.

[52] H.-C. Yang and M.-S. Alouini, "Performance analysis of multibranch switched diversity systems", *IEEE Trans. Commun.*, vol. 51, pp. 782-794, May 2003.

[53] A. A. Abu-Dayya and N. C. Beaulieu, "Analysis of switched diversity systems on generalized-fading channels", *IEEE Trans. Commun.*, vol. 42, pp. 2959-2966, Nov. 1994.

[54] B. Barrow, "Diversity Combination of Fading Signals with Unequal Mean Strengths", *IEEE Trans. Commun.*, vol. 11, pp. 73-78, Oct. 1963.

[55] A. Afrashteh and D. Chukurov, "Performance of a novel selection diversity technique in an experimental TDMA system for digital portable radio communications", in *Proc. IEEE Global Telecomm. Conf., GLOBECOM '88*, Nov.-Dec. 1988, pp. 810-814.

[56] J.C.-I. Chuang and N.R. Sollenberger, "Burst coherent demodulation with combined symbol timing, frequency offset estimation, and diversity selection", *IEEE Trans. Commun.*, vol. 39, pp. 1157-1164, Jul. 1991.

[57] A. Tucker, *Applied Combinatorics*, New York: J. Wiley, 1995.